THE PENNSYLVANIA STATE UNIVERSITY

Ionospheric Research
NASA Grant No. NsG 134-61
Scientific Report
on

"F REGION ANALYSIS FROM RADIO PHASE DISPERSION MEASUREMENTS BETWEEN SEPARATING ROCKET CAPSULES"

by

J. C. Widmaier
March 20, 1966

IONOSPHERE RESEARCH LABORATORY

The Pennsylvania State University
College of Engineering
Department of Electrical Engineering

Ionospheric Research

NASA Grant No. NsG 134-61

Scientific Report

on

"F Region Analysis from Radio Phase Dispersion Measurements Between Separating Rocket Capsules"

by

J. C. Widmaier

March 20, 1966

Scientific Report No. 267

Ionosphere Research Laboratory

Submitted by: J. S. Nisbet (au)

John S. Nisbet, Associate Professor of Electrical Engineering, Project Supervisor

Approved by: G. H. Waynick

A. H. Waynick, Director, Ionosphere Research Laboratory

The Pennsylvania State University

College of Engineering

Department of Electrical Engineering

TABLE OF CONTENTS

Abstract 30605

A unique high resolution technique has been employed to obtain absolute electron densities of the upper F region of the ionosphere. Propagation of two harmonic radio signals between two slowly separating rocket capsules and a measure of the ionospheric phase dispersion of these two signals with respect to a higher harmonic frequency reference was the essential principle employed.

A successful payload was launched on May 19, 1965 from Wallops Island. The data reduction technique and results of the experiment are presented. An error analysis also accompanies the final electron density profile. Also presented with these results of the Mother-Daughter experiment are comparisons with simultaneous measurements of the electron density from an onboard planar ion probe, the topside sounding satellite Alouette, and a ground ionosonde at Wallops Island.

CHAPTER I

Introduction

1.1 General Statement of the Problem

Numerous rocket and satellite experiments have been devised within the last decade to measure electron densities above the F_2 density maximum. The purpose of this experiment was to obtain with minimum error an absolute measure of the electron density in the F region extending from 250 to 1000 km.

When lower region direct measurement and propagation techniques are extended to the upper regions of the ionosphere many inherent complications exist and reduce the degree of accuracy. Calibration of direct measuring Langmuir probes becomes extremely com plicated and often inaccurate when considerations must be given to vehicle potential, the ion sheath formed around the vehicle, shock-waves in the plasma created by the vehicle, given transparency of the probe, and outgassing. Theoretical calibration of these probes, unless verified by experimental testing, is often a difficult basis for assessing the absolute degree of accuracy. Rocket propagation to ground is, a reliable method in the lower regions where horizontal stratification of the ionosphere is assumed. When the propagation techniques are extended to higher altitudes, especially above the F_2 peak, the presence of horizontal gradients and small irregularities in the F region and the ducting of radio waves along extended paths are a few of the problems reducing the degree of accuracy. The integrated density along these longer paths of propagation becomes, at best, by these techniques an average value.

These limitations gave rise to the idea of propagating between two sections of a rocket with an immediate advantage of obtaining an absolute measurement and a high degree of resolution. The method appeared promising for the study of the detailed structure of the upper ionosphere and the calibration of direct measurement devices. After further evaluation it was proposed to NASA by Pennsylvania State University in December 1959 and a feasibility study was written by Nisbet, Quinn, and Carlson (1961). Based on this study it was decided to develop a payload for an Argo D-4 rocket and make a series of measurements in this fashion up to 1000 km. It was also proposed to investigate the accuracy of the method and make preliminary studies of the applicability of this technique. The payload design has been described by Cantrell of Space Craft, Inc. (1964).

A successful Javelin firing on May 19, 1965 at Wallops Island, Virginia yielded very fruitful results. The major part of this work was devoted toward the development of a reliable data reduction technique relating phase changes of propagated waves to electron densities, calculation of electron density profiles, and the deduction of basic properties of the ionosphere from these profiles.

1.2 Previous Related Studies

There are essentially four propagation techniques used for investigating the upper ionosphere. Pulse-delay comparison, Faraday rotation, integrated phase analysis, and topside sounding propagation constitute the basic methods employed.

1.2.1 Pulse Propagation

Of the earliest techniques developed was pulsed radio frequency propagation. Dow (1946) at the University of Michigan first suggested the method using pulse propagation to determine electron density in an ionized layer. The basic experiment consisted of equipment for the transmission of two synchronized pulse signals from ground to an ascending rocket. The frequency of one of the pulse signals was near the critical penetration frequency of the layer and thus was measurably retarded. The other higher frequency signal suffered little retardation along the propagation path and was indirectly used as a reference. Upon reception in the rocket, the pulse signals triggered reply pulses transmitted to ground on a u. h. f. channel. The time difference between the two u. h. f. reply signals contained a measure of the retardation time of the probing low frequency pulse. This retardation time was then proportional to the equivalent electron density.

Linford (1952) at the University of Utah improved the experiment and later conducted rocket flights in 1953. Moore and Law (1953) of Boston University also conducted a series of h. f. pulse propagation rocket experiments. According to Lien, Marcou, Ulwick, Aaron, and McMarrow (1954) the failure of Moore and Law to identify various pulse modes throughout portions of their flights reduced the reliability of the underlying applicability of ray theory to pulse propagation through extended path lengths.

The most recent version of this method has been developed by Pfister and Ulwick (1959) and Ulwick, Pfister, Vancour, Bettinger,

Haycock, and Baker (1962). Pfister and Ulwick (1959) have obtained volumes of data in obtaining this integrated electron density along the path of the rocket. Considerable fluctuations in time delay of the pulses occurred, however; and in later flights they analyzed these delays to be enhanced by intervening clouds of electrons along the ray path. A smoothing process in their data was necessary to obtain more realistic electron densities; the smaller time delays were weighted more than the larger ones. In a later Astrobee firing Pfister, Ulwick, Vancour, Bettinger, Haycock, and Baker (1962) showed that these density irregularities had effects on the two pulse frequencies such as to cause different ray paths. They also pointed out that it was necessary to take into account effects of the earth's magnetic field for tracing the oblique rays and for the equivalent path of the wave packet.

1.2.2 Faraday Rotation

The method of Faraday rotation was first employed by Brown, Evans, Hargreaves, and Murray (1956). In a series of observations from 1953 to 1955 they obtained a measure of the total electron content of the ionosphere from the angle of rotation of radio signals reflected from the moon.

The basic technique involves a continuous measurement of the angle of rotation of the plane of polarization of a linearly polarized wave which propagates through a homogeneous ionized medium. The ordinary and extraordinary components of a linear wave are elliptically polarized; they rotate in opposite senses and travel with different velocities. Combined rotation of each mode results in a rotation of the plane of polarization of the linear wave. Then the rotation angle as

measured on the ground is essentially the product of electron density and magnetic field component integrated along the path of propagation.

Ross (1959) used the Faraday rotation of radio signals from the Delta 2 satellite to obtain electron content and density profiles. Blackband, Burgess, Jones, and Lawson (1959) also studied electron density and content using the Faraday rotation of signals from Sputnik I and II. Bowhill (1958) conducted numerous experiments from Cape Kennedy using long range ballistic missiles. Nisbet (1959) along with Bowhill later conducted a series of seven high altitude rocket experiments dealing with Faraday rotation. Nisbet (1959) made an extensive analysis of the errors inherent in the technique. He concluded that horizontal gradients in the intervening region, refractive bending of the rays, and non-vertical trajectories could introduce serious errors in calculating density profiles.

Ross and Solomon (1965) did extensive studies of the columnar electron content for altitude ranges between 250 and 300 km. From these satellite investigations using Faraday rotation, Solomon also noted that second order corrections due to nonuniform distribution of ionization, non-coincidence of wave normals and rays for particular frequency modes, and a nonlinear refractive index in electric density and magnetic field intensity appeared twice as great, for closely spaced frequency polarization, as that for the polarization rotation itself.

1.2.3 Phase Comparison

The method of comparing phases of two CW harmonically related frequencies radiated to ground stations to obtain measurements

of the ordinary and extraordinary indices of refraction was first used from 1946-1947 by Seddon (1953), (1954). With restrictive vertical propagation the ordinary and extraordinary modes of the propagated (4.274 and 25.644 Mc) waves were separated by crossed dipoles. After frequency multiplication by a factor of six, each component was heterodyned separately with the 25.644 Mc reference frequency. From the resulting beat frequency and the measured radial velocity of the rocket, the index of refraction of the medium was calculated with the Appleton-Hartree equation. Seddon did encounter complications in his records. Irregularities along the path of propagation from rocket to ground showed added frequencies in the ordinary modes of the A. V. C. records. Further evidence of the effects of irregularities upon the path of propagation was obtained after an S. I. D. in 1947 which occurred just before launch. Resultant sporadic E stopped signal propagation at 111 km and caused a loss of transmission data at higher altitudes.

Berning (1951) conducted similar phase propagation experiments but employed a radio Doppler electronic tracking system. Later flights using Seddon's phase comparator method were conducted by Jackson (1954). In analysis Jackson considered the errors of the method arising from nonvertical trajectories and low vertical rocket velocities. For further simplification signals were assumed to travel according to the line of sight when the rocket wasn't overhead. Deviations in propagation path were neglected. Jackson believed the method also limited to conditions when there were no rapid changes in regions traversed by the low frequency rays.

Jackson and Seddon (1957) continued density measurements of

the upper ionosphere using Seddon's original method. Seddon, Pickar, and Jackson (1954) again used the basic experiment but changed propagation frequencies to 7.75 and 46.5 Mc; both signals were above the F_2 layer critical frequency. Berning in 1960 using frequencies of 37 and 148 Mc/sec has obtained reasonable profiles at altitudes extended above the F region; but, Bowhill (1961) emphasized also that nearly vertical rocket trajectories were essential for the method if effects due to horizontal gradients were to be neglected.

Bauer and Jackson (1962) described a Doppler phase comparison method for obtaining densities to 2500 km. The integrated densities along the path of propagation at best corresponded to three point averages over height intervals of the order of 25 kilometers. At altitudes higher than 900 km they reported that density measurements were only possible over intervals which increased to 300 kilometers. Corrections were also necessary for error introduced by the explicit time variation of the ionosphere and horizontal gradients.

Blumle at G.S.F.C. is currently using a low altitude phase comparator method in obtaining electron density profiles.

1.2.4 Topside Sounding

In topside sounding devices similar in principle to a ground based ionosonde are located in a rocket or satellite above the ionosphere. Pulses of discrete radio frequencies or sweeping radio frequency waves are transmitted and then later received at the vehicle. From the group delay as a function of frequency the characteristics of the ionosphere below the vehicle can be calculated. Two versions of this type of device have been described.

The most highly developed application of the swept frequency technique is the Canadian satellite Alouette described by Chapman (1963). Jackson (1963) discussed two basic sources of error in Alouette measurements. The first dealt with the propagation of waves along loss-free aligned ducts and the second dealt with the methods used to reduce the ionograms. From a simultaneous experiment with a rocket and ground ionosonde, Jackson, Donley, Blumle, Bauer, and Fritzenreiter (1963) detected a ducting of the sounding radio waves. They have found that the density profile from Alouette showed a much lower F_2 peak than those obtained from the rocket and ionosonde. They speculated this lower height of the peak to be due to an increase of path length; and, the increase of path length was a result of ducting of the waves along field lines. Independent methods of reducing the ionograms have been developed by Doupnik and Schmerling (1965), Fitzenreiter and Blumle (1964), and Thomas, Briggs, Colin (1965). Profiles and electron content deviate slightly from each other according to reduction techniques. Thomas, Briggs, Colin, Rycraft, and Covert (1965) discussed the errors in ionogram scaling.

The first fixed frequency sounders were those in rockets devised by Knecht and Van Zandt (1961). The records of their two frequency pulsed sounder were described as being liable to errors caused by wave scattering irregularities in the 700-1000 km range. Knecht and Russel (1962) from topside pulsed soundings have also indicated that the path lengths for diffuse echoes was probably greater than normal because of a deviation of propagated waves to paths along field lines between the sounder and reflection level.

The most recent version of a fixed frequency topside satellite is a six harmonic frequency sounder described by the Central Radio Propagation Laboratory at N. B. S. According to Jackson (1963) this new S-48 satellite does, however, have limited resolution in depth on each of the twelve data point ionograms.

1.3 Specific Statement of the Problem

1. To devise methods of analyzing the electron density profile in the F region from propagation measurements between two sections of a rocket.

2. To determine the absolute accuracy of the above methods and to select techniques which will minimize the effects of any inherent errors present.

3. To apply these techniques to the reduction of data from rocket experiments and to determine electron density profiles.

4. To examine the electron density profiles deduced from the rocket propagation studies and to relate the measurements to basic properties of the ionosphere with particular emphasis on the detailed studies of the profiles such as density, density gradients, and irregularities of structure.

5. To compare results from the propagation study with those obtained by other means such as incoherent backscatter soundings, planar ion probes, topside sounding, and bottomside ionosondes.

1.4 Definitions and Notations

The MKS system of units, unless otherwise specified, is

used throughout this report including equations, tables of data, and figures. A right-handed Cartesian coordinate system is also used.

Symbols found within this paper are:

e = electron charge

m = electron mass

c = velocity of light in vacuum

ϵ_o = permittivity of free space

f = wave frequency

ω = angular frequency

t = time

Z_o = impedance of free space

$\overline{H}$ = magnetic field vector

$\overline{E}$ = electric field vector

$\overline{B}$ = earth's magnetic field vector

B_L = component of earth's field along direction of propagation

B_T = total earth's magnetic field

f_H = $\omega_H/2\pi$ electron gyrofrequency

ν_e = collision frequency

Z = ν_e/ω

T_e = electron temperature

T_i = ion temperature

K = Boltzman's constant

k_o = free space propagation constant

θ = propagation angle with respect to earth's field

Y_L = $\omega_H \cos\theta/\omega$

Y_T = $\omega_H \sin\theta/\omega$

$Y = [\, Y_T^2 + Y_L^2 \,]^{\frac{1}{2}}$

$\omega_N = N_e e^2 / \epsilon_o m$ plasma frequency

$X = \omega_N^2 / \omega^2$

$W = \dfrac{Y_T^2}{2Y_L(1 - X - jZ)}$

$R = W + \sqrt{1 + W^2}$

ρ = polarization

μ = index of refraction

Φ = total phase difference

ϕ = phase of individual wave

CHAPTER II

Theoretical Description Relating Phase to Electron Density for the Mother-Daughter Experiment

2.1 Phases for Electromagnetic Waves Propagating in a Homogeneous Anistropic Media

Budden (1961) describes radio wave propagation in a homogeneous anisotropic media such as the F region where the effects of the earth's magnetic field are included but also where electron collisions may be excluded. For a wave propagating in the z direction and normally incident upon the layer, he gives the solutions of Maxwell's equation in the prescribed media as:

$$E = A_o e^{-jk_o \mu z} \tag{2.1}$$

or

$$E = A_o e^{-j\phi(z)} \tag{2.2}$$

The amplitude of the field quantity is given by A_o. The factor exp $j\omega t$ has been omitted. The complex index of refraction μ is given in complete form by the Appleton-Hartree formula in Appendix A.

Differentiating equations (2.1) and (2.2) with respect to z yields:

$$\frac{d\phi}{dz} = k_o \mu + \frac{1}{2\mu} \frac{d\mu}{dz} \tag{2.3}$$

During the course of this experiment the linearly increasing separation distance between the transmitting Daughter and receiving Mother sections never exceeded 5 km. Within these short distances the ionosphere can be represented by a thin discrete stratum in which the medium is homogeneous and the electron density constant. Thus,

the derivative on the right side of equation (2.3) vanishes.

$$\frac{1}{2\mu} \frac{d\mu}{dz} = 0 \tag{2.4}$$

and thus

$$\frac{d\phi}{dz} = - k_o \mu \tag{2.5}$$

When (2.5) is integrated and simplified, the expression for the phase shift, ϕ, between the signal transmitted from the Daughter at $z = D$ and the signal received in the Mother at $z = M$ will be

$$\phi = \frac{2\pi f_1}{c} \int_D^M \mu dz = \frac{2\pi f_1}{c} \mu S_{MD} \tag{2.6}$$

where f_1 is the propagating frequency and S_{MD} is the relative separation distance between the two sections.

2.2 Relative Phase Shifts

If two harmonic signals are such that $f_2 = Nf_1$ and the phase comparison is made at the frequency of the higher harmonic, then the total phase shift between the signals is:

$$\Phi = \phi_2 - N\phi_1 = \frac{2\pi f_2}{c}(\mu_2 - \mu_1) S_{MD} \tag{2.7}$$

Each phase is given by relations above in (2.6) and the complex quantities μ_2 and μ_1 representing the indices of refraction are given in form similar to that of Appendix A. These indices of refraction are principally dependent upon the electron density, the mode of propagation - ordinary or extraordinary, the local earth's magnetic field

vector, and the propagation angle with respect to the magnetic field vector.

The relative phase of two harmonic signals of specified modes is thus shown to be essentially the product of separation distance and the difference of refractive indices. The separation velocity between the Mother and Daughter can be accurately measured; therefore, relative separation distances are easy to calculate. The earth's total magnetic field vector has been extensively investigated and is also known along the payload trajectory. Using known values of the total field and measurements of the component of the earth's field along the direction of propagation from a payload magnetometer, it is possible to find the angle of propagation with respect to the field vector. Then from a measure of relative phase along the trajectory, the electron density becomes uniquely determined.

2.3 Total Relative Phases of Propagated and Received Waves

The radio waves transmitted by the Daughter have the waveform:

$$E_T = E_{1T} \sin \omega_1 t + E_{2T} \sin (N\omega_1 t + \theta_N) \qquad (2.8)$$

The constant phase shift θ_N is introduced when both harmonic signals are derived from the same local oscillator. Frequency multiplication of ω_1 by a factor N introduces θ_N.

After the signals propagate through the homogeneous anisotropic ionosphere, the Mother antennas see waves given by the form:

$$E_R = E'_{1R} \sin [\omega_1 t + \phi(t)] + E_{2R} \sin [N\omega_1 t + \theta_N + \phi_2(t)] \qquad (2.9)$$

Phases $\phi_1(t)$ and $\phi_2(t)$ are the phases previously discussed in (2.6) which are functions of separation distance, electron density, propagation angle, and the total magnetic field. Amplitudes of the pair of transmitted and received waves are given by E_{1T}, E'_{1R}, E_{2T}, and E'_{2R}.

At the receiving antennas in the Mother the two frequency components of the received signal given in (2.9) is coupled to its appropriate receiver. The antenna matching unit introduces, however, a phase shift at each frequency and the waves, before phase comparison is made, have the form:

$$E_{1R} = E'_{1R} \sin [\, \omega_1 t + \phi_1(t) + \theta_1 \,] \qquad (2.10)$$

$$E_{2R} = E'_{2R} \sin [\, N\omega_1 t + \phi_2(t) + \theta'_2 \,] \qquad (2.11)$$

where θ'_2 is the sum of phase shift from the matching antenna θ_2 and the phase shift θ_N given in (2.8).

When the two signals received E_{1R} and E_{2R} are mixed with their local oscillator frequencies ω_i and $N\omega_i$ and the lower sideband is selected, the output of the I. F. amplifier is given by:

$$E_3 = E''_{1R} \sin [\, (\omega_i - \omega_1)t + \theta_3 - \phi_1(t) - \theta_1 \,] \qquad (2.12)$$

$$E_4 = E''_{2R} \sin [\, (\omega_i - \omega_1)Nt + \theta_4 - \phi_2(t) - \theta_2 \,] \qquad (2.13)$$

Then as E_3 is frequency multiplied by a factor N and passes through a phase comparator, the following phase difference results:

$$\Phi(t) = N\phi_1(t) - \phi_2(t) + \phi_o \qquad (2.14)$$

where ϕ_o is the combined time independent phase shifts of (2.12) and (2.13). Since phase comparison begins immediately with separation of the Mother and Daughter sections, the total phase difference at any time t' after separation is:

$$\Phi(t') = N\phi(t') - \phi_2(t') \qquad (2.15)$$

Receiver delays caused by a change in signal strength were not considered in the original analysis. These phase shifts which are dependent on variations of signal levels, do have a significant effect especially at time of Mother-Daughter separation. These contributions to the accumulative phase difference will be defined and appropriately analyzed in a later part of this paper. Also in a later chapter the secondary effects and the accuracy with which they are determined will be discussed.

Two such sets of phase comparison are employed in the Mother-Daughter experiment. One is made at 6.13333 Mc and 73.60 Mc; and the other phase comparison is at 12.26667 Mc and 73.60 Mc. This system is depicted in Figure 2.1.

There are two distinct advantages in using two comparisons of the described type. The first deals with the improved resolution at extended altitudes. A continuity of phase measurements from one phase channel to another also becomes possible as the experiment passes through different density regions. A more quantitative discussion of resolution is found in Chapter VI. Proper selection of propagation frequencies makes this possible. The upper limit for the frequencies is determined by the sensitivity desired. The lower limit

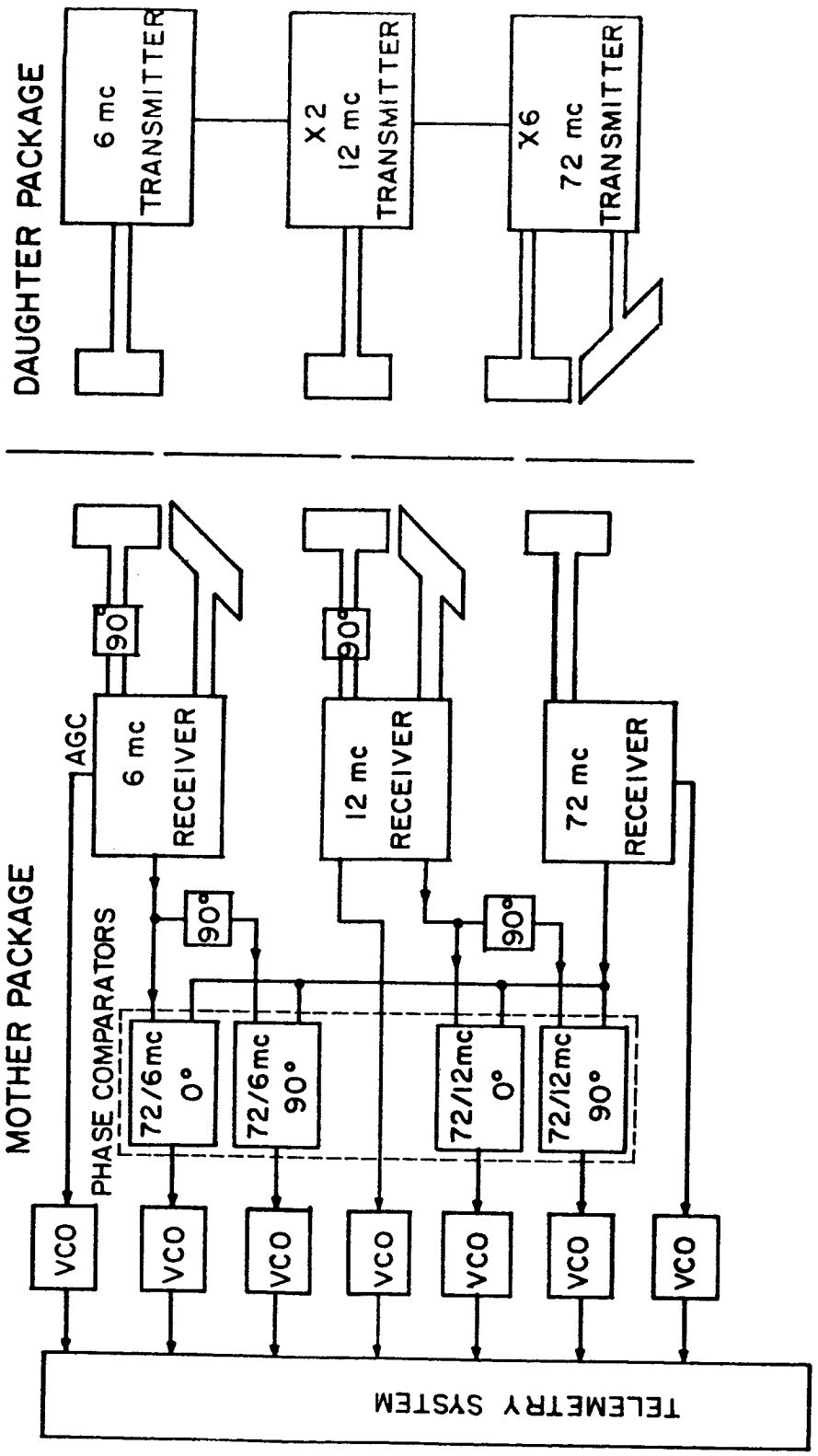

BLOCK DIAGRAM OF MOTHER – DAUGHTER INSTRUMENTATION

FIGURE 2.1

is determined by the largest density desired to measure with that particular frequency channel. With these considerations in mind one probing frequency at 12.26667 Mc was chosen. At a designed separation time the payload passes through the F_2 peak density. At that time the 12.26667 Mc wave gives maximum sensitivity and spatial resolution while also being higher than the plasma frequency. Then at the higher altitudes where electron density is smaller, the 6.13333 Mc signal gives maximum sensitivity and spatial resolution. The reference signal, the extraordinary mode of 73.60 Mc signal was of high enough frequency to propagate nearly unchanged through transition regions.

The second advantage is the increase degree of reliability of the absolute measurement. A duplication of the measurement occurs. For instance, if one pair of phase measurements were lost during some interval of experiment flight-time, it would be possible to reconstruct the total phase of that channel during its blackout time. Knowing the total accumulative count of phase for both pairs up to the blackout and polarizations of the transmitting and receiving antennas partially enable the calculation.

CHAPTER III

Description of Mother-Daughter Payload

3.1 General Description of the Payload

Following the feasibility study, it was decided to start the rocket experiment program and a payload was designed, developed, and tested by Space Craft, Inc. of Huntsville, Alabama under the technical direction of the Pennsylvania State University. The payload has been described in detail by Cantrell (1964). Only those portions necessary for the interpretation of data will be repeated here.

3.2 Electrical Design of the Mother-Daughter Payload

3.2.1 Design Considerations

Because of the stringent power, weight, and phase resolution problems, great care was devoted to the design and specification of the electrical and mechanical systems.

Receivers were required for each of the propagation frequencies and stability requirements limited the minimum bandwidth obtainable with available rocket equipment. The bandwidth requirements did allow, however, calculation of signal strengths necessary for the propagation experiment. The minimum signal strengths required for the receiving antenna and antenna matching units were then compared with those required from consideration to galactic and atmospheric noise. From the minimum signal strengths required, currents in the transmitting antenna were calculated and used for calculating the required transmitter power.

Frequency stability of this unit was 2 parts in 10^9. This high frequency stability was important not only because of bandwidth considerations in the receiver, but also because it enabled one way Doppler tracking of the Daughter section of the payload.

C. Temperature Changes and Detuning of I. F. Filters

In the original proposal it had been intended to use superheterodyne receivers. Improved transistors and design techniques, however, resulted in the selection for the final design of the tuned radio frequency receivers. In these receivers the individual stages were made extremely broad band to minimize the phase shifts in the individual stages due to temperature changes. Receiver selectivity was controlled by crystal filters. Figure 3.1 shows phase changes induced in the receivers of the Mother due to temperature changes. The limiting choice of the bandwidth was this phase-temperature curve of the receiver and not the Doppler shifts. Bandwidths for the 6 Mc, 12 Mc, and 73.6 Mc receivers were chosen to be 2 Kc, 4 Kc, and 24 Kc respectively because of the phase-temperature curve of the receiver. They were also chosen so that the power output was high enough to get the signal sufficiently above the noise.

3.2.3 Antenna Systems

A. Receiving Antenna System

For the Mother-Daughter system three antenna systems were required in the Mother package. It was desired to have a circularly polarized antenna for each low frequency measuring channel and a linearly polarized antenna for the high frequency reference channel.

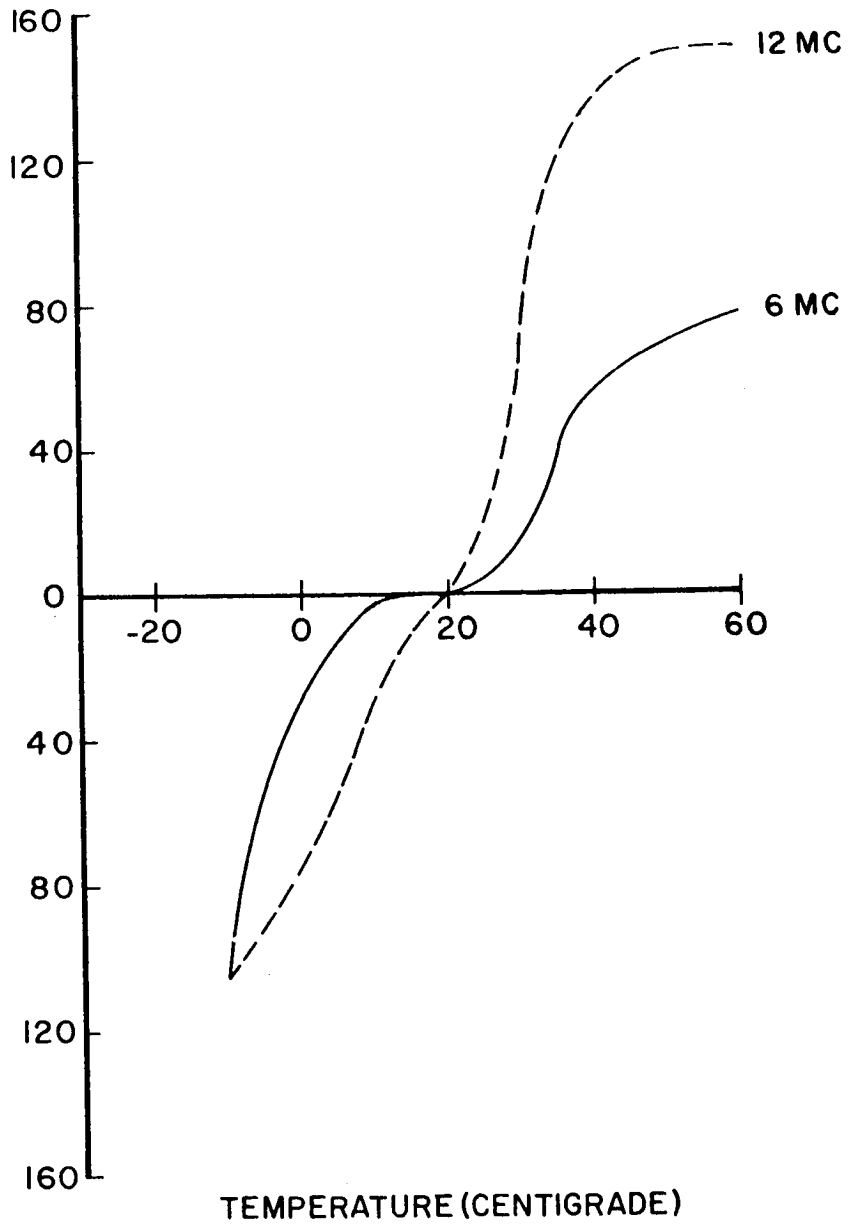

MOTHER PAYLOAD RECEIVER PHASE CHANGE RELATIVE TO 73.6 MC VS. TEMPERATURE

FIGURE 3.1

Loop antennas were chosen because of their reduced mechanical complexity and because they were insensitive to phase shifts and detuning resulting from the changing dielectric constant of the ionosphere. However, calculations showed that adequate power could be received using transmitter powers less than one watt.

B. Transmitting Antenna System

Linearly polarized loop antennas were required for the transmitted 6 Mc and 12 Mc signals. In addition to the advantages discussed for loop antennas for this application for the receiving antennas, an important advantage was that since the loop antenna Q remained high out to large departures of the refractive index from unity the current from which the distant field depended remained sinusoidal. This was important because the nonlinearity in the antenna system, which was dependent upon the ionospheric refractive index, could have caused a phase shift between the transmitted 6 and 12 Mc components. These components were, however, dependent upon the electron density which the experiment was designed to measure.

The antenna matching circuit for the 6 Mc and 12 Mc signals is shown in Figure 3.2. At the end of the transmitters the 6 Mc and 12 Mc signals were diplexed through phasing and trapping circuits onto the single linearly polarized loop antenna composed of a metal braid and the Daughter nosecone locking ring. This single antenna caused no diplexing problems with the 73.6 Mc signal because the frequencies were so different.

Two 1:1 isolation transformers were used for the balanced to unbalanced transformation. Both transformers were necessary to

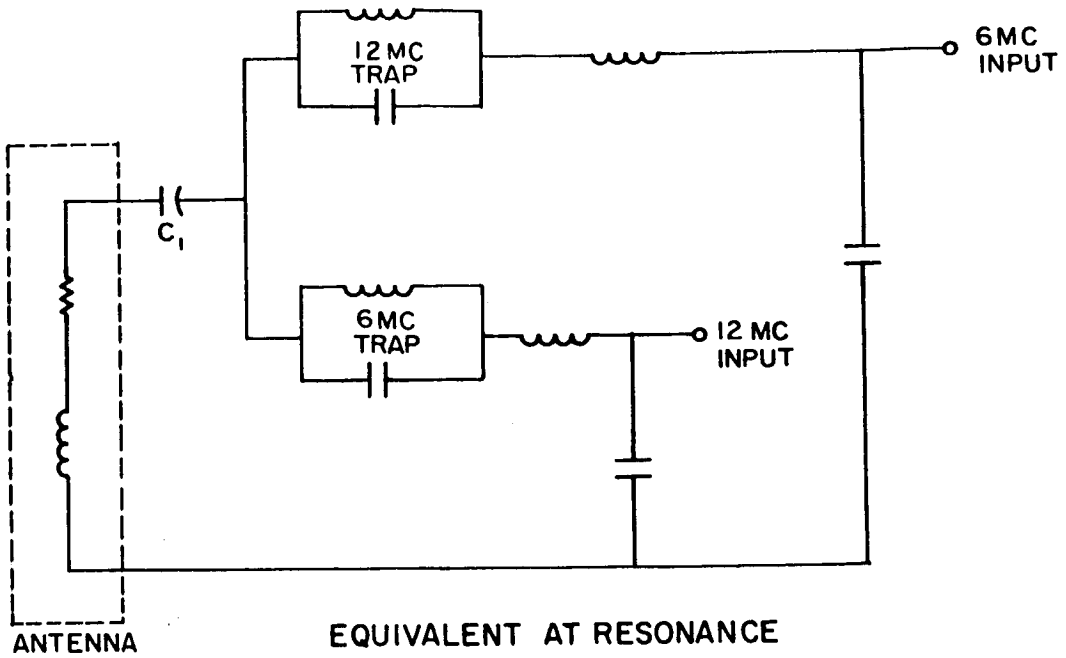

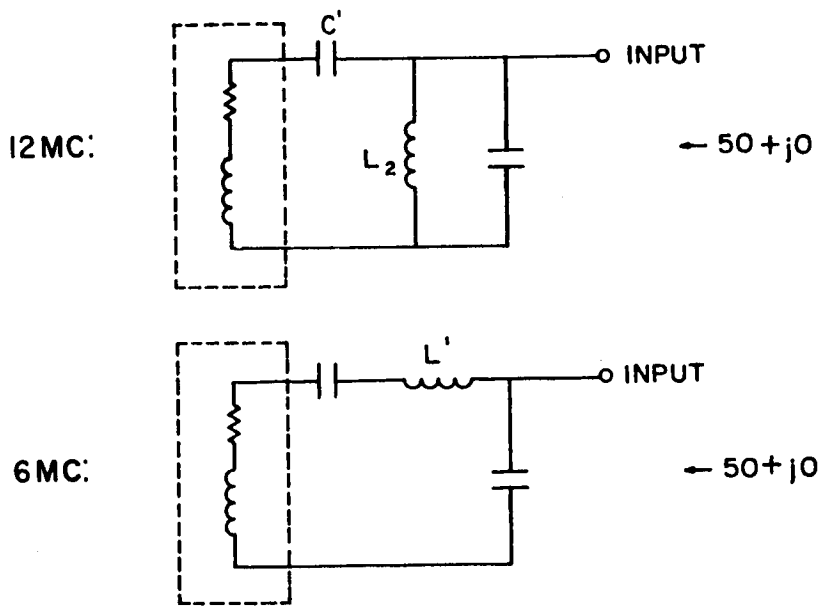

6MC AND 12MC ANTENNA MATCHING UNITS

FIGURE 3.2

avoid using a broad band transformer which was not as efficient as a transformer designed for a specific frequency. The circular ring in the top leg of the loop which was necessary for payload separation, prevented the balanced to unbalanced transformation by coaxial techniques. A 50Ω resistive impedance as shown in Figure 3.2 was present at the transmitter's input terminals.

Four loops in a phased array formed the 75.6 Mc transmitting antenna. A three db elliptical polarization which was used for SSD tracking and vehicle spin rate determination on the AGC records, was achieved by feeding the 73.6 Mc transmitter output through an impedance matching-phase shifting circuit. Polarization was obtained by the proper phasing of two equal amplitude signals. Using this method it was easier to adjust the phasing and ellipticity of the signals. Figure 3.3 shows the equivalent circuit of the antenna matching unit and the impedances presented to the transmitter input. The same $\lambda/8$ matching networks described here were also used on the receiving antennas. Since the antennas were detuned when the Mother and Daughter payload were assembled together, the transmitter was designed to be able to operate into the mismatched impedances without damage. Nearly zero phase angle impedance matching between the antennas and the receivers and transmitters was maintained over the range of normal operation.

The entire transmitting and receiving systems as they appeared in the Mother and Daughter capsules is seen in Figure 3.4. Table 3.1 summarizes important parameters of both the receiving and transmitting antennas.

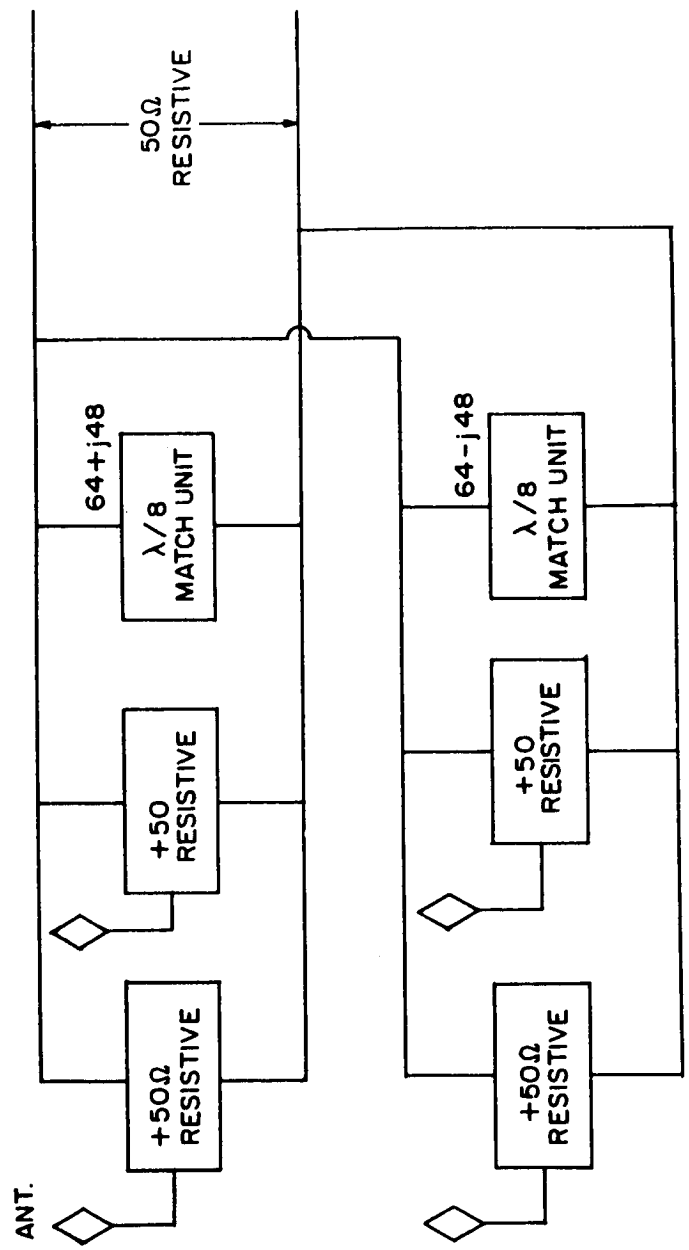

73.6 MC TRANSMITTING AND RECEIVING ANTENNA MATCHING UNIT

FIGURE 3.3

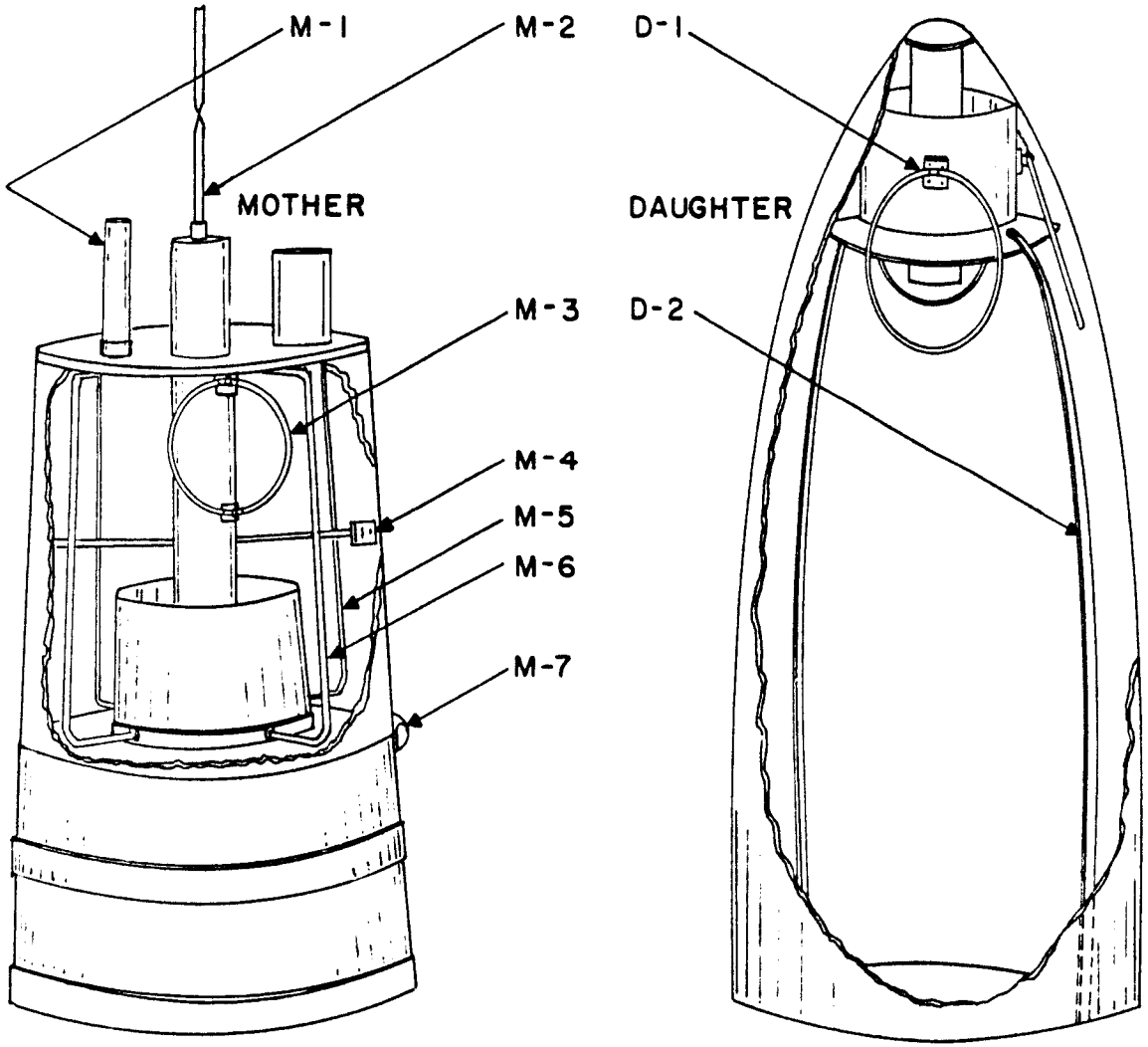

MOTHER

M-1 MAGNETOMETER
M-2 VELOCITY TAPE
M-3 73 MC RECEIVER
M-4 240 MC TELEMETRY TRANSMITTER ANT.
M-5 } 6 MC RECEIVER ANT.
M-6 } 12 MC RECEIVER ANT.
M-7 SOLAR ASPECT SENSOR

DAUGHTER

D-1 73 MC TRANSMITTER ANT.
D-2 6MC-12MC TRANSMITTER ANT.

MOTHER DAUGHTER ANTENNA SYSTEMS
FIGURE 3.4

C. Noise Considerations

From a study of the galactic noise of the upper ionosphere, noise bandwidth, receiver noise, and predicted signal to noise ratios, it was possible to calculate signal strengths needed from the transmitting loop antennas. Table 3.2 is a partial summary of these noises investigated by Nisbet (1961) and Cantrell (1964).

D. Transmitter Power Design

Transmitter power and bandwidth requirements were probably two of the most important considerations controlling the design of the experiment. Considerations to the maximum separation distance between the transmitting Daughter and receiving Mother sections, anticipated noise levels, antenna performance, and payload weight restriction determined these powers.

System calculations were based on the following equations for loop antennas:

$$E = \frac{120\,\pi^2}{d} N \frac{A}{\lambda^2} I_o \cos\theta \qquad (3.2)$$

$$V = 2EN \frac{A_R}{\lambda} \cos\theta \qquad (3.3)$$

$$\frac{P_T}{P_R} = \frac{1}{14400} \frac{R_T R_R}{A_T A_R^2} \frac{d^2 \lambda^6}{\pi^6} \qquad (3.4)$$

where E = field strength

d = distance

N = number of turns in loop

A_T = area of transmitting loop

Table 3.1

Receiving and Transmitting Antenna Parameters

Frequency	Mc	6.13333	12.26666	73.6
Transmitting loop area	$A_T(m^2)$	0.266	0.266	0.0187
Receiving loop area	$A_R(m^2)$	0.159	0.159	0.0187
Transmitting loop resistance	$R_T(\Omega)$	1.5	2.8	2.9
Receiving loop resistance	$R_R(\Omega)$	1.7	3.2	2.9
Number of turns in loop	N	1	1	1
Antenna polarization loss	db	3	3	3

Table 3.2

Noises Considered in the Mother-Daughter Experiment

Channel Frequency	Receiver Noise Figure (db)	Noise Bandwidth (Kc)	Noise Power (dbm)	Cosmic Noise Power (dbm)	Total Noise Power (dbm)	S/N Required at Receiver (db)
6.13 Mc	4	1.86	-137.3	-137.4	-134.3	20
12.26 Mc	4	3.72	-134.3	-142.8	-133.7	20
73.6 Mc	4	22.3	-130.5	-131.3	-127.9	20

A_R = area of receiving loop

λ = wavelength

I_o = loop current

θ = angle with respect to plane of loop

P_T = transmitter power

P_R = power delivered to receiver terminal

V = voltage induced into receiving loop

R_T = total series resistance of transmitting loop, sum of loss and radiation resistance

R_R = total series resistance of receiving loop, sum of loss and radiation resistance

A typical transmitter power requirement calculation is presented for the maximum expected separation distance of 5 km. The calculation made with equations (3.2), (3.3), and (3.4) are seen in Table 3.3.

Below is a summary of a signal strength test evaluation for the Mother-Daughter 8.29 payload. This shows the output voltage into the matched 50 ohm resistive load for a given input signal level.

System	Field Strength at 5 km	Signal Input
6.13333 Mc	8 μv/m	0.164 μv
12.26666 Mc	1.07 μv/m	0.044 μv
73.6 Mc	84 μv/m	2.37 μv

A complete evaluation of the signal strengths was made when the Mother and Daughter were separated by 20 meters in two ground towers. Figure 3.5 shows the results when extrapolated through the entire range of expected Mother-Daughter separation distances.

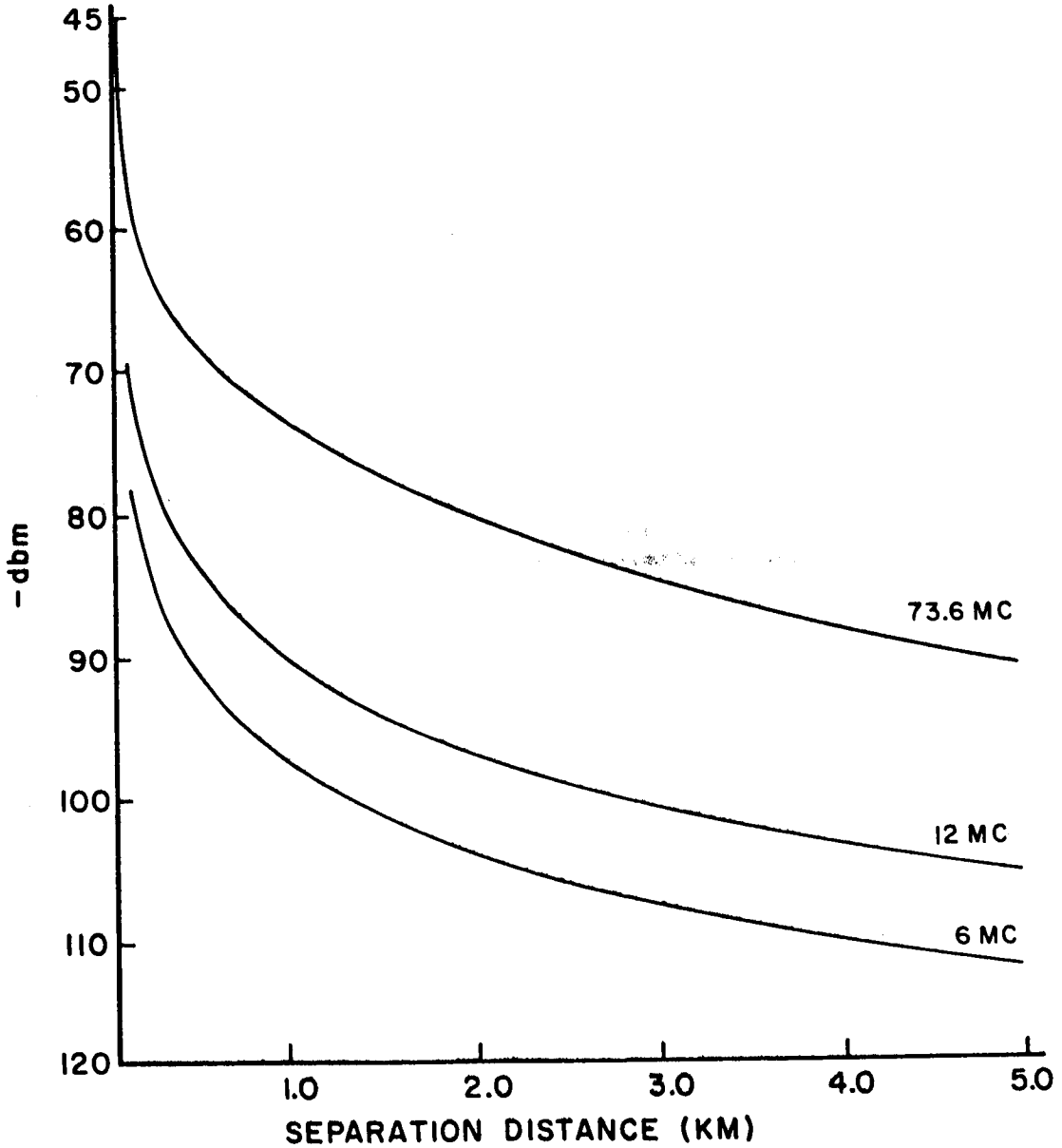

FIELD TEST SIGNAL STRENGTH EVALUATION

FIGURE 3.5

Table 3.3

Transmitter Power Requirement Calculations

Frequency	Mc	6.13333	12.26666	73.6
Distance (maximum)	Meters	5000	5000	5000
Transmitting loop area	$A_T(m^2)$	0.266	0.266	0.0187
Receiving loop area	$A_R(m^2)$	0.159	0.159	0.0187
Transmitter loop resistance	$R_T(\Omega)$	1.5	2.8	2.9
Receiver loop resistance	$R_R(\Omega)$	1.7	3.2	2.9
Number of turns in loop	N	1	1	1
Angle with respect to plane of loop	0	0	0	0
Antenna polarization loss	db	3	3	3
Total path loss from transmitter to receiver	$\frac{P_T}{P_R}$ (dbm)	138.5	125.9	120.5
Noise bandwidth	B (Kc)	1.86	3.72	22.3
Receiver noise figure	F (db)	4	4	4
Receiver noise power	dbm	-137.3	-134.3	-130.5
Cosmic noise power	dbm	-137.4	-142.8	-131.3
Total noise power	dbm	-134.3	-133.7	-127.9
Required S/N at receiver	db	20	20	20
Required power at receiver (minimum)	dbm	-114.3	-113.7	-107.9
Minimum transmitter power $[(P_T/P_R)-P_{min}]$	dbm	24.2	12.2	12.6
Minimum transmitter power	milliwatts	260	16.6	18.2
Designed transmitter power	millivolts	600	30	1000

Attenuation due to the ionosphere has not been accounted for in these graphs.

E. Receiver and Transmitter Units

The TRF receiver circuit design has been described in detail by Space Craft - Cantrell (1964), especially those aspects concerned with the actual electronics.

Holding the signal input to the phase-comparator at relatively constant amplitude was an AGC system incorporated in each receiver. The AGC voltage, which measured the receiver input signal amplitude, was also telemetered to ground receivers to provide a record of the signal strength of the three channels and a measurement of the relative spin rate between the separating Mother and Daughter sections. Sensitivities of the 6 Mc, 12 Mc, and 73.6 Mc sections were -120 dbm, -110 dbm, and -90 dbm, respectively.

The Daughter's transmitter, which provided the coherent 6.13333, 12.26666, and 73.6 Mc signals, is seen in the block diagram of Figure 3.6. A basic frequency of 6.13333 Mc was derived from a stable oscillator provided by the Manson Company. This crystal controlled source was housed in a vacuum-type dewar with thermal control achieved by a thermostatic heater wire. Stability was 2 parts in 10^9. The output frequency was then amplified and multiplied to produce the desired power levels at all three frequencies.

3.2.4 Phase Comparator Design

This phase comparator resolution required for the experiment was determined largely by the magnitude of the phase shifts introduced

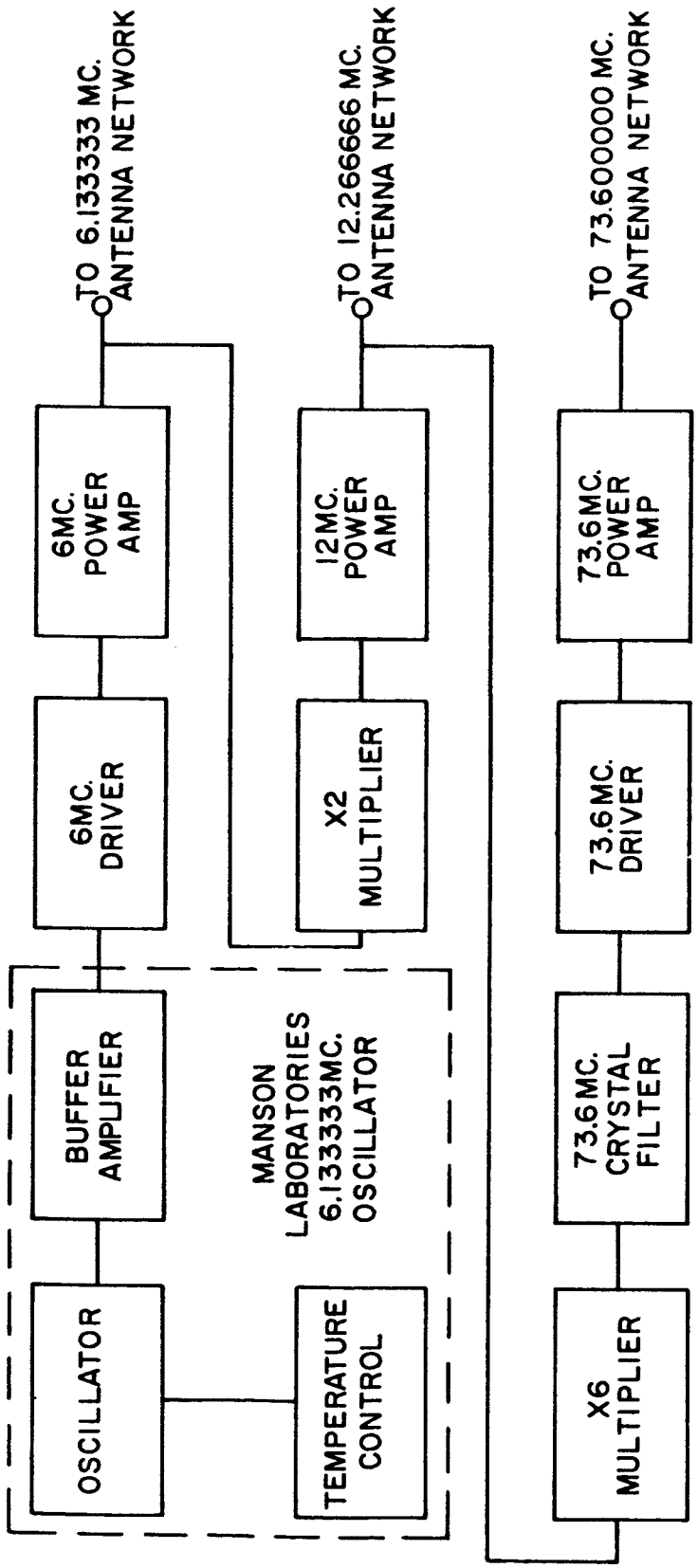

BLOCK DIAGRAM

DAUGHTER TRANSMITTER

FIGURE 3.6

in the antenna matching units and the receivers. A vector rectifier unit for phase comparison with the required $\pm 5^{o}$ resolution was designed by Fisher of Space Craft, Inc. and described in detail by Froehlich (1964).

The diode bridge type comparator gave an output proportional to the cosine of the angular phase difference between the two input signals summed by the vector difference rectifier. However, the resolution in the region of 90^{o} phase shift was poor and the direction of phase change was ambiguous for deployment of only one comparator. Since increasing and decreasing phase angles were expected in the ionospheric experiment, the ambiguity was resolved by using two similar phase comparator circuits and by the introduction of a 90^{o} phase shift between the reference voltages applied to their diode bridges. This was accomplished by simply detuning the output feeding the bridges to provide a 45^{o} phase shift in each channel for a resultant total phase shift of 90^{o}. In this way one comparator was always operating in a region of maximum sensitivity with the least sensitivity of the combination occurring at 45^{o}. The second comparator also eliminated the ambiguity of the direction of phase change.

Figure 3.7 shows the complete phase comparator circuit. The required phase shift for quadrature outputs was developed by achieving the $\pm 45^{o}$ displacement with two separate RL and RC branches.

There were four main sources of error in the phase comparator according to Froehlich. He found that if the ratio of the input voltages was maintained greater than 6, a sinusoidal output could be assumed to obtain the desired phase measurement within $\pm 5^{o}$. For values of

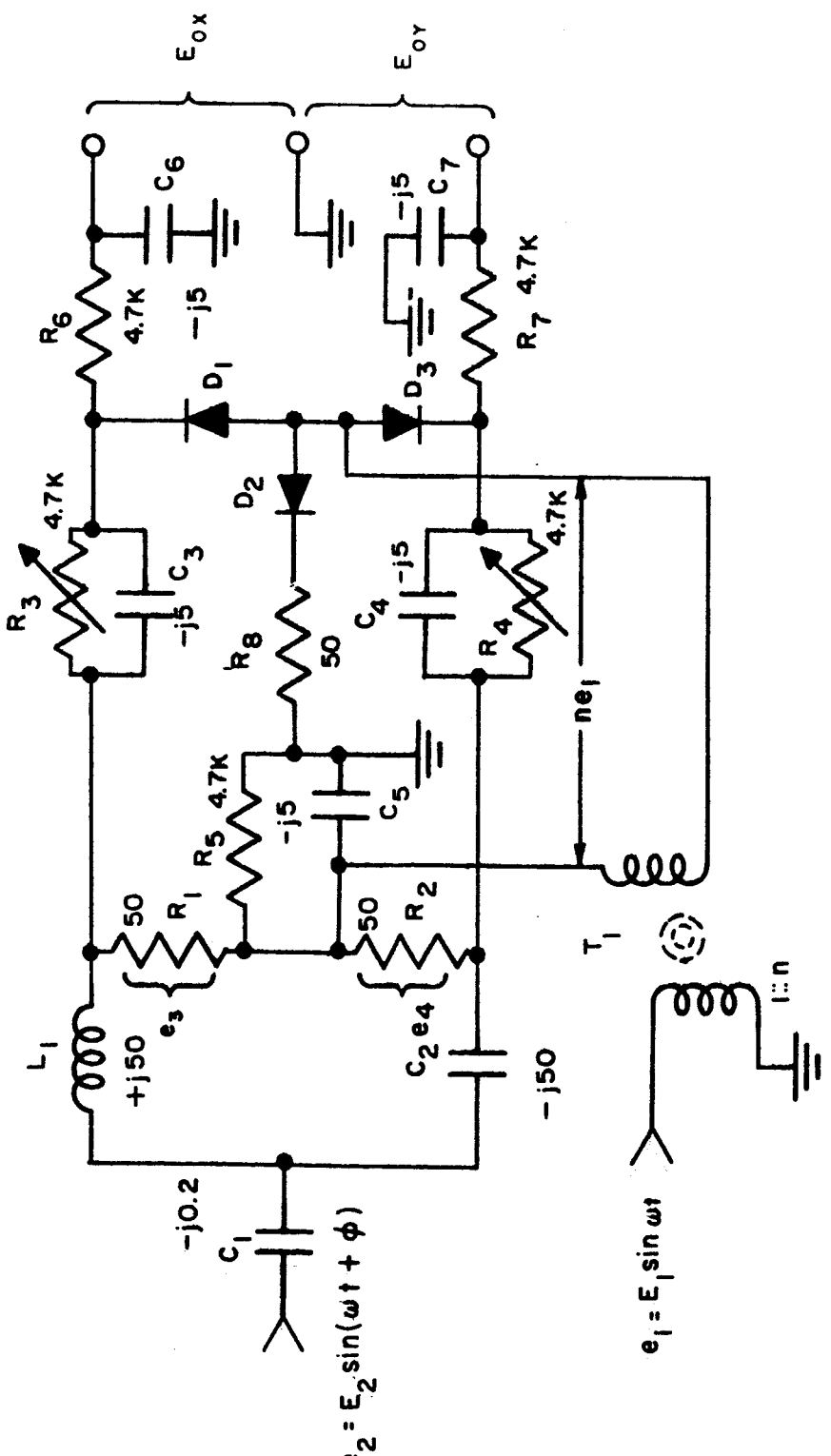

PHASE COMPARATOR CIRCUIT

FIGURE 3.7

the ratio less than 6, error from this source was minimized by using the appropriate calibration curve for the phase angle measurement. Secondly, Froehlich showed that considerable error could have been introduced by incorrect alignment of the phase shifters if a division process were used to determine ϕ. The division did not reduce the error caused by a fluctuation in the input provided the ratio was maintained above 6 and the phase splitting network was properly aligned. Temperature fluctuations and resultant detuning of the inductors in the bridge constituted the third source of error. Phase shifts introduced resulted in deviations from quadrature. A 20 percent deviation between parameters was estimated to correspond to a phase error of 6.4°. The error, however, was calculable with an occurrence of several cycles of phase change. The fourth source of error was the noise present in the comparator. Noise generated in the resistive elements and shot noise was, however, negligible.

The actual errors encountered in the M-D Flight 8.29 phase comparator under test were, however, different from those described above. Dependence of relative phase shift under temperature fluctuations is seen in the receiver test calibrations of Figure 5.21. The fluctuation in signal strength was also a source of phase error. Figure 5.18 shows that variation of the AGC voltage due to fluctuation in signal strength. Figure 5.19 shows how this fluctuation is directly related to induced phase shifts.

Preflight calibrations of the phase comparator were made using a calibrated 10 db attenuator into a 73.6 Mc reference

transmitting test loop and a discrete 30^{o} phase shifting network. Thus, it was possible to vary the power and phase within the Mother's receivers. Difficulty in these calibrations was principally caused by loss of phase resolution for small reference voltages. Figure 3.8 shows how the error increases for smaller reference voltages. In the actual flight these calibration curves were unusable because of the superimposed relative spin phases.

3.2.5 Separation Velocity Design

The separation velocity of the Mother and Daughter capsules was measured at separation time with a 15 foot fiberglass tape painted with conductive stripes equally spaced every 1.5 inches and folded in an accordian fashion in the Mother. The loose end was fed between a pair of metallic contacts connected through signal conditioning circuits to telemetry and attached to the Daughter. As the Mother and Daughter separated the tape slid through the contacts, caused momentary shorting, and thereby superimposed pulses on a telemetry channel. A typical output of the device is presented in a later figure (Figure 5.4). The rate of change of the spacing of the pulses determined the initial acceleration imparted by the separation spring. The spacing of pulses gave the constant separation speed of the two bodies.

The accuracy of the device was critical. Preflight and flight data showed separation speed measurements were obtainable to within ±0.106%.

3.2.6 Magnetometer Design

A magnetometer-Schonstedt type RAM-5A was mounted on

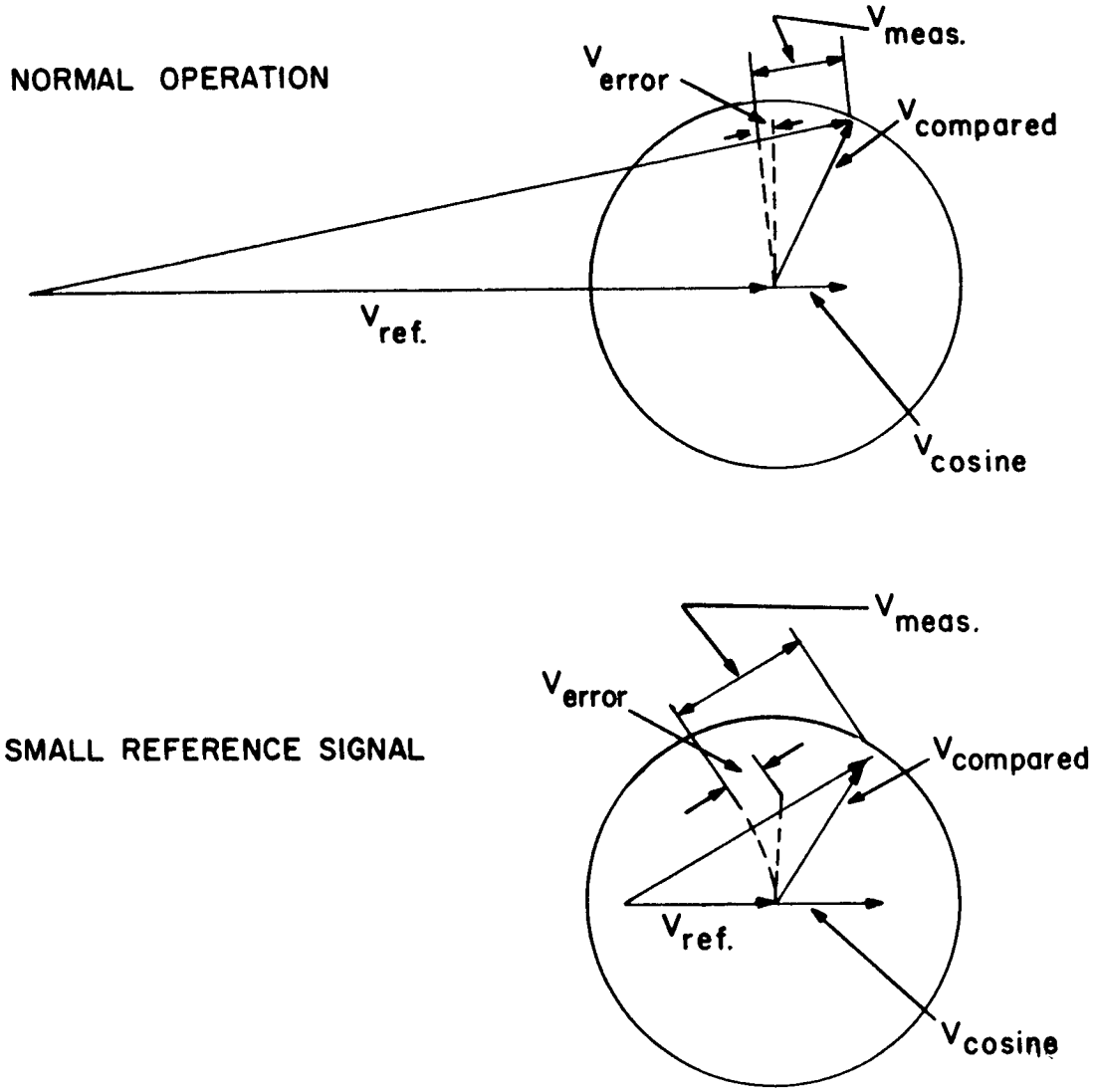

PHASE DETECTOR VECTOR DIAGRAM

FIGURE 3.8

the Mother payload to obtain continuous measurements of the longitudinal component of the earth's magnetic field. The device was aligned along the axis of the Mother payload which was also the direction of propagation. From field measurements by the magnetometer, it was then possible to determine the angle of propagation with respect to the theoretical total magnetic field vector. Payload spin rate was also measurable from fluctuations about the output voltage level of the device. The accuracy of the magnetometer was 1 milligauss in 500. A portion of the output is seen in Figure 5.6A.

3.2.7 Solar Aspect Design

For Javelin 8.29 a solar aspect sensor was employed to determine both payload attitude and payload spin rate. The pulse width output of the device exhibited in Figure 5.6B was proportional to the payload attitude with respect to the sun. Time between the pulses determined the spin rate and the width of the pulse enabled a determination of the attitude.

A silicon photodiode was used as the sensor. It was mounted at the center of a carefully designed shield. The shape of this shield was such that the length of time the photodiode was illuminated during any one rotation was dependent upon the angle between the sun and the axis of the rocket. Figure 3.9 shows the design of the device.

3.2.8 Telemetry System Design

The telemetry system which was used to relay the Mother-Daughter experimental data operated at 240.2 Mc and was a 2 watt

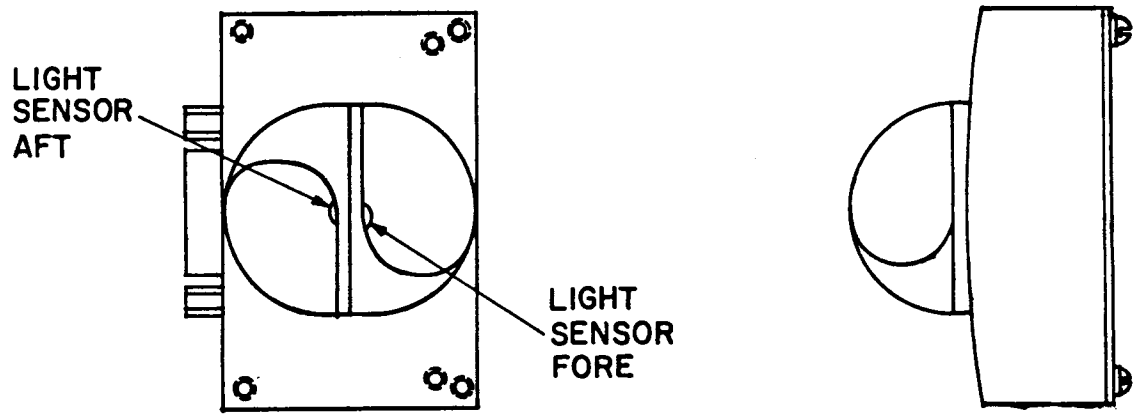

ASSEMBLY ASPECT SENSOR

MOTHER DAUGHTER

FIGURE 3.9

PM type, vector Model No. TRPT-2W. Detail on the circuitry is provided by Cantrell (1964). All the information in the form of voltages was fed into the transmitter from twelve frequency-modulated subcarrier oscillators. Channel assignments were made according to anticipated data sequence and rate. The channels and functions are tabulated in Table 3.4.

Table 3.4

Telemetry Channel Assignment

TM Channel	Subcarrier Frequency (Cps)	Function and Description
5	1,300	Magnetometer
6	1,700	6 Mc AGC
7	2,300	12 Mc AGC
8	3,000	73.6 Mc AGC
9	3,900	6 Mc phase 1
10	5,400	6 Mc phase 2
11	7,350	12 Mc phase 1
12	10,500	12 Mc phase 2
13	14,500	Ion Current
14	22,000	Electron Temperature
15	30,000	Commutator
D	52,500	Vibration before Separation
		Separation Position and Velocity during Separation
		Optical Aspect after Separation

CHAPTER IV

Data Reduction Procedure

4.1 Complete Expressions for Refractive Indices

Dependence of the ionospheric phases on the indices of refraction was given in Chapter II as:

$$\Delta\Phi = \frac{\omega_2}{c} (\mu_2 - \mu_1) V_{MD} t \tag{4.1}$$

For the ordinary and extraordinary modes of the three propagation frequencies, the complete form of the Appleton-Hartree equation was used:

$$\mu^2 = 1 - \frac{X}{1 - jZ - \frac{Y_T^2}{2(1-X-jZ)} \pm \left[Y_L^2 + \frac{Y_T^4}{4(1-X-jZ)^2} \right]^{\frac{1}{2}}} \tag{4.2}$$

For this analysis of the F region it was justified as is shown in Appendix B to assume $Z = \nu_e/\omega \doteq 0$. A computer program devised by T. A. Seliga was slightly modified to make these computations of μ. The input parameters to this program were electron density, total magnetic field, and angle of propagation with respect to this field vector.

A solution of equation (4.2) required a knowledge of both the longitudinal and transverse components of the magnetic field. The effect of the longitudinal component predominates; and it was measured in flight using an axially mounted payload magnetometer described in Chapter III. The total field B_T and longitudinal component B_L were related by the propagation angle θ:

$$B_L = B_T \cos \theta$$
$$\theta = \cos^{-1} B_L/B_T \qquad (4.3)$$

The theoretical total field values were calculated along the trajectory using a digital computer program furnished by J. R. Doupnik. Latitude, longitude and altitude were the input parameters for this essentially inverse cube calculation best fitted to actual data described by Hendricks and Cain (1966).

By comparison with theoretical field values and B_L the vehicle attitude could be determined and checked for consistency with trajectory parameters available from other sources as radar tracking. The expression for the attitude is obtained from equation (4.3):

$$\theta' = \Delta B_L/B_T \sin \theta \qquad (4.4)$$

Propagation frequencies specified for the main program were the 73.6000 Mc, 12.26667 Mc, and 6.13333 Mc signals. It was thus possible to calculate the phase shift divided by the separation distance as a function of the electron density. In this way when the experiment was analyzed it was possible to calculate the electron densities from the observed phase shifts. This procedure is discussed in the following section.

4.2 Calculation of the Curve for Reducing Phase Measurements to Electron Densities

Equation (2.7) may be re-expressed as:

$$\frac{\Phi}{V_{MD}t} = \frac{\omega_2}{c}(\mu_2 - \mu_1) \qquad (4.5)$$

With the experimental value of ω_2 and c equation (4.5) reduces to:

$$\frac{\Phi}{S_{MD}} = 1.541(\mu_2 - \mu_1) \qquad (4.6)$$

Thus, the ratio on the left side of equation (4.6) which was measured at each instant of time during the experiment, was essentially the difference between the refractive indices of the extraordinary mode of the 73.6 Mc signal and the indices of the extraordinary mode of the 6 Mc or the ordinary mode of the 12 Mc signal. To simplify the final computation of electron densities from measured phase shifts and calculated separation distances the curves of the type shown in Figure 4.1 were developed.

Using the digital computer values of phase shift divided by separation distance were then calculated for thirty suitable chosen electron densities between 10^9 and 10^{12} electrons meter^{-3} for a number of values of the longitudinal magnetic field B_L, the angle θ between the propagation direction, and the magnetic field vector B_T. Using these thirty sets of calculations, the actual electron density could be found by numerical interpolation for the actual electron densities observed in the flight.

When actual flight data was reduced to electron densities, it was only necessary to calculate Φ/S_{MD} from phase data and apply the correct reduction curve upon specifying the propagation angle and total field. Using actual payload trajectory data separation velocity

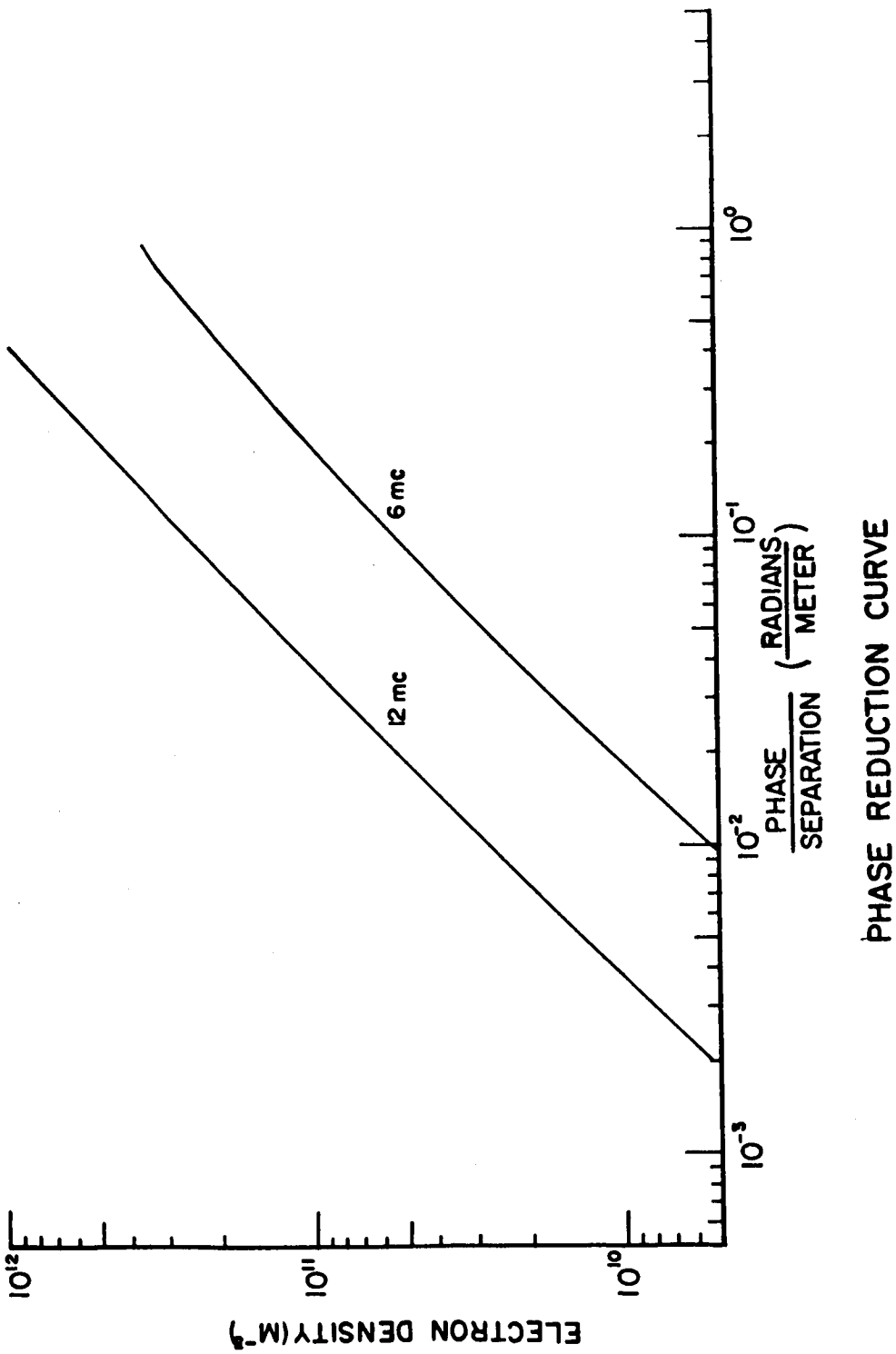

PHASE REDUCTION CURVE

FIGURE 4.1

measurements, range time, and the measured values of the longitudinal component of the magnetic field, the electron density profiles could be calculated. Figure 4.1 shows then a typical curve for reducing phase measurements to electron densities.

CHAPTER V

Experimental Results of Mother-Daughter Javelin 8.29 Flight

5.1 General Background

A Mother-Daughter payload, Javelin 8.29, was designed, developed, and tested to perform all of the previously mentioned functions within the allowable tolerances. A four stage rocket was successfully launched from Wallops Island on May 19, 1965 at 20 hours 11 minutes 00 seconds zebra time. Payload trajectory was nominal and the final parameters are shown in Figures 5.1 and 5.2.

Telemetered data was received continuously from launch until re-entry. Phase data was obtained from the time of Mother-Daughter separation at an altitude of 266 km to 968 seconds at which time the altitude was 350 km. The 73.6 Mc receiver sensitivity was lower than nominal during an early portion of flight time; however, this did not compromise the analysis of the results of the phase measurements. Figure 5.3 shows an actual section of the telemetry recording of the four phase channels.

The ionospheric phase shift was obtained by subtracting the effect of the relative spin between the Mother and Daughter sections of the payload as well as minor phase shifts dependent upon signal strength fluctuations and receiver temperature variations.

5.2 Telemetered Data

5.2.1 Separation Velocity

The separation velocity between Mother and Daughter sections

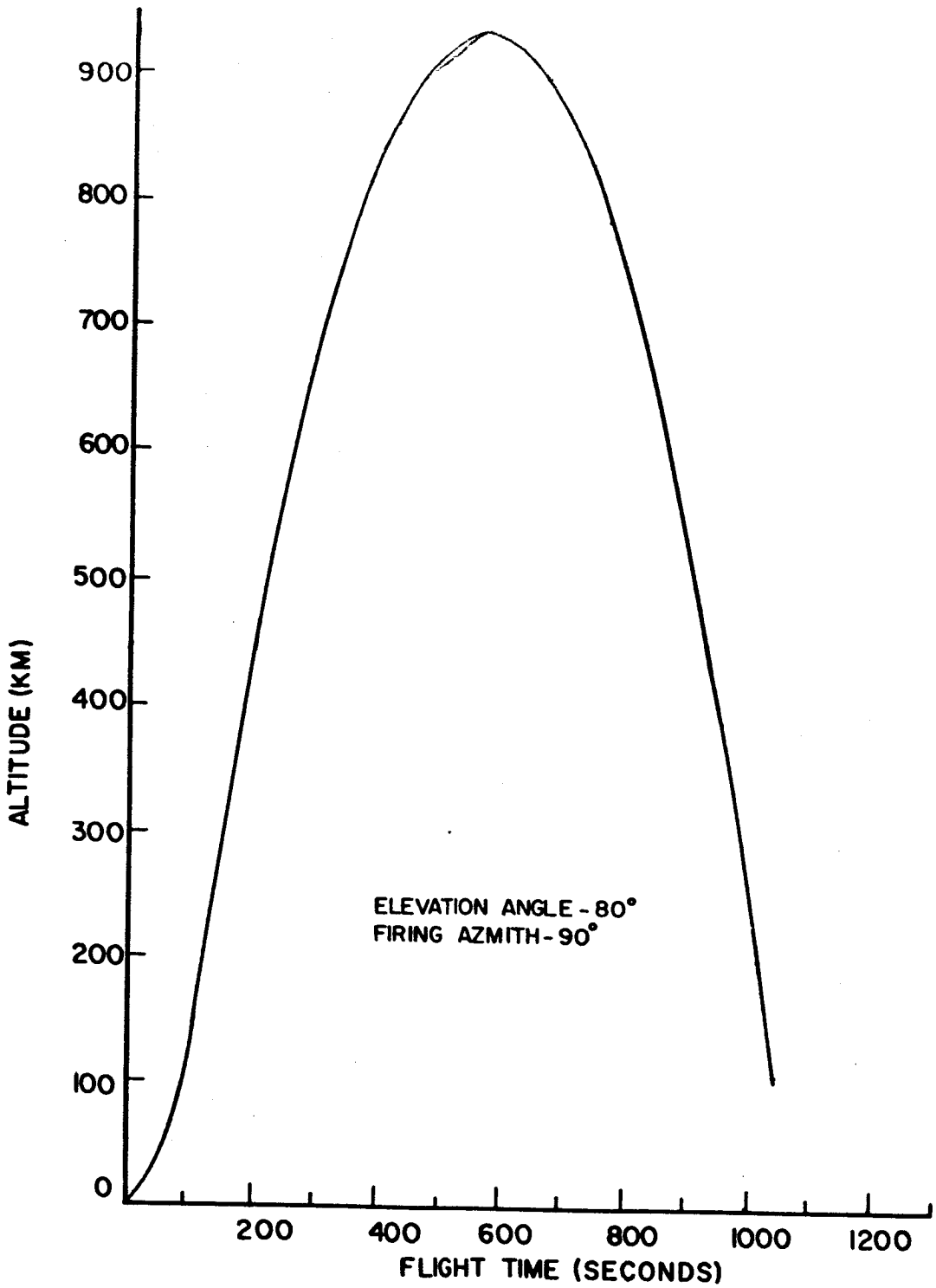

TRAJECTORY NASA JAVELIN 829

FIGURE 5.1

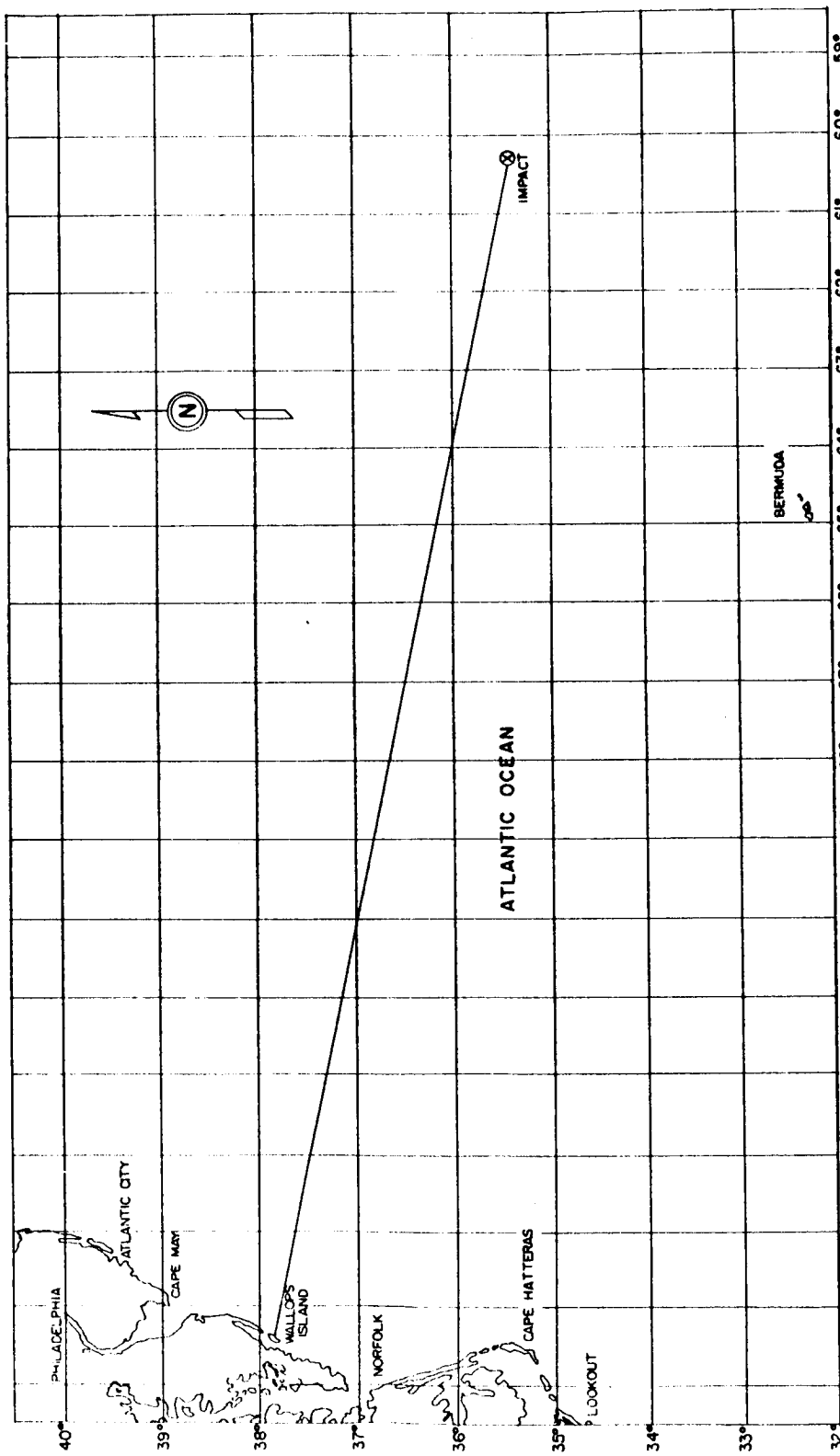

WALLOPS ISLAND ROCKET RANGE
JAVELIN 8.29 (5-19-65) HORIZONTAL FLIGHT PATH
FIGURE 5.2

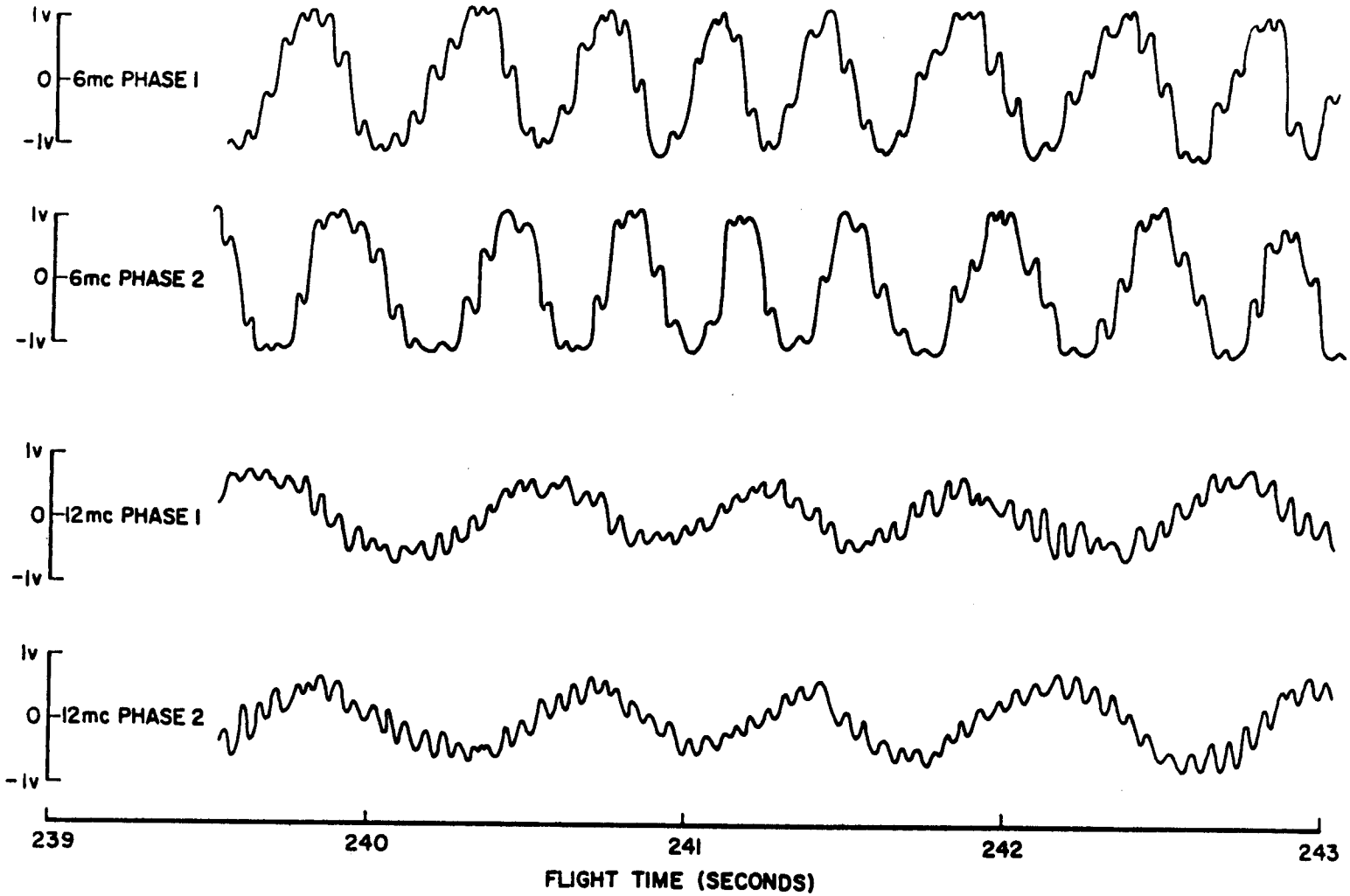

TELEMETRY RECORD OF PHASE DATA

FIGURE 5.3

was measured from time spaced telemetered voltage spikes on commutator channel 15. The circuit operation has been described in Chapter III. A typical section of the output waveform was traced for Figure 5.4. Not only the total separation velocity was determined, but the record was examined for evidence of relative nutation of the two bodies. No evidence of relative nutation was observed, and a value of 5.3397 ± 0.0057 meters/seconds was measured. The separation distance as a function of time is shown in Figure 5.5.

5.2.2 Magnetometer

Signal channel 5 was assigned the function of recording the output voltages of the magnetometer. Figure 5.6A shows the output of the magnetometer before and after payload separation. In the closed configuration when the Mother and Daughter were together, the force of the separation spring produced a distortion in the Mother payload. This distortion caused the axis of the magnetometer and the Mother axis to diverge less than 2.5 degrees. The modulation shown prior to separation was a result of the changing orientation of the magnetometer to the earth's magnetic field. Vehicle rotation was responsible for the changing orientation of this offset magnetometer. For this flight the vehicle nutation was less than 5 degrees in the open and closed configurations.

The voltage levels from the output of the magnetometer were reduced to field readings with the aid of the calibration curve of Figure 5.7. The expression of the longitudinal component of the field along the trajectory is seen in Figure 5.8.

Payload spin rate was easily determined from the small

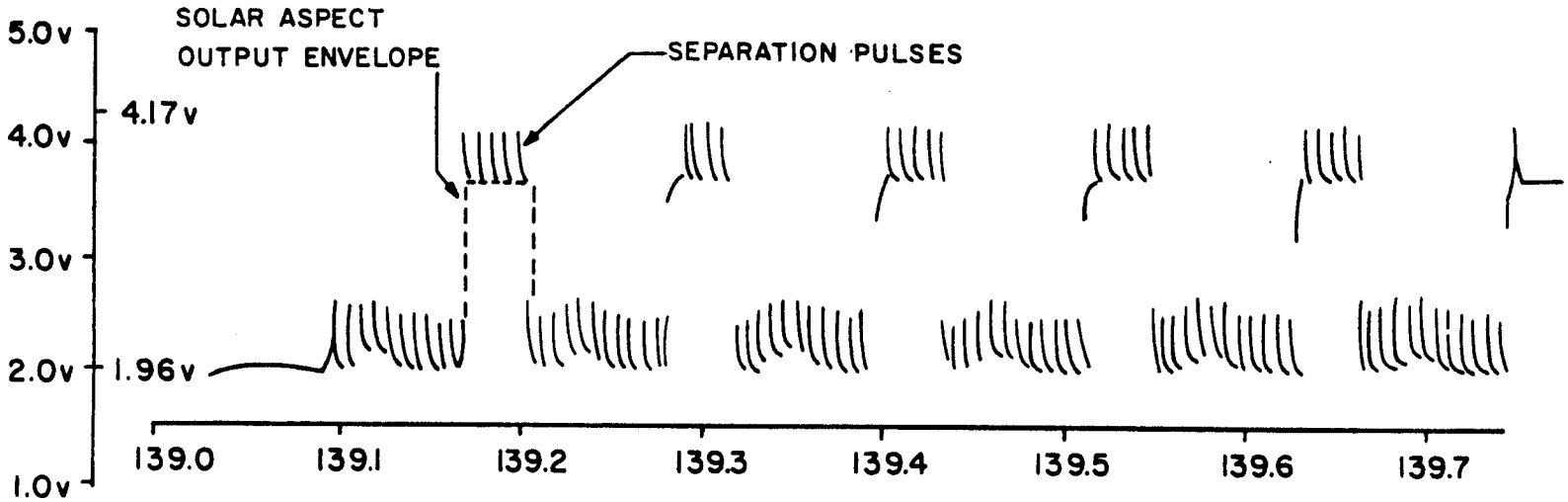

SEPARATION VELOCITY OUTPUT

FIGURE 5.4

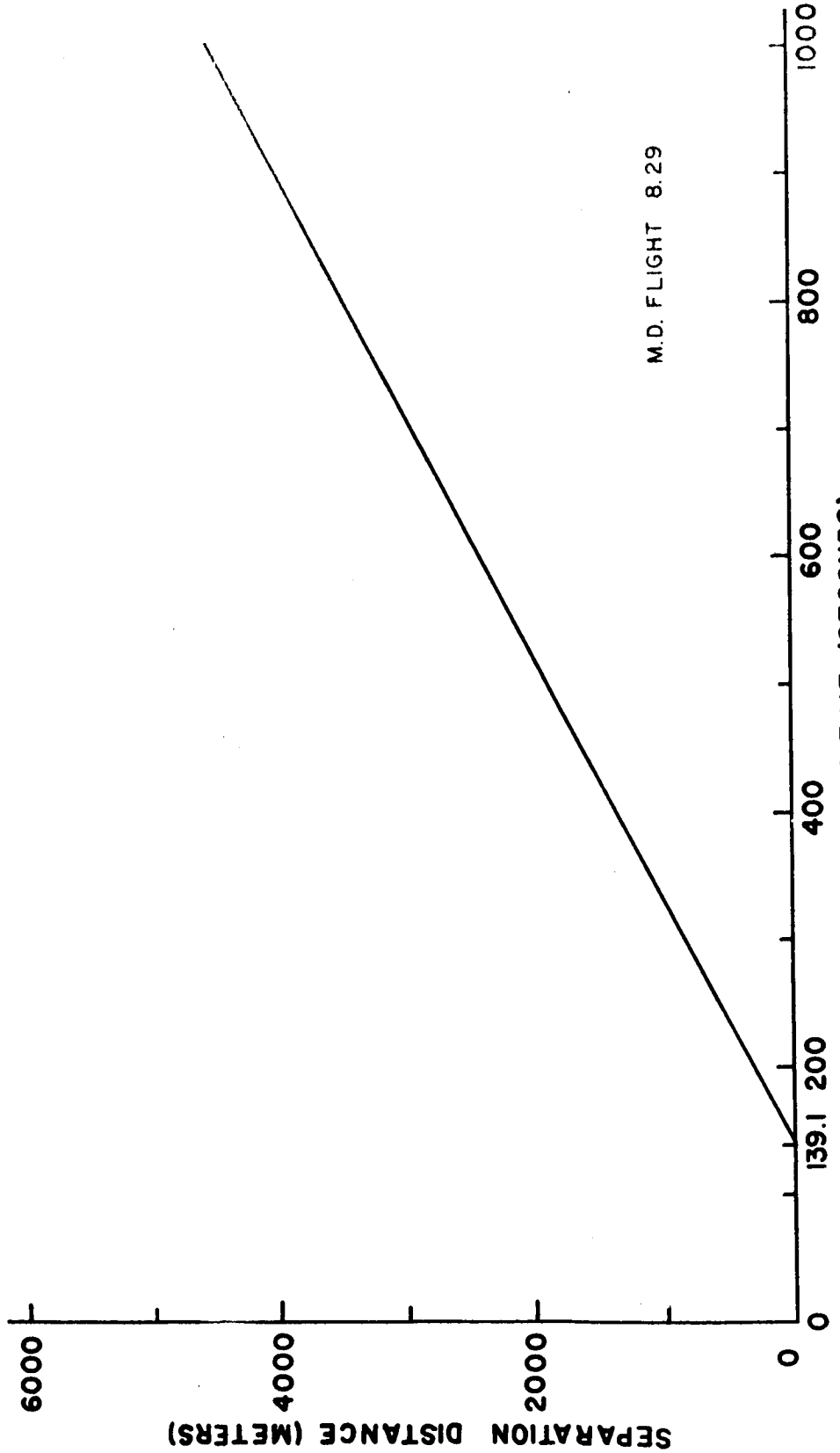

MOTHER DAUGHTER SEPARATION DISTANCE

FIGURE 5.5

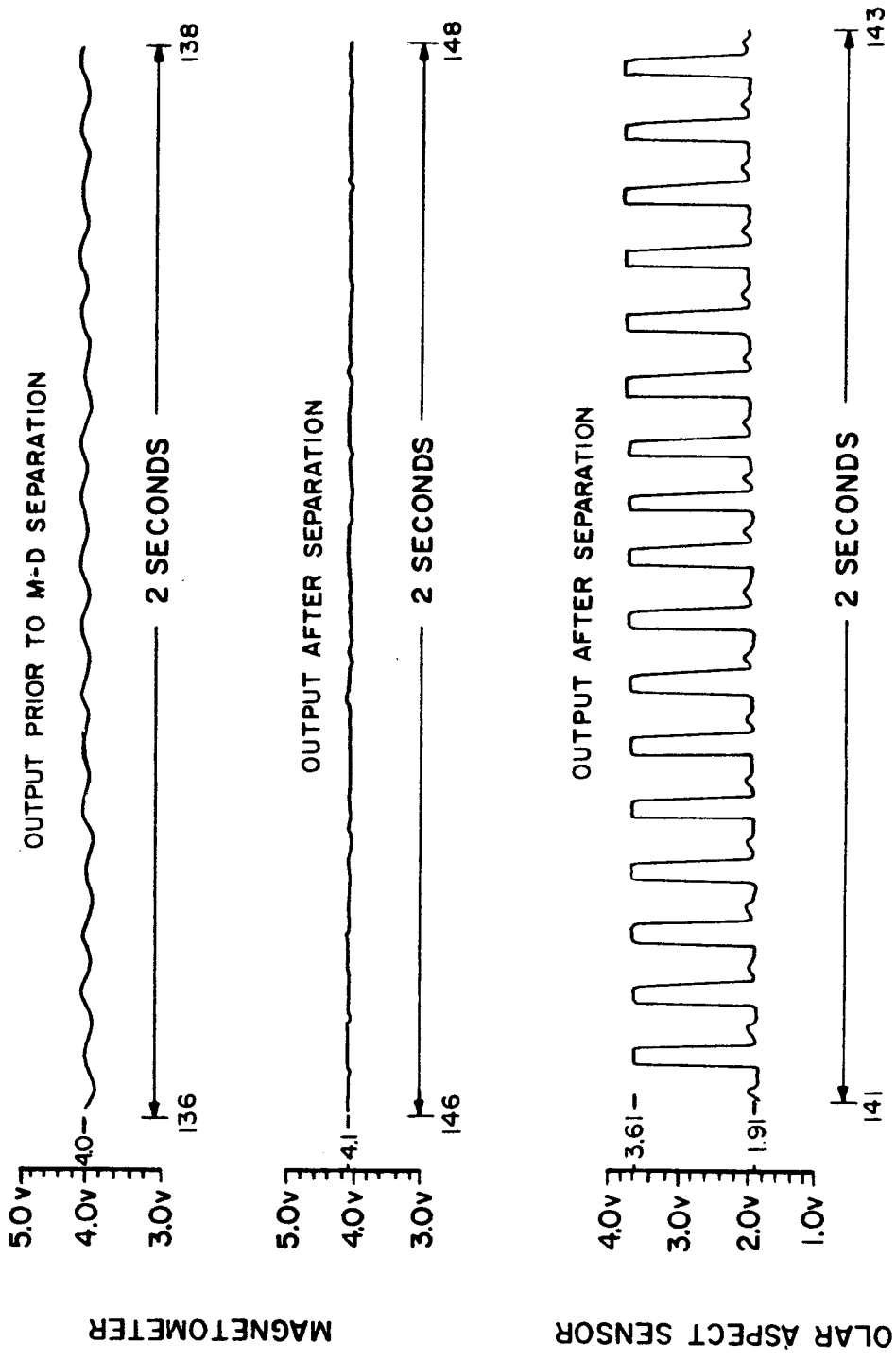
MAGNETOMETER
OUTPUT PRIOR TO M-D SEPARATION
5.0v
4.0v
3.0v
4.0
136
2 SECONDS
138
OUTPUT AFTER SEPARATION
4.1
146
148
SOLAR ASPECT SENSOR
OUTPUT AFTER SEPARATION
4.0v
3.0v
2.0v
1.0v
3.61
1.91
141
143
FLIGHT TIME

FIGURE 5.6

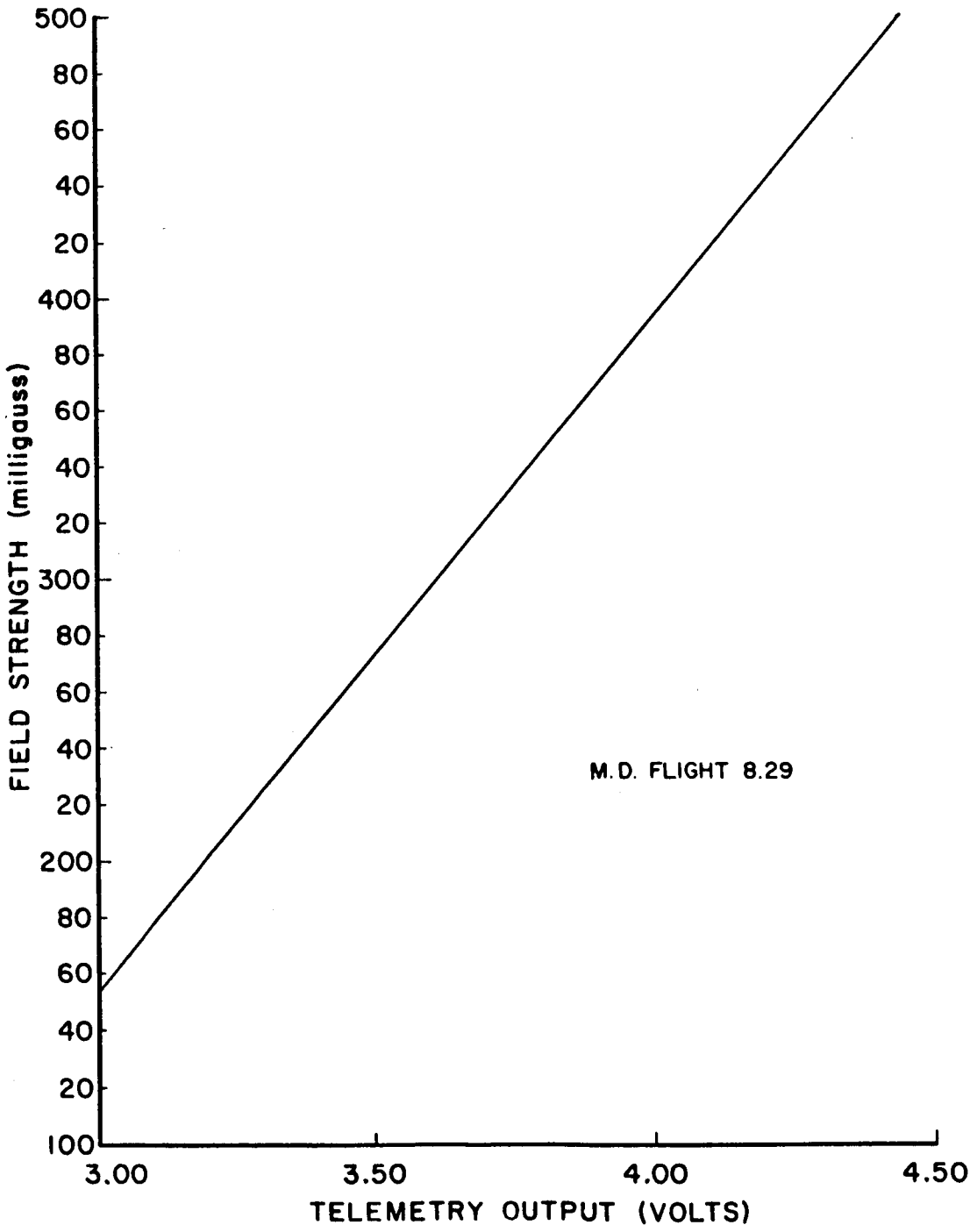

MAGNETOMETER CALIBRATION

FIGURE 5.7

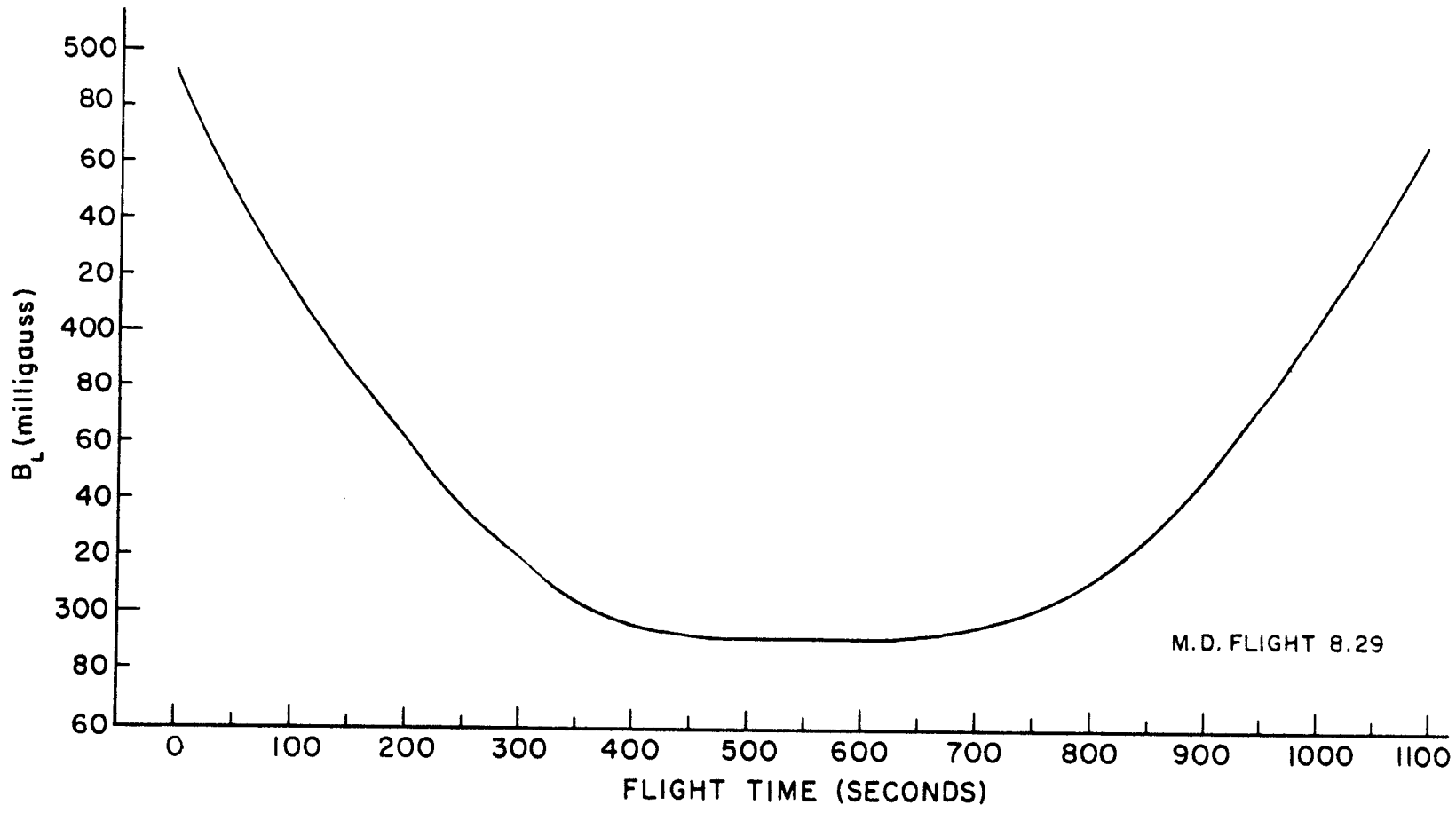

COMPONENT OF EARTH'S MAGNETIC FIELD ALONG DIRECTION OF PROPAGATION

FIGURE 5.8

sinusoidal modulations on the voltage output of the magnetometer. One cycle of the modulating voltage corresponded to one payload revolution. Immediately before Mother and Daughter separation the spin rate was determined as 8.695 ± 0.095 revolutions/second. After Mother-Daughter separation the magnetometer shoed the Mother to have a spin rate of 8.69 ± 0.01 revolutions/second. Also upon separation of the two sections the solar aspect sensor described in Chapter III was used to determine the Mother payload spin rate. The output of this device is seen in Figure 5.6B. The spin rate measured from this device was determined at 8.695 ± 0.008 revolutions/second.

The total magnetic field vector was computed along the payload trajectory in Figures 5.1 and 5.2 using the computer program described in Chapter IV. Figure 5.9 shows these results which were then used in the calculation of the propagation angle.

The propagation angle θ for the three CW signals with respect to the earth's magnetic field vector was calculated throughout the flight and expressed as a function of flight time. Figure 5.10 which gives these results distinctly indicates a variation of ten degrees in θ which was measured from Mother-Daughter separation at 139 seconds to splash at about 1100 seconds. The theoretical propagation angle expected is also seen in Figure 5.10; it was found using the actual separating payload trajectory, the initial separation axis angle taken with respect to the local vertical, and the theoretical total field from Doupnik's computer program. This variation in θ demanded the use of the entire family of data reduction curves discussed in Chapter IV when the $\Phi(t)/S_{MD}$ ratios were found

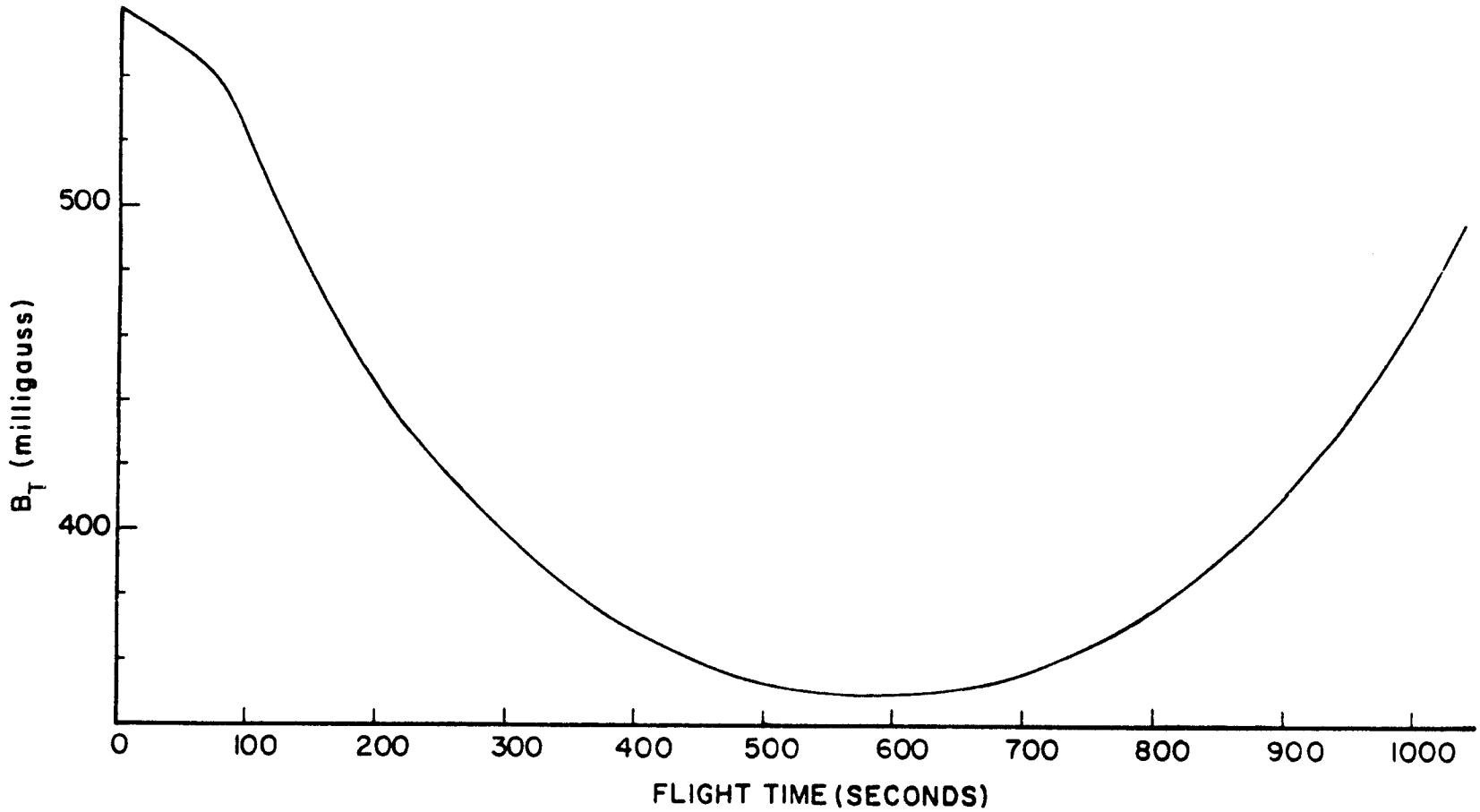

TOTAL MAGNETIC FIELD ALONG TRAJECTORY

FIGURE 5.9

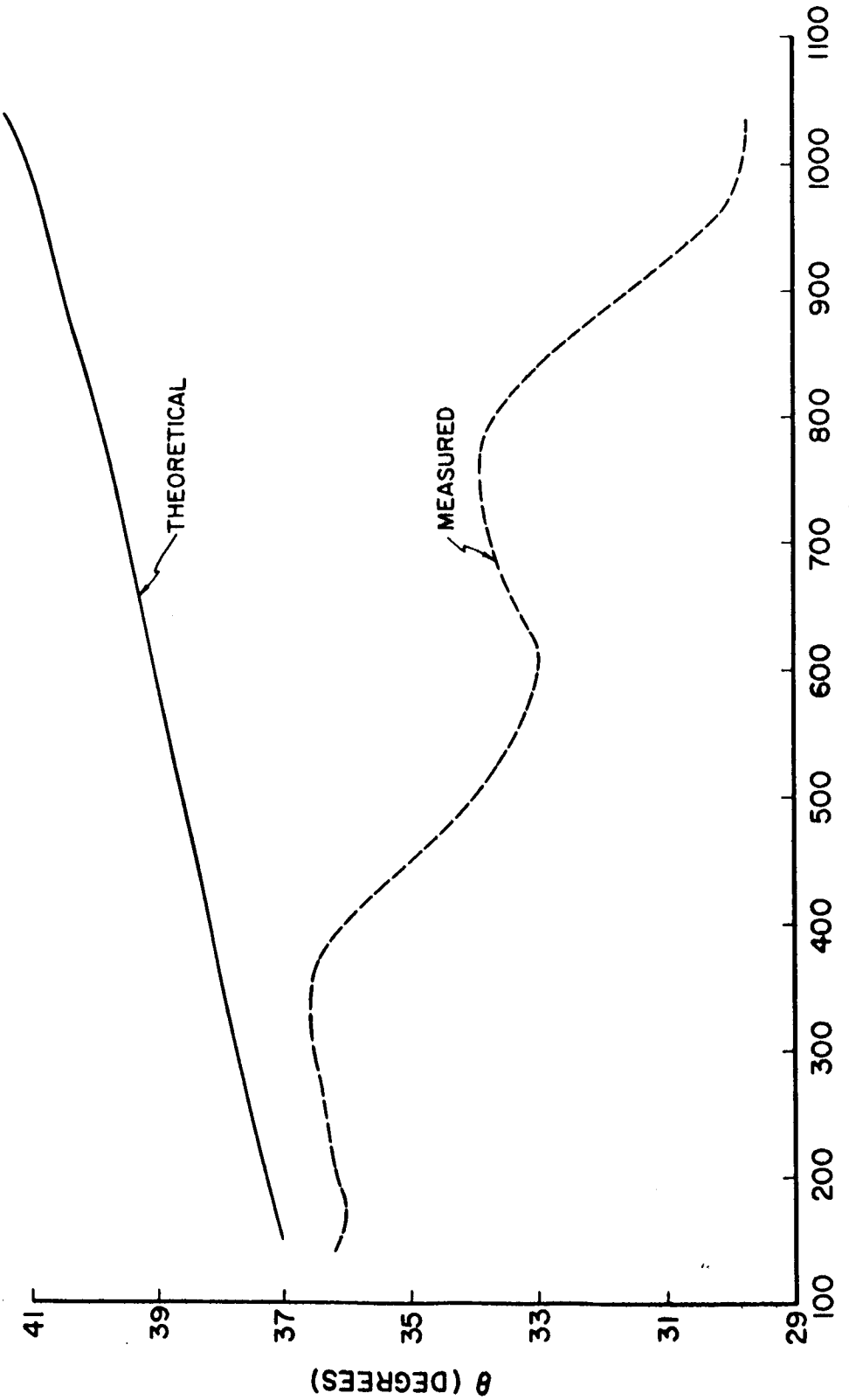

ANGLE OF PROPAGATION

FIGURE 5.10

experimentally and reduced to densities.

The attitude of the Mother section was evaluated before and after separation using magnetometer data. At separation the Mother's attitude was calculated as 26° with respect to the local vertical. From calculations later in the flight the variation in attitude was less than 2° from the original 26°. Thus, the variation of the angle of propagation in Figure 5.10 was not caused by possible changes in attitude of the vehicle. Rather, it was surmised that the actual total magnetic field vector did not follow the uniform total field vector given by the computer program. A magnetic field irregularity was the possible cause of the change in the actual total field, the longitudinal component of which was measured and used in the experimental θ calculations.

5.2.3 Temperature Sensors

Temperatures were measured by thermistors attached to the Mother package. Measured temperatures are shown in Figure 5.11. Preflight calibration of the receiver delays dependent on temperature variations is shown in Figure 5.21. The resulting delays are seen in Figure 5.22.

5.2.4 Signal Strengths and 6, 12, 73.6 Mc AGC Channels

Telemetry channels 6, 7, 8 were used for monitoring signal strengths of the 6, 12, 73.6 Mc waves received at the Mother. When the recorded voltages on these channels were reduced to signal strength measurements, the behavior of the three waves was found throughout the flight. Figure 5.12, 5.13, and 5.14 show the results

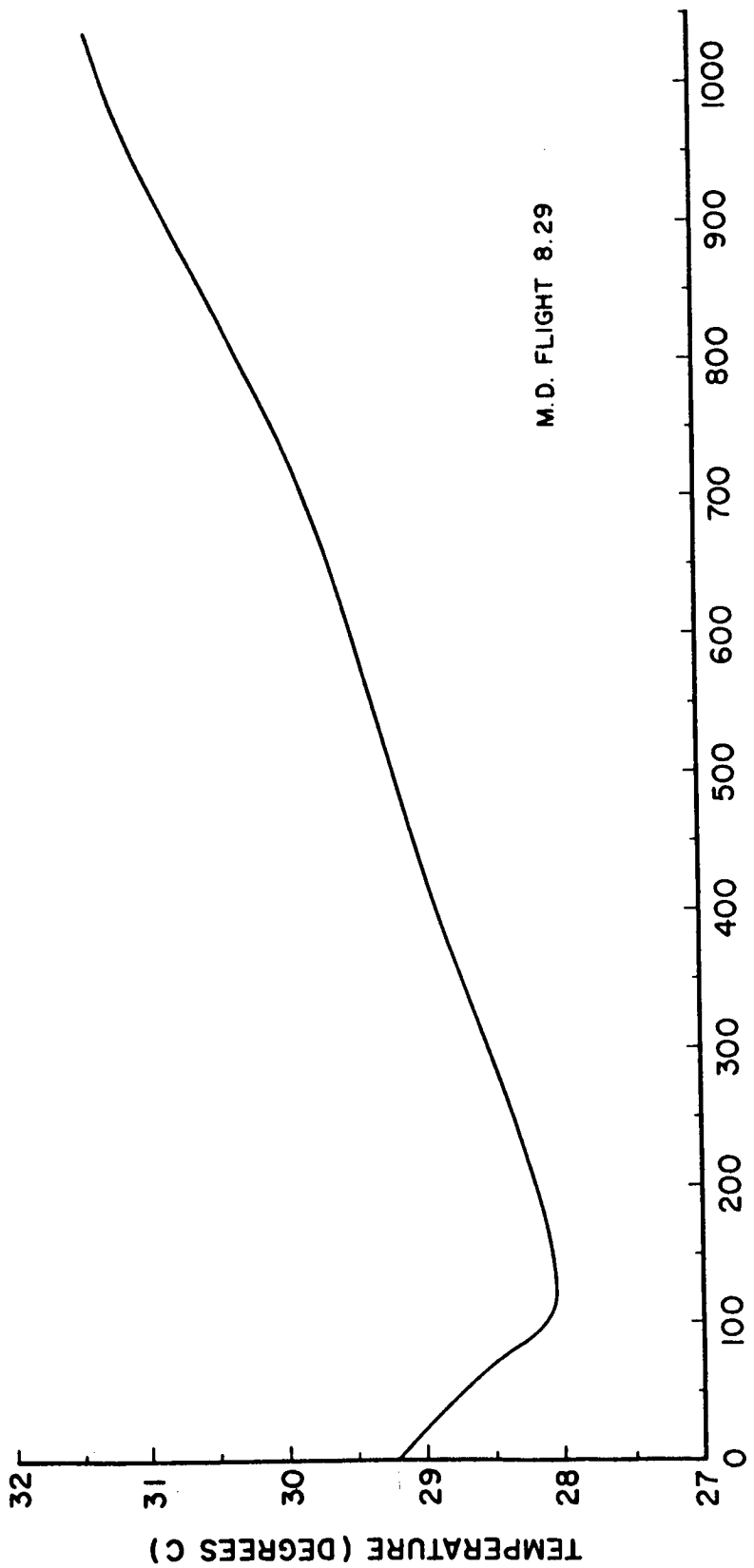

TEMPERATURE MONITORED ON RECEIVERS AND PHASE COMPARATOR

FIGURE 5.11

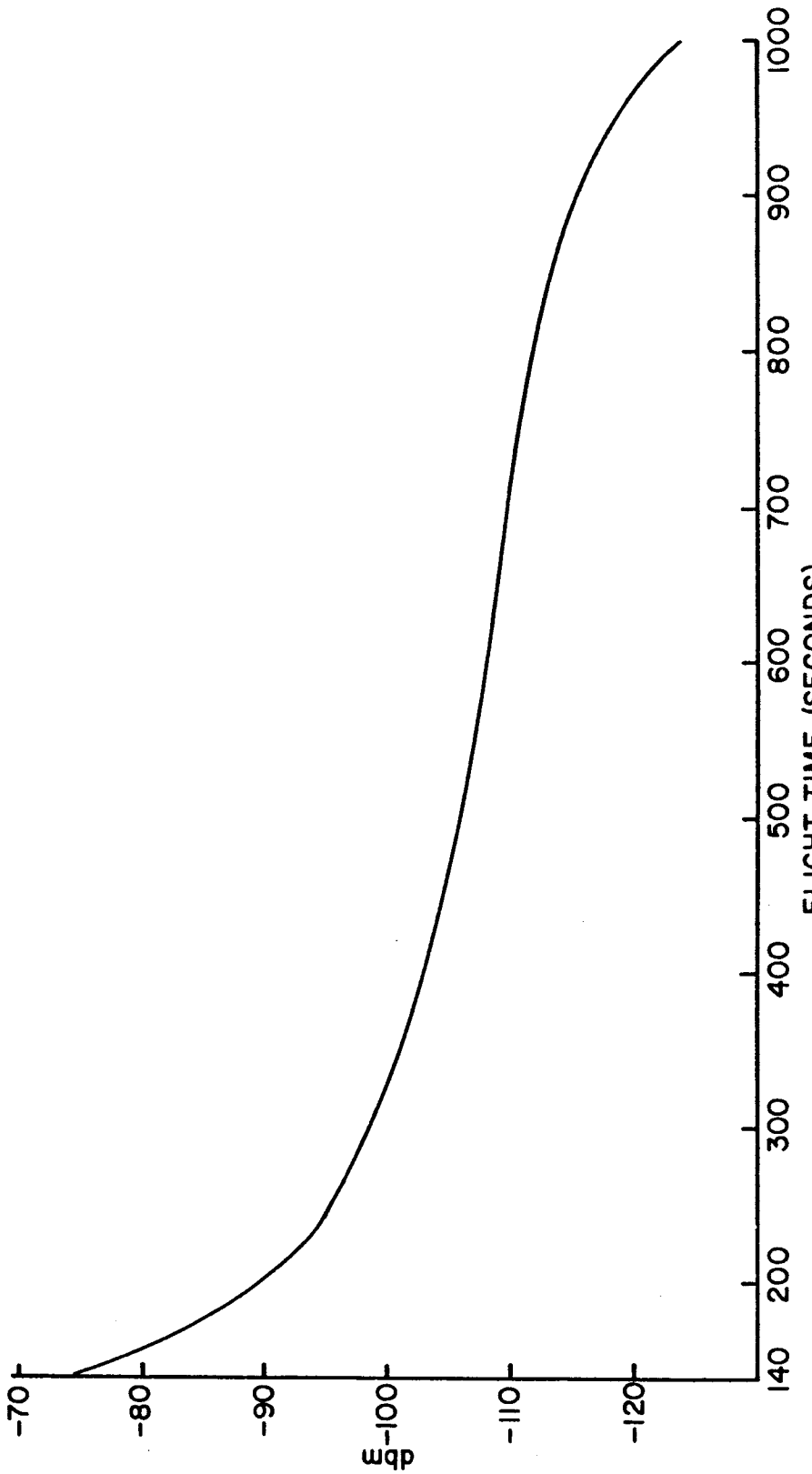

6 MC SIGNAL STRENGTH
FIGURE 5.12

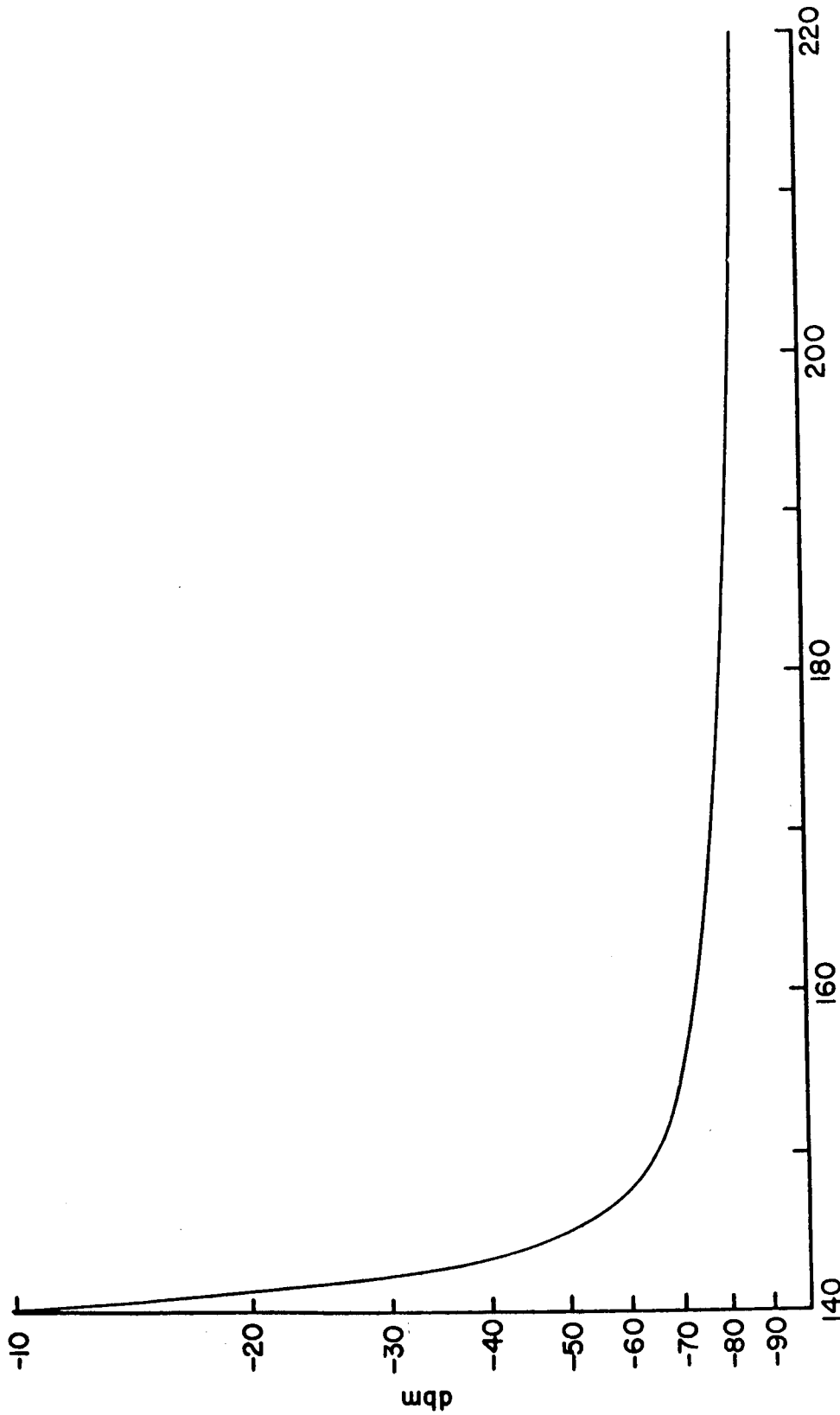

12 MC SIGNAL STRENGTH

FIGURE 5.13

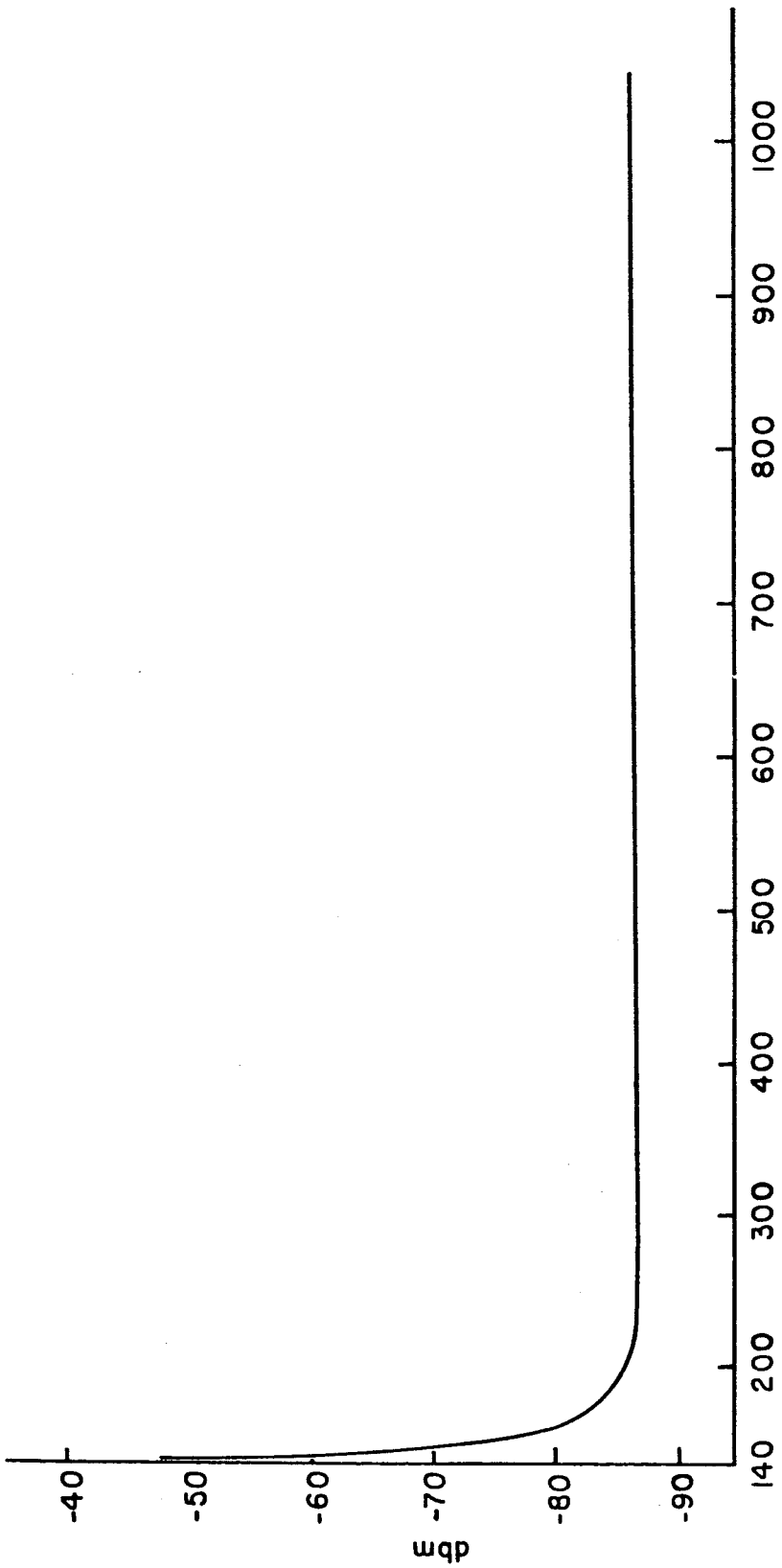

72 MC SIGNAL STRENGTH

FIGURE 5.14

of the computations using flight data. There was an abrupt drop in the 73.6 Mc receiver sensitivity from separation at 139 seconds to approximately 150 seconds. Ground receivers showed the signal strengths were nominal for the transmitter. However, the loss in sensitivity did give rise to receiver delays and corresponding phase shifts. The delays were accurately analyzed using a preflight simulated calibration curve and the 73.6 Mc signal strength of Figure 5.14. Even though the 73.6 Mc signal was used as a reference for the 6 Mc and 12 Mc signals, the 73.6 Mc delays occurred and ended before 12 Mc and 6 Mc calculations were made.

From the analysis of the 12 Mc AGC channel data it was apparent that the 12 Mc AGC levels were well below nominal. The 12 Mc transmitter power was known to have been nominal because ground based measurements of the signal strength were available and compared well with other flights. The fault, therefore, was in the receiver. Receiver calibrations immediately prior to flight showed no abnormalities and the signal strength measurements on a subsequent 12 Mc channel were nominal. It has, therefore, been concluded that the trouble arose in the 12 Mc receiver after preflight checks. However, no means have been found to define the problem more accurately. Subsequent vibration and mechanical checks have failed to show a design weakness in the unit. The uncertainty in this stage was responsible for the loss in signal strength and has complicated the analysis of the arising phase delays. This has been taken into account in the analysis that follows.

The 6 Mc signal strengths measured were nominal throughout

the flight. Rapid attenuation of this wave near the end of the flight was caused by the re-entry of the payload in a region of high electron density where the plasma frequency was nearly the same as the propagating frequency.

Superimposed on all three AGC channels was a spin modulation caused by the relative rotation of the Mother and Daughter sections. Analysis of this relative spin phase is discussed in the following section.

5.3 Calculation of Electron Densities from Ionospheric Phase Shifts

The recorded output on the four phase channels, a portion of which was depicted in Figure 5.3, was mentioned previously as a combined result of not only ionospheric phases but also of phase shifts from the relative rotation of the two sections. Secondary contributions to the total recorded phase also arose from receiver delays dependent on signal strength and temperature fluctuations. The 6 Mc and 12 Mc phases also had a minor contribution due to a Faraday rotation of the propagating frequencies.

5.3.1 Relative Rotation of Mother and Daughter

The first major correction to the total recorded phases was the extraction of phases due to the relative spin which was detected and accurately measured on the 6 Mc AGC channel. The method of calculating this value from the 6 Mc channel included a correction due to the effect of Faraday rotation. The Faraday rotation arises because of the factor $W = Y_T^4/(2Y_L)(1 - X - jZ)$. If W is large, there will be significant Faraday rotation; and this occurs at the lower altitudes of the F region where the density is high. However, near apogee W is

small and so is the Faraday rotation. First, an estimate of the spin rate was made near the peak of the trajectory on the 6 Mc AGC channel. Then the electron density, which was estimated using this spin rate, was used to calculate the Faraday rotation. With the Faraday rotation known a new estimate of the relative spin rate was used. Figure 5.15 shows how the number of phase cycles on the 6 Mc channel varied throughout the flight. Figures 5.16 and 5.17 show the Faraday rotation calculations. An average relative spin rate of 0.2130 ± 0.0001 revolutions/second was obtained on the 6 Mc channel from calculations using the results of the above figures.

5.3.2 Receiver Delays

A. Signal Strength Dependent Delays

The first major secondary correction to the phase data, especially to the 12 Mc data, was the receiver delays dependent upon a rapid change in signal strength. It was imperative to initiate this correction for 12 Mc data for the time region of 139.1 seconds to 172 seconds where the small signal drop-out occurred. Calculating the rate of change of 12 Mc signal strength from data in Figure 5.13 and using preflight delay testing results exhibited in Figures 5.18 and 5.19 the relative phase shifts of ϕ_D of the receiver delays were found. Figure 5.20 shows that the correction from the receiver delay to spin corrected phases was most significant near 151 seconds but less than 1% thereafter in the experiment.

The 6 Mc signal strength suffered no delays of this nature and thus phases were uncorrected for this effect.

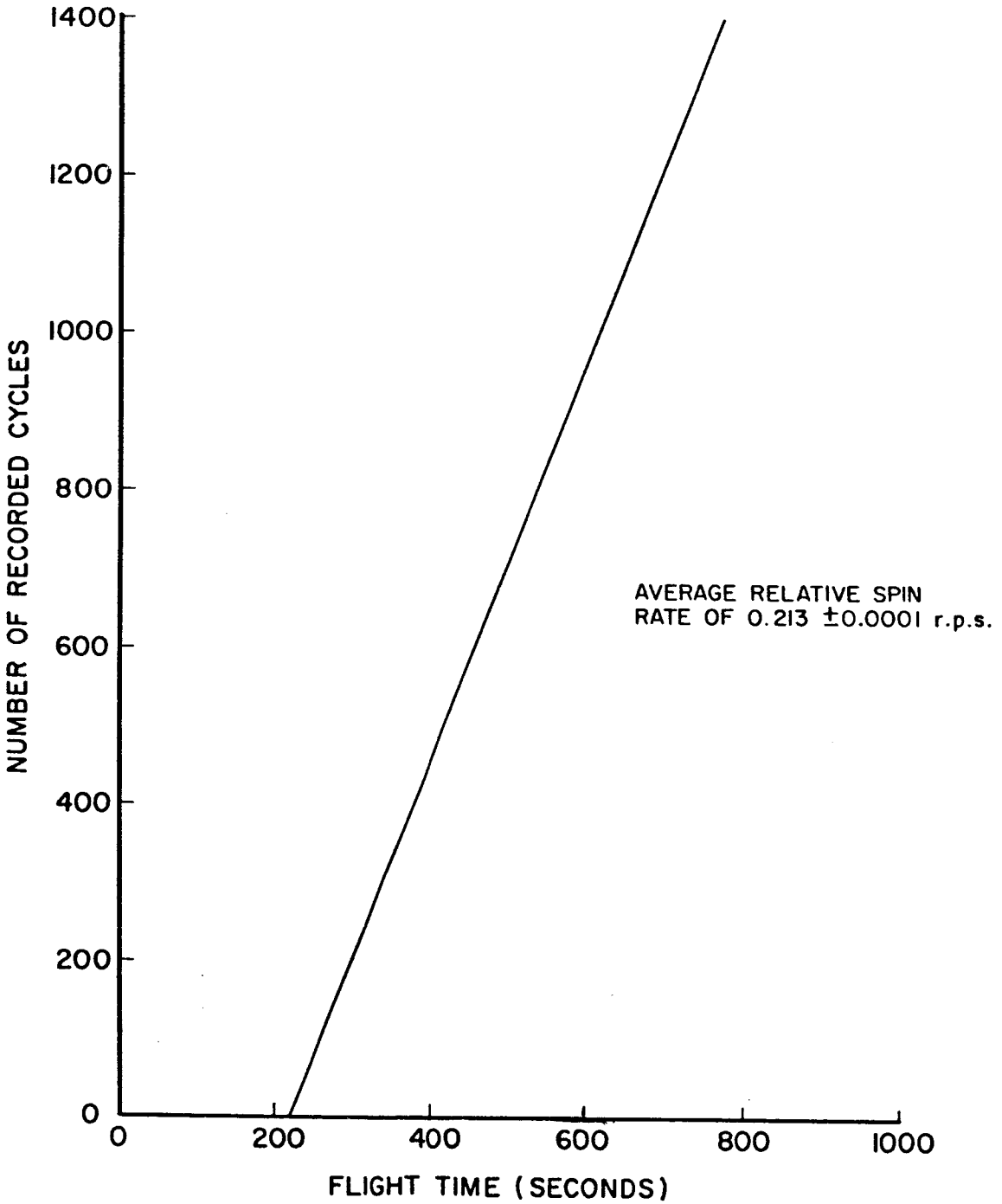

6 M.C. AGC CYCLES ARISING FROM RELATIVE ROTATION

FIGURE 5.15

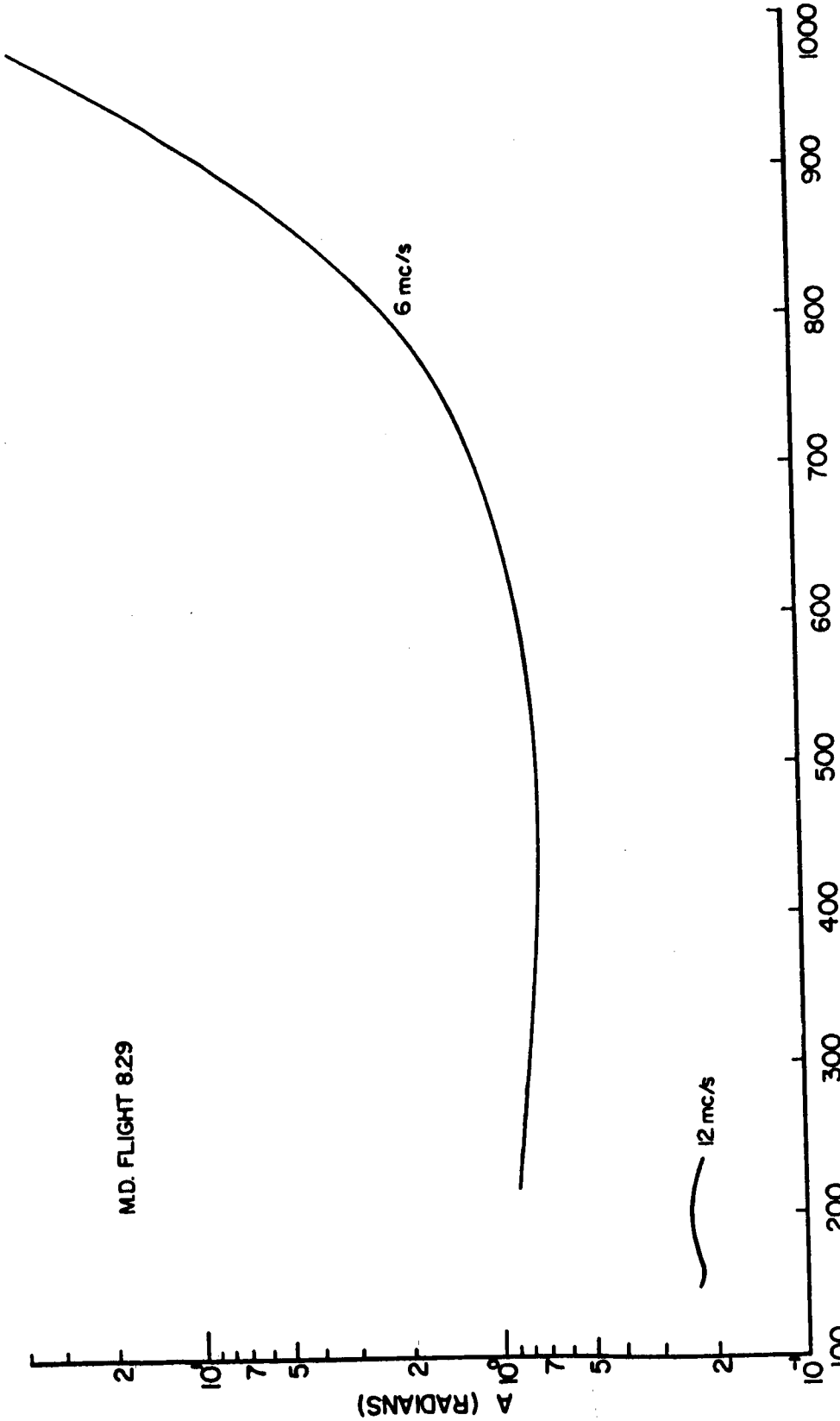

FARADAY ROTATION OF 6 AND 12 MC WAVES

FIGURE 5.16

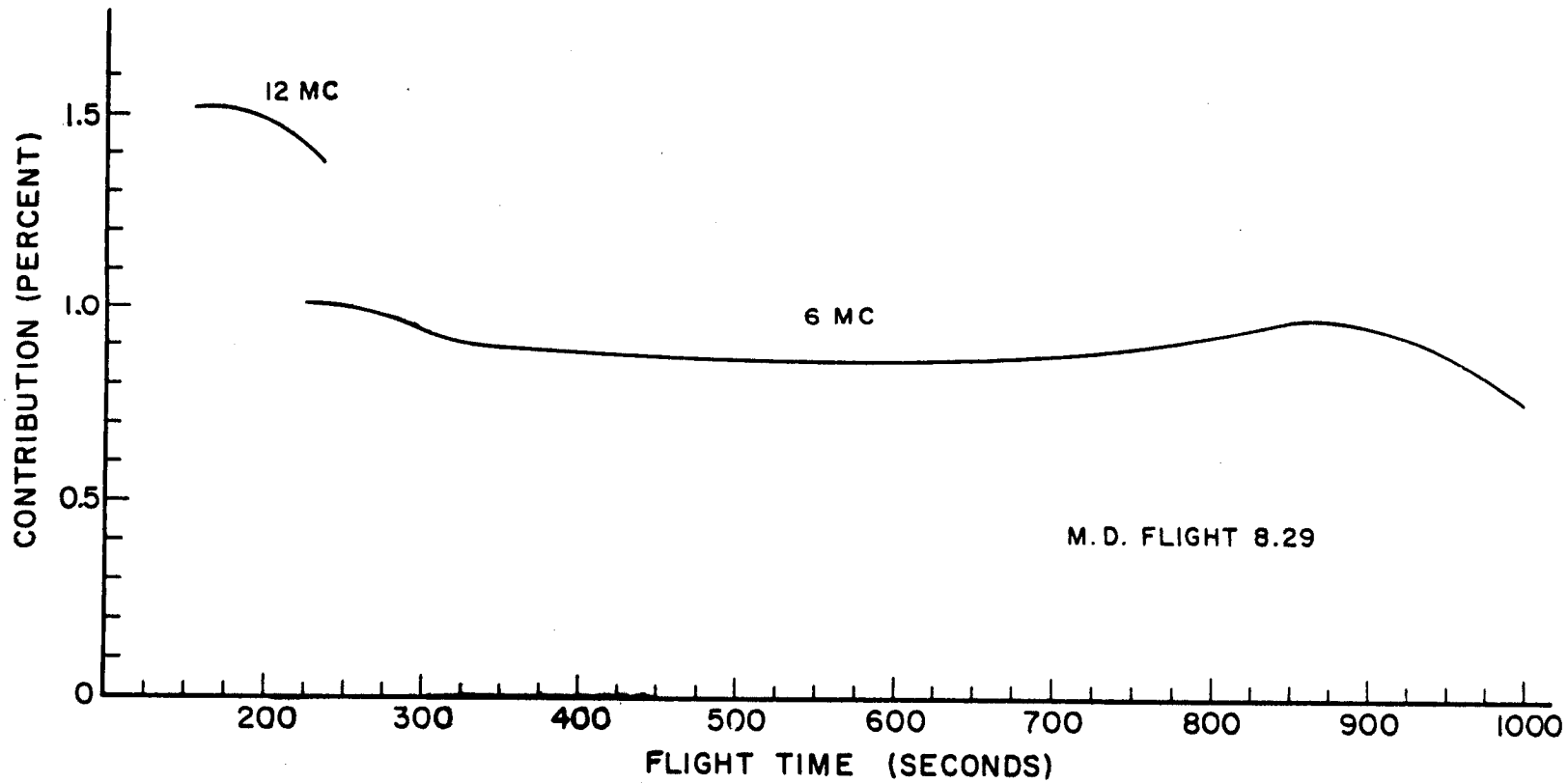

CONTRIBUTION OF FARADAY DELAYS ϕ_F TO 6MC AND 12MC PHASES $\phi_R - \phi_S$

FIGURE 5.17

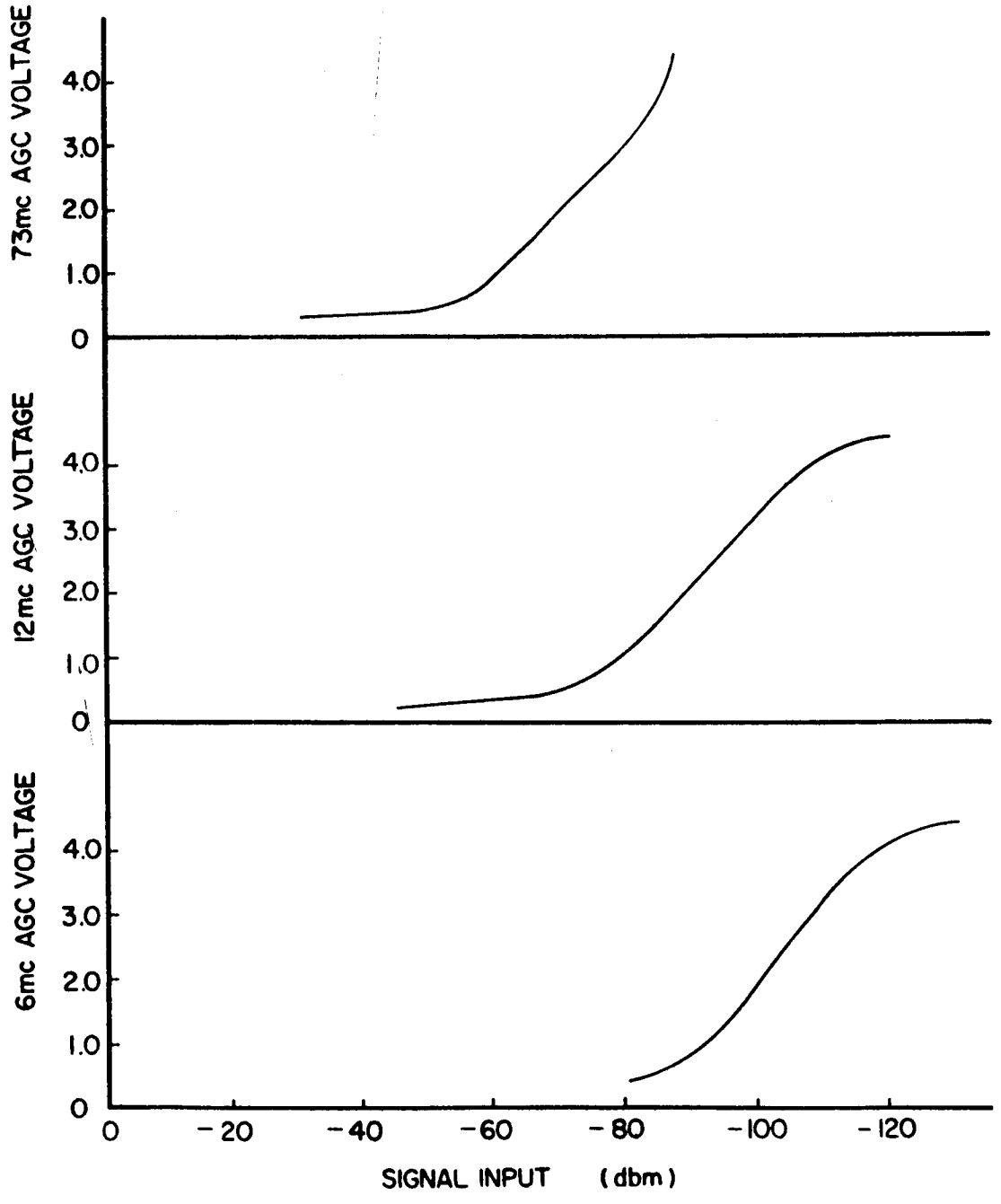

RECEIVER IB AGC VS SIGNAL INPUT

FIGURE 5.18

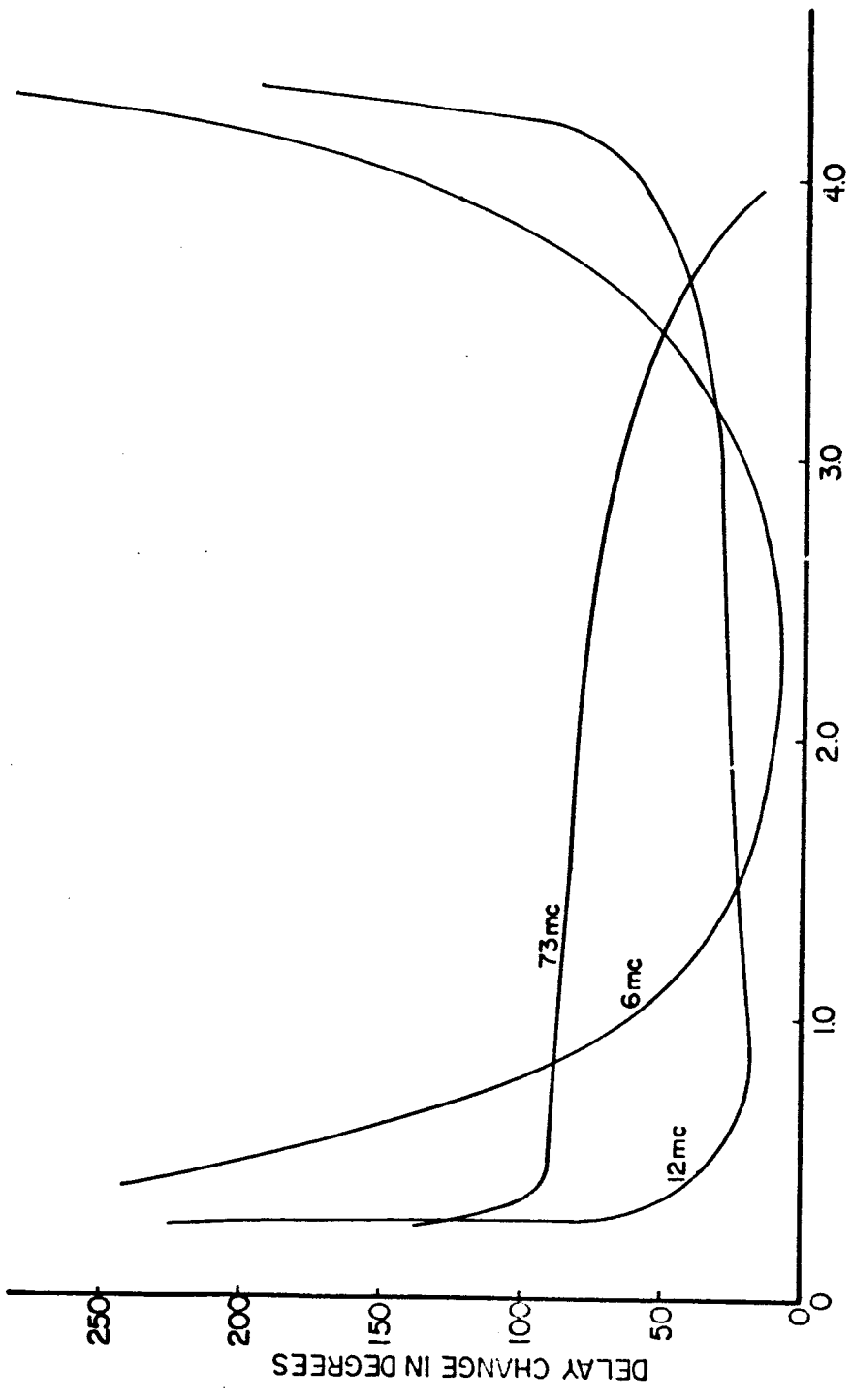

RECEIVER IB RECEIVER DELAY VS AGC

FIGURE 5.19

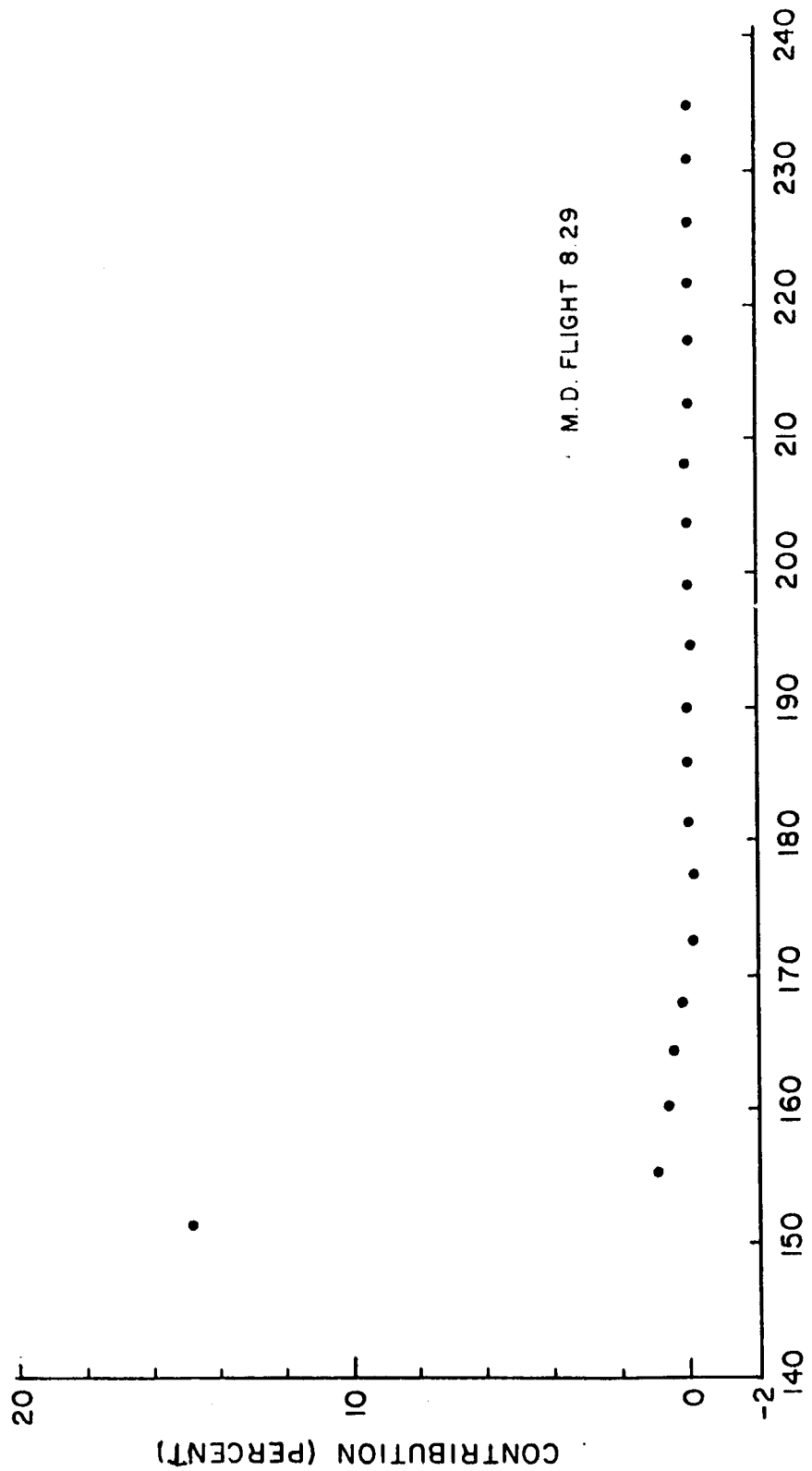

PERCENTAGE CONTRIBUTION OF 12 MC RECEIVER DELAY ϕ_D TO ABSOLUTE PHASE $\phi_R - \phi_S$

FIGURE 5.20

B. Temperature Dependent Delays

An analysis of the phase comparator and receiver delays which were related to changes in device operating points caused by temperature variations, was also made. From the calibration curve of Figure 5.21 and the temperatures in Figure 5.11, receiver delays were computed. Figures 5.22 and 5.23 show these delays and their contribution to relative spin corrected phase which were then directly related to computed electron densities by Figure 4.1. From Figure 5.23 it is seen that the effects of these delays were extremely small compared to the phase shifts introduced by the ionosphere.

5.3.3 Final Corrected Phases

Thus, the final corrected phases were those dependent only on the electron density variations in the ionosphere. Figure 5.24 and 5.25 show the corrected phases which accounted for the relative spin, Faraday rotation, and receiver delays. From these phases, the separation distances of Figure 5.5, the reduction curves of 4.1, and the trajectory of 5.1, the electron density profile became uniquely determined.

5.4 Electron Density Profile

5.4.1 Accuracy of Measured Parameters and Subsequent Density Errors

A. Separation Distances

One of the critical measurements was the separation velocity between the Mother and Daughter sections. The velocity measuring device was described in Chapter III. Calculated from flight data was

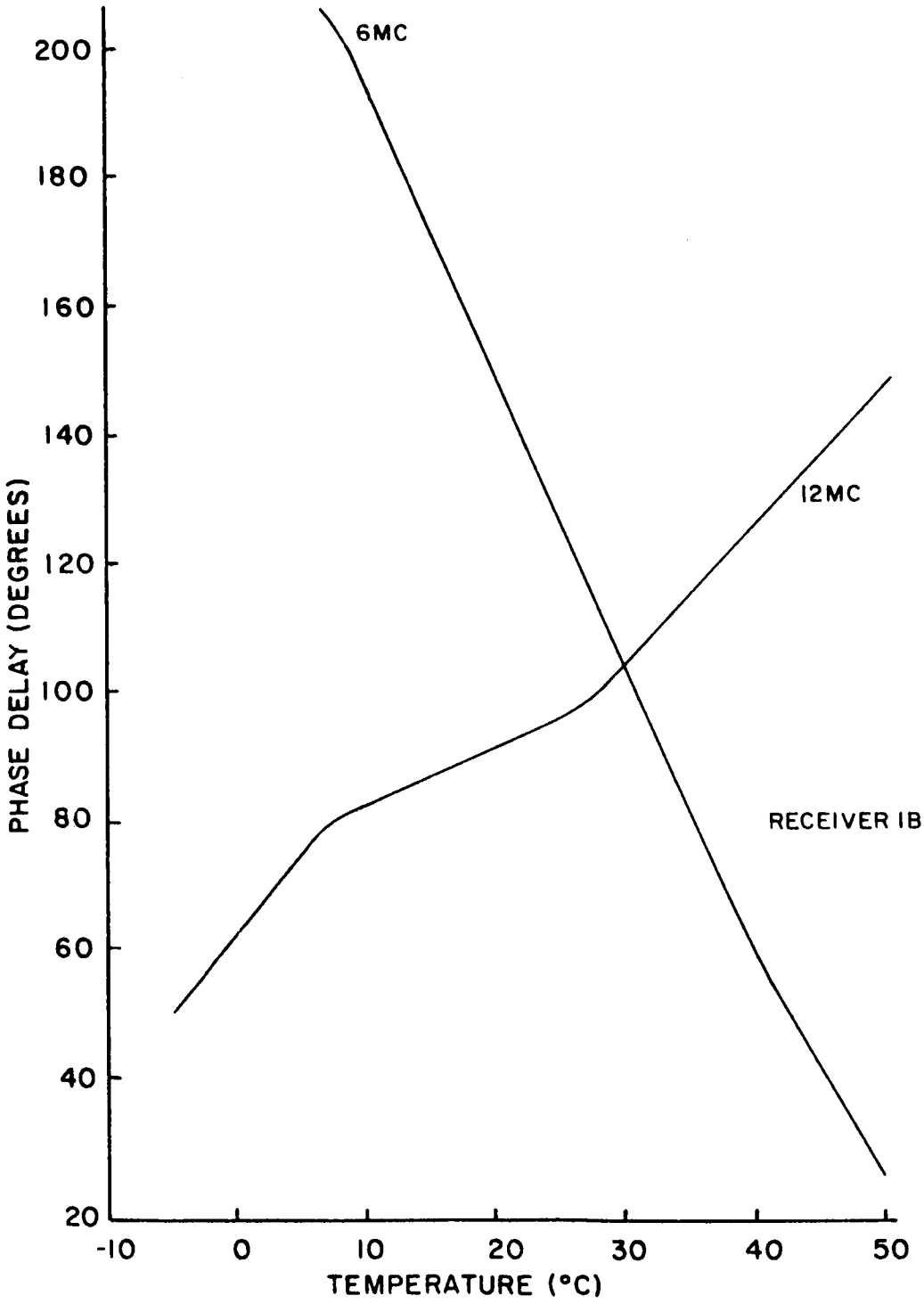

CALIBRATION CURVE FOR TEMPERATURE DEPENDENT RECEIVER DELAYS

FIGURE 5.21

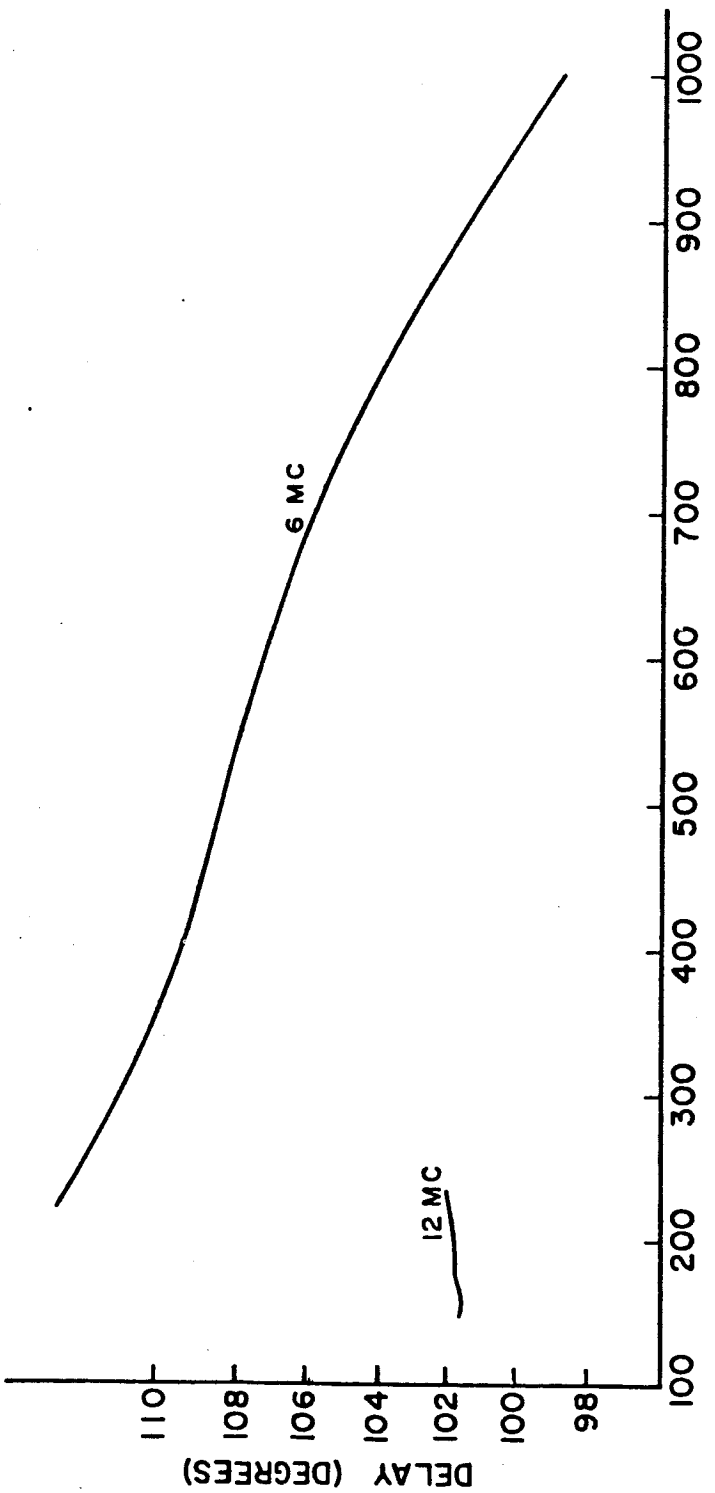

RECEIVER DELAYS CAUSED BY TEMPERATURE VARIATION

FIGURE 5.22

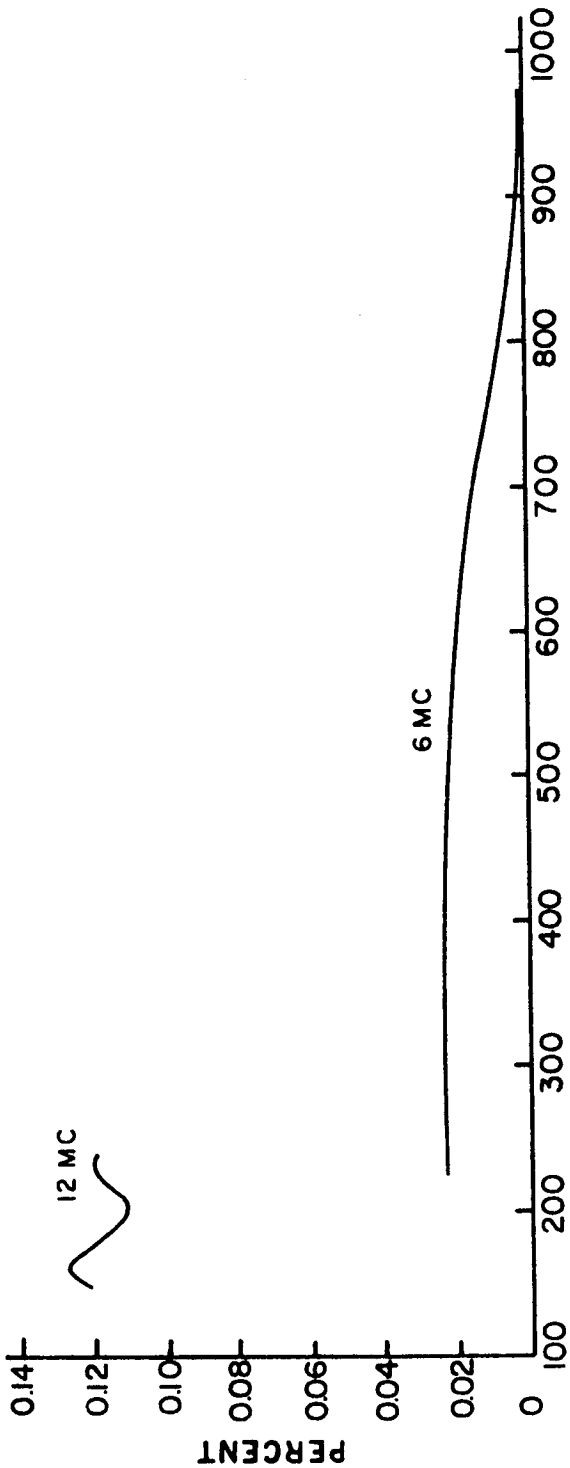

PERCENT CONTRIBUTION OF TEMPERATURE DELAYS TO ABSOLUTE PHASE

FIGURE 5.23

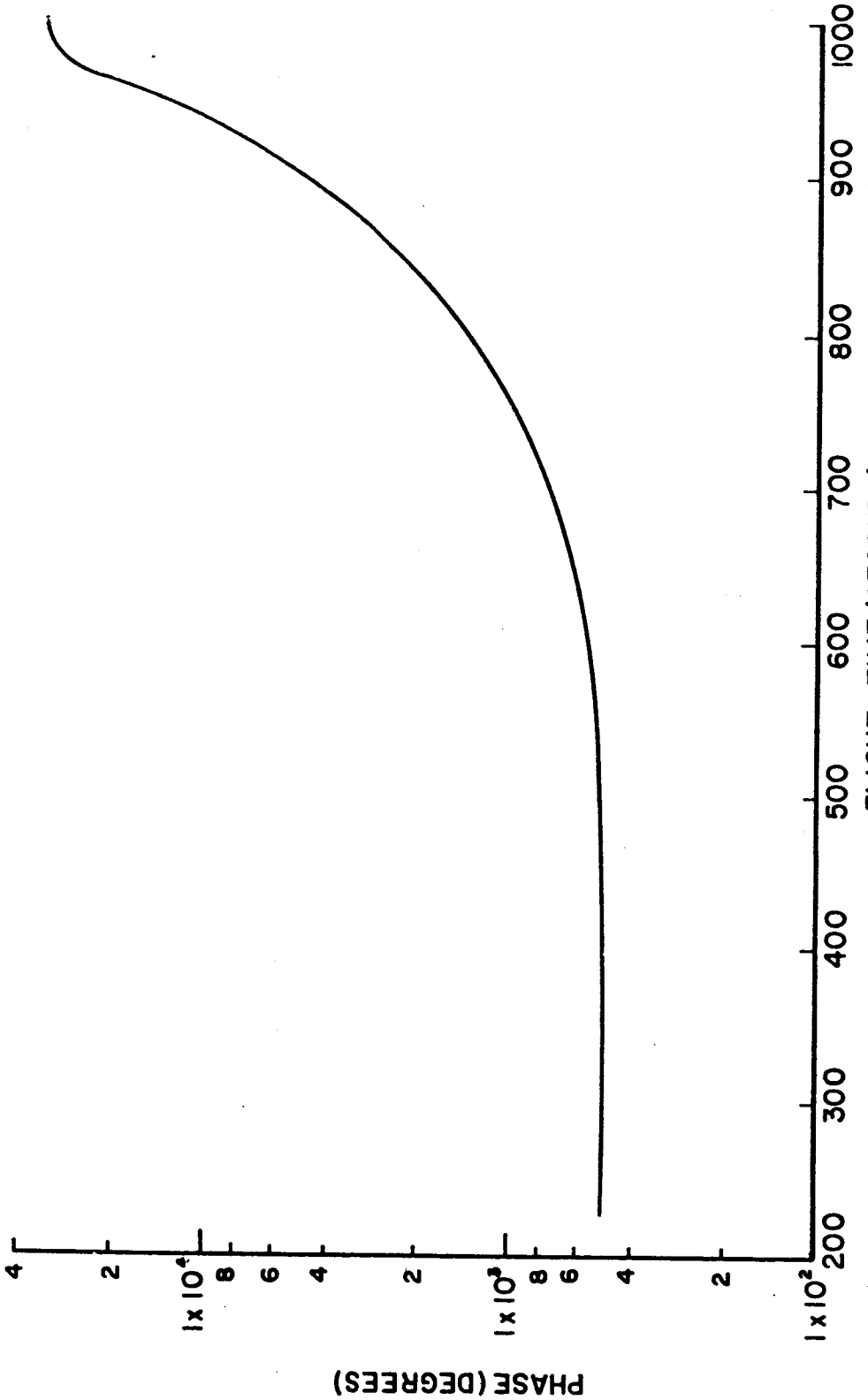

6MC IONOSPHERE PHASES

FIGURE 5.24

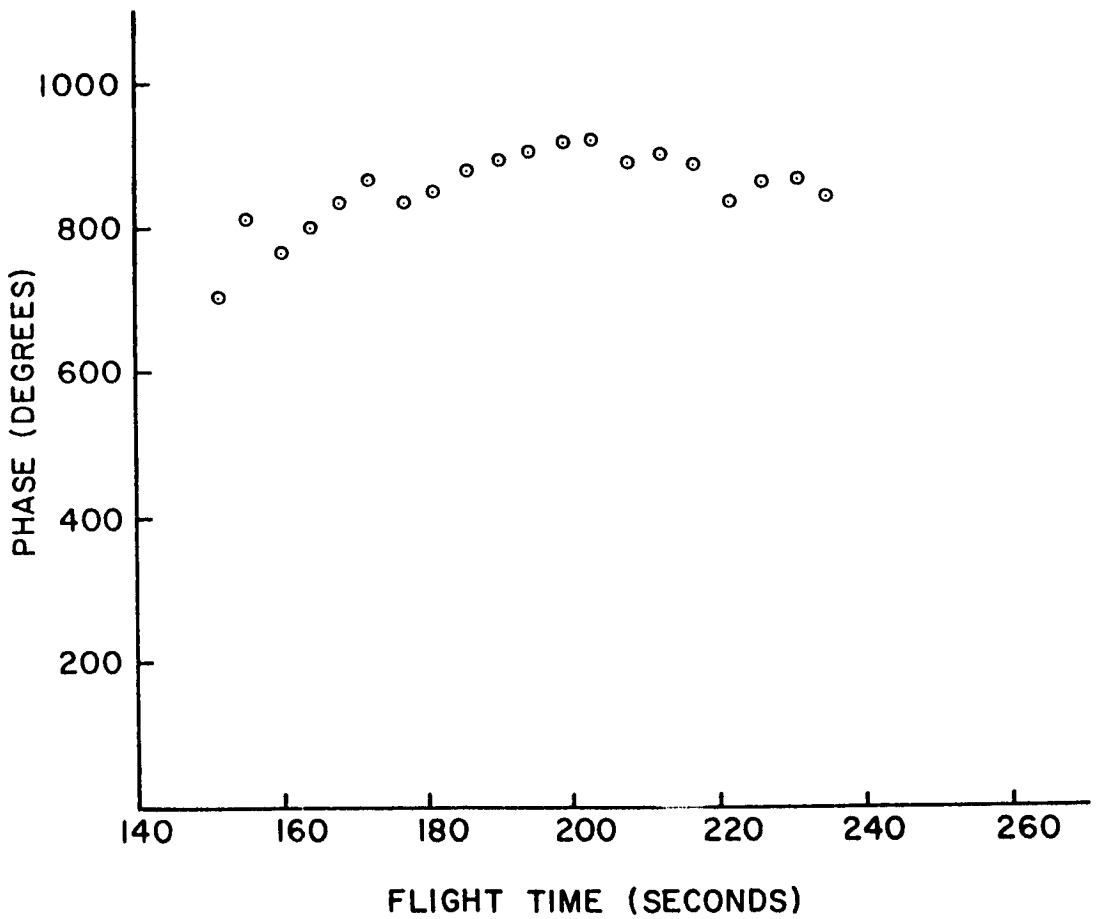

12 MC IONOSPHERE PHASES

FIGURE 5.25

the average value of 5.3397 ± 0.0057 meters/ second from three overlapping time intervals in the total recorded spike output time of 0.7 seconds. Since the electron density and separation distance were inversely related by Figure 4.1, the ± 0.106% uncertainty in the value of V_{MD} made all 12 Mc (phase/separation) ratios liable to an error of ±0.106%; and, all 6 Mc ratios were also liable to this constant error of ±0.106%. These errors were then converted by Figure 4.1 directly to errors in the electron densities. Figures 5.26 and 5.27 show the density errors arising from the separation velocity uncertainty.

B. Longitudinal Component of the Magnetic Field and the Propagation Angle

The propagation angle θ defined by $\theta = \cos^{-1} B_L/B_T$ also affected all densities calculations because it appeared in Y_L and Y_T found the formula for μ. Uncertainty of the value of θ arose from a 2.65% error in B_L measurements and error in all theoretical total field values B_T. The combined error for B_L and B_T was best estimated as a maximum error in θ calculations between 25^o and 40^o as a $\pm 2^o$ uncertainty throughout the entire flight. Figures 5.28 and 5.29 show the variation of electron density with the refractive index as a function of the propagation angle. Each figure was for one particular flight condition encountered. Figure 5.28 shows that an uncertainty of $\pm 2^o$ corresponded to a maximum uncertainty in electron density of ±2.32% for the actual 6 Mc density. For Figure 5.29 a $\pm 2^o$ uncertainty implied a ±1.44% error in density calculated from the actual 12 Mc flight data. Figure 5.26 shows these propagation

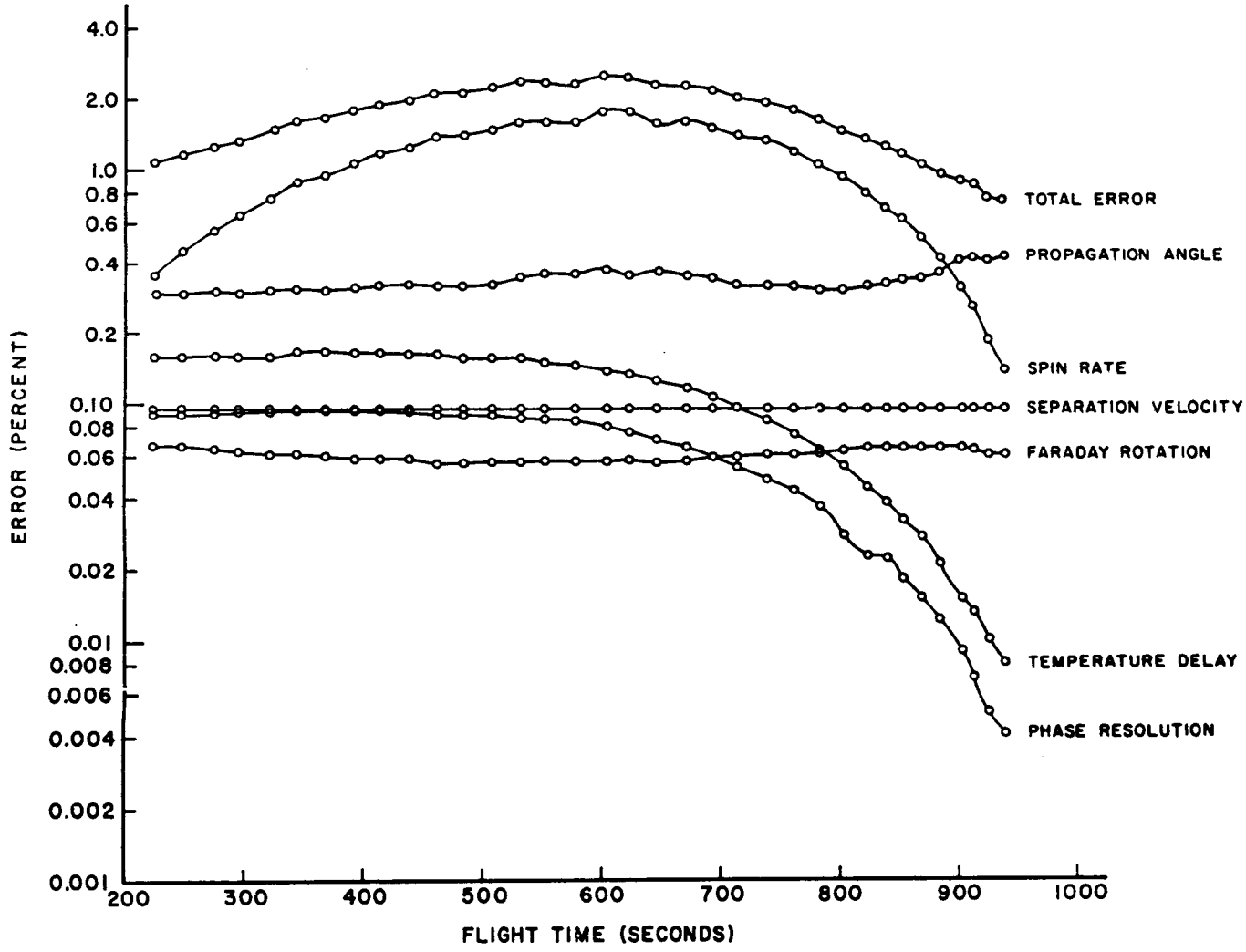

6 MC ELECTRON DENSITY ERRORS

FIGURE 5.26

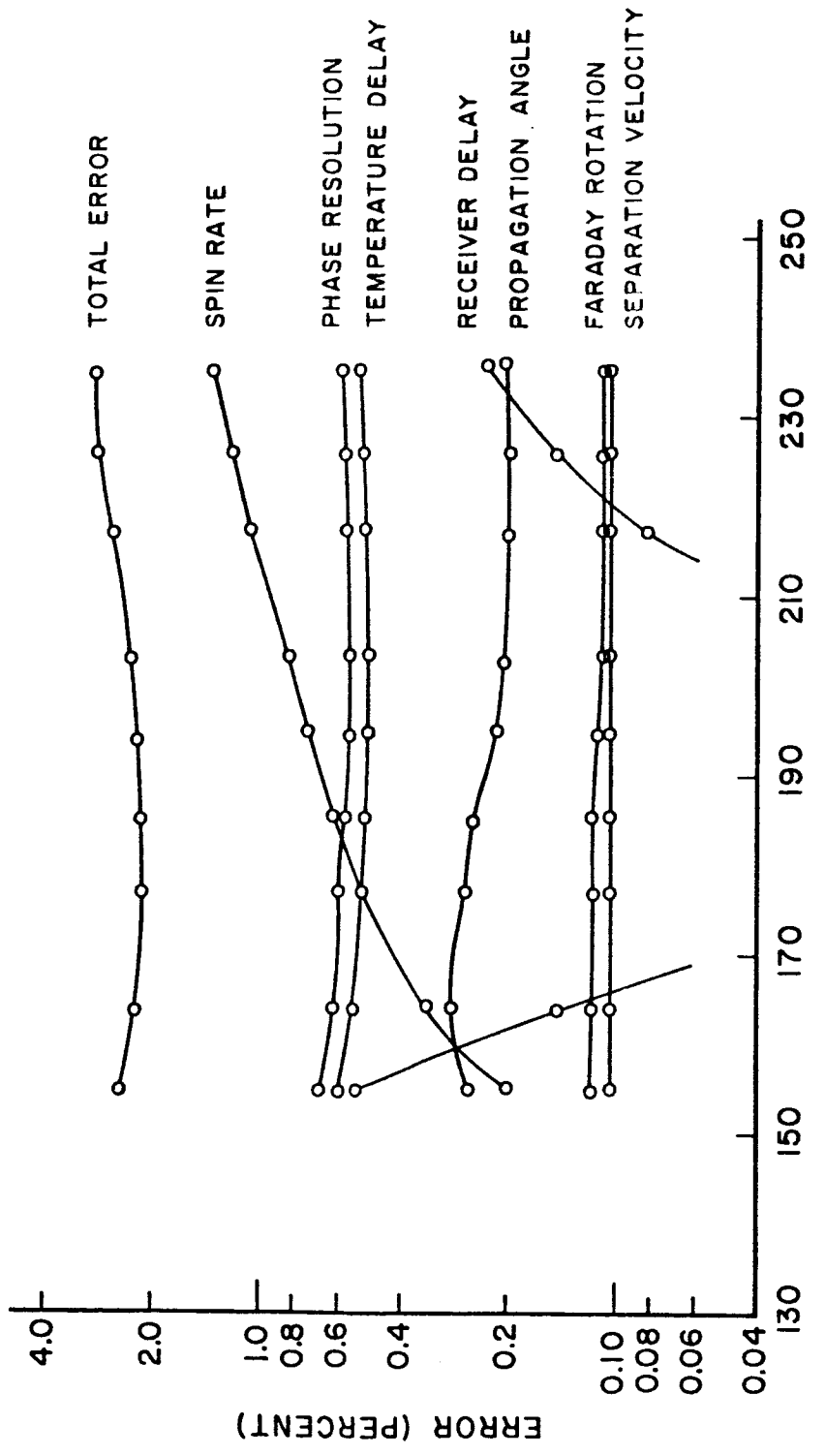

12 MC ELECTRON DENSITY ERRORS

FIGURE 5.27

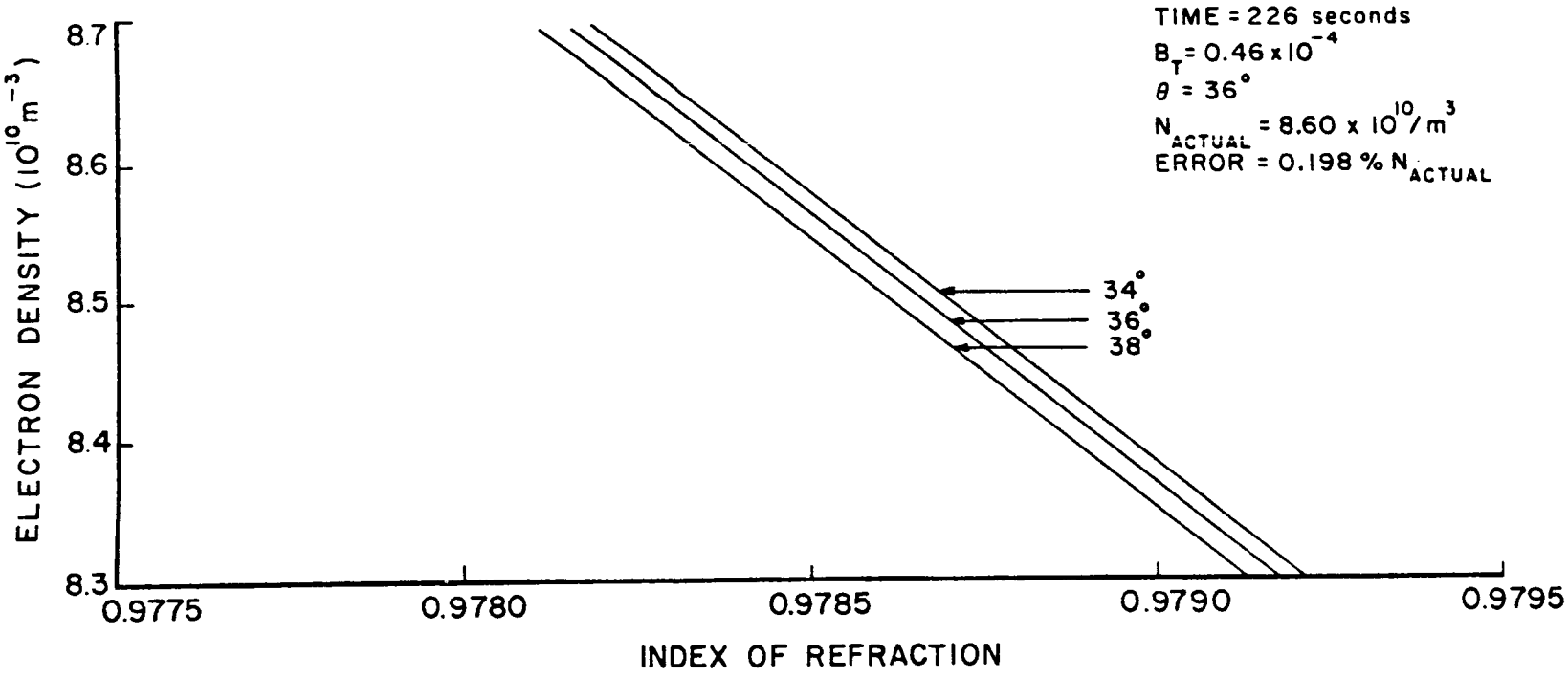

VARIATION OF 6 MC INDEX OF REFRACTION WITH ELECTRON DENSITY AS A FUNCTION OF THE PROPAGATION ANGLE

FIGURE 5.28

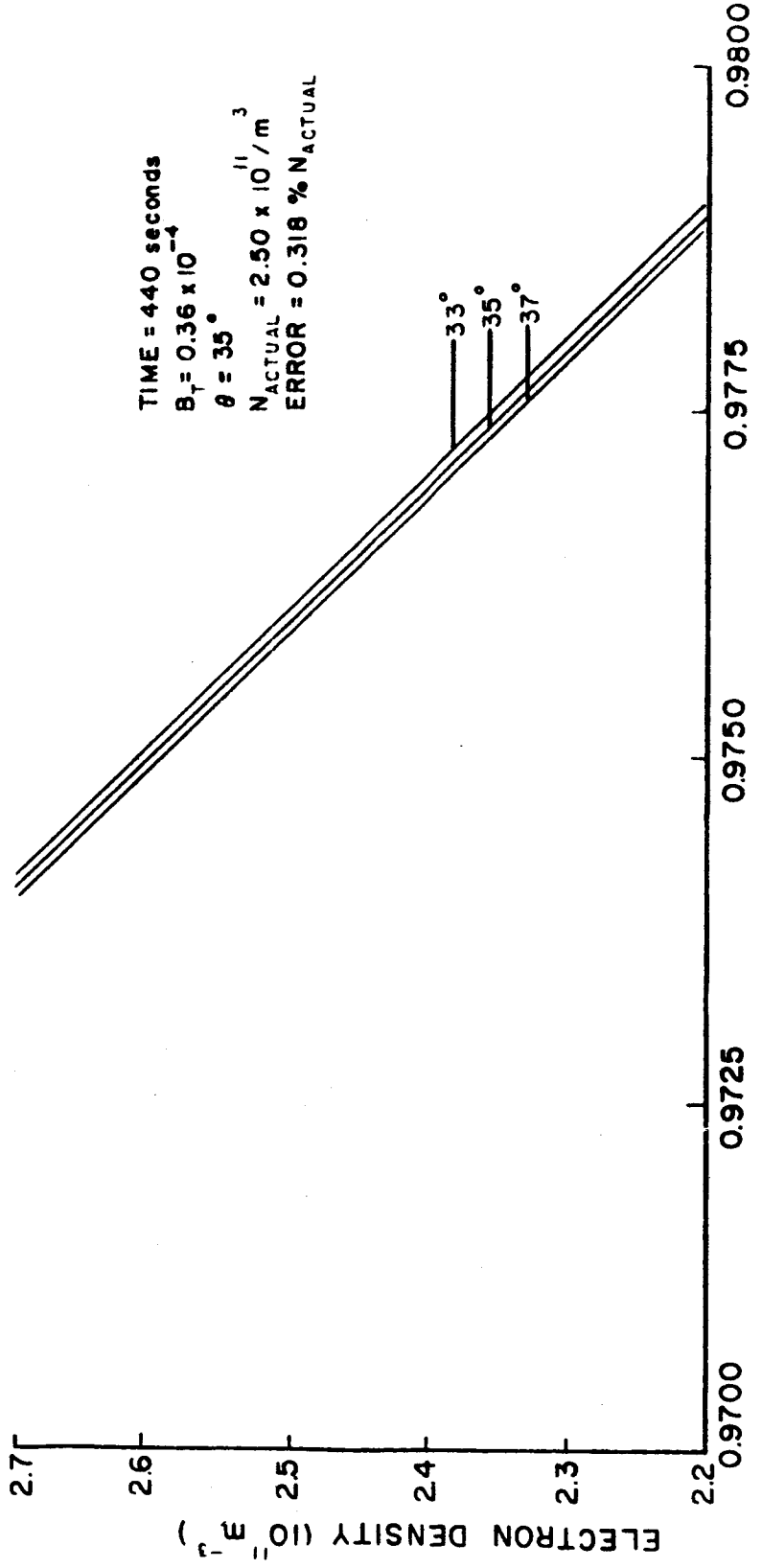

VARIATION OF 12 MC INDEX OF REFRACTION WITH ELECTRON DENSITY AS A FUNCTION OF THE PROPAGATION ANGLE

FIGURE 5.29

errors in time as 6 Mc density errors while Figure 5.27 shows the density errors due to θ uncertainty for the 12 Mc densities throughout the flight.

C. Phase Measurements

Phase measurements from the vector diode bridge were inherently limited to a detection accuracy of $\pm 5^{\circ}$. The 12 Mc phase data uncertainty amounted to a decreasing 0.63% error at 151 seconds or 302 km to 0.45% at 235 seconds or 536 km. An error of 0.09% for 6 Mc data at 225 seconds steadily decreased to less than 0.009% at 900 seconds or 506 km on re-entry. Figures 5.26 and 5.27 show these errors throughout the flight.

D. Phase Corrections - First and Second Order

The relative spin rate and the subsequent determination of spin phases were the most important correction to phase data. An accurate determination of these phases was important. The relative spin rate was described previously as being measured from the 6 Mc AGC channel and determined to be 0.2130 ± 0.0001 revolutions/second. The uncertainty in calculated ionospheric phases caused by the uncertainty in the spin rate was converted to errors in the electron densities by use of Figure 4.1. Figures 5.26 and 5.27 also show these errors expressed as a function of flight time.

Receiver delays dependent on temperature and signal strength variations were the cause of second order corrections to phase data. Measurement of the signal strengths were critical in regions where drop-out occurred on the 12 Mc channel and where the receiver delays

contributed to the recorded phases. An uncertainty of ±1 dbm occurred in all readings of signal strength made between -68 dbm at 151.43 seconds to -115 dbm at 235 seconds. The accuracy of calculating the receiver delays for the 12 Mc phase correction stems directly from the ±1 dbm error. The ±1 dbm error was related to an error in the receiver delays by Figures 5.18, 5.19, 5.20; and this error in receiver delay was related to the corresponding errors of corrected densities by Figure 4.1. Figure 5.27 shows these errors in the density expressed as a function of time. The 6 Mc channel suffered no receiver delays. Phase delays from the significant 73.6 Mc loss of receiver sensitivity at separation to 150 seconds were negligible by the time 12 Mc delays were calculated. At 151.43 seconds where the first 12 Mc delay was computed, the 73.6 Mc signal had already suffered maximum rate of decrease of sensitivity and was leveling off nominally.

Receiver delays dependent upon temperature variations were also analyzed for their accuracy. Data reduction and calibration errors combined for an uncertainty no greater than 2° C uncertainty in all temperatures. The uncertainty in these phases was also related to density uncertainty using Figures 5.21, 5.22, 5.23 then Figure 4.1. The density errors are expressed for both channels in Figures 5.26 and 5.27.

Faraday rotation angle introduced another type of second order correction to the phases on the 6 Mc and 12 Mc AGC channels. The uncertainty in the angle itself was 7.5% because it was only a first order calculation from electron densities uncorrected for this factor.

Using results from Figures 5.16 and 5.17 then Figure 4.1, the Faraday uncertainty was converted to density uncertainty. The error in the corrected densities for the 12 Mc calculations and all 6 Mc densities is exhibited in Figures 5.26 and 5.27.

E. Tracking Errors

Data on trajectory parameters such as longitude, latitude, and altitude was supplied by NASA. The largest error in altitude throughout the entire flight was a 2% uncertainty at one instant during payload re-entry. This error was one of the largest sources of error in the entire experiment, but it was determined at points in time by comparing results from the 5 independent radar tracking units. The trajectory error bars in Figure 5.31 show these nonlinear errors.

5.4.2 Summary of Significant Parameter Errors

The above errors in recorded phases which contributed directly in the calculation of electron densities are summarized in the curves of Figure 5.26 and 5.27. Total uncertainty is also expressed as error bars in Figure 5.31.

5.4.3 Electron Density Profile and Analysis

The final electron density profile is exhibited in Figures 5.30 and 5.31 with error bars about each calculated density. The theoretical errors for 12 Mc densities (which extended from 302 km to 526 km) and for 6 Mc densities (which extended from 511 km on the upleg to 357 km on the downleg) were mainly caused by the fore-mentioned uncertainty in the propagation angle θ and spin rate. All other combined sources of error on the 6 Mc and 12 Mc channels

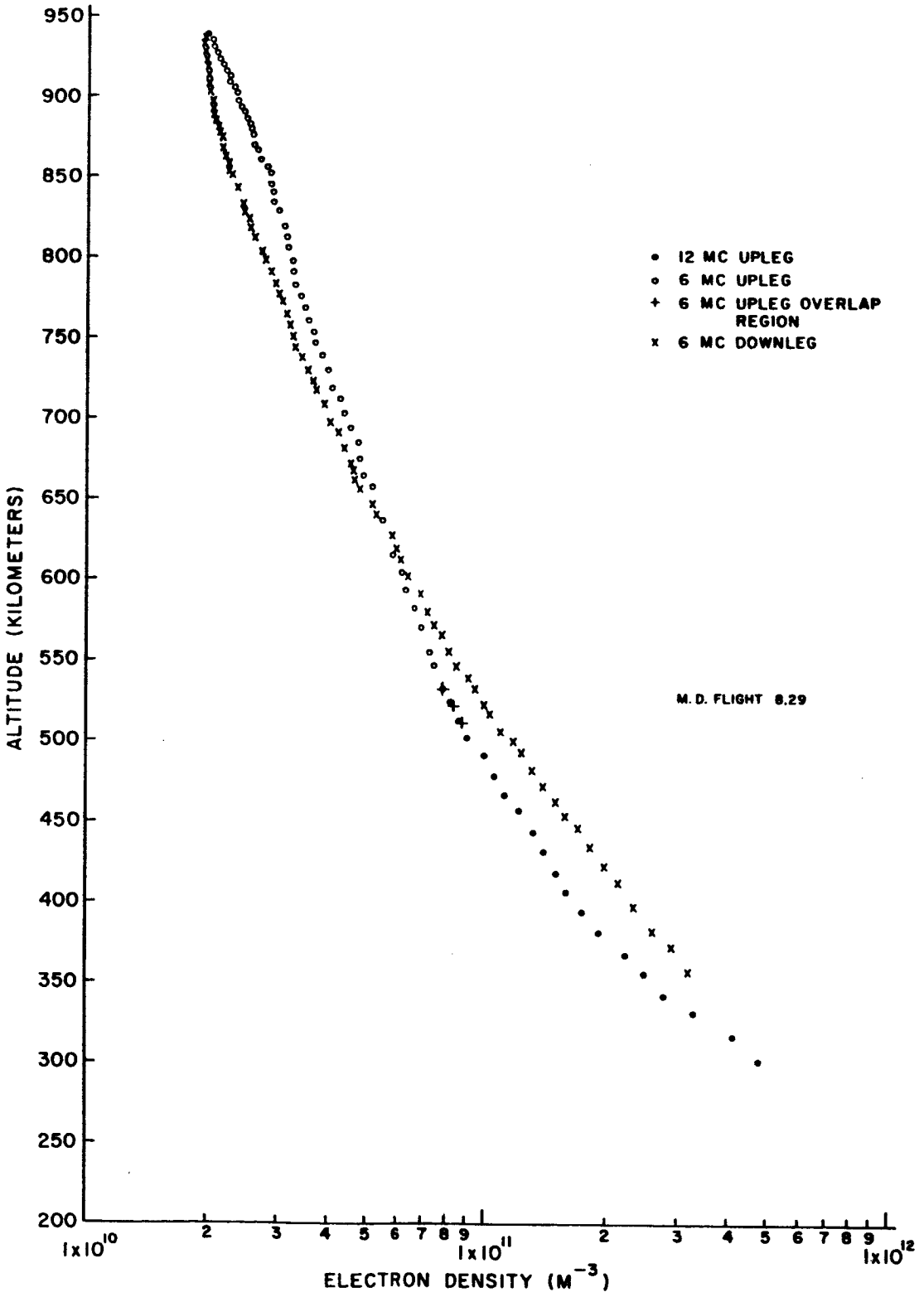

ELECTRON DENSITY PROFILE

FIGURE 5.30

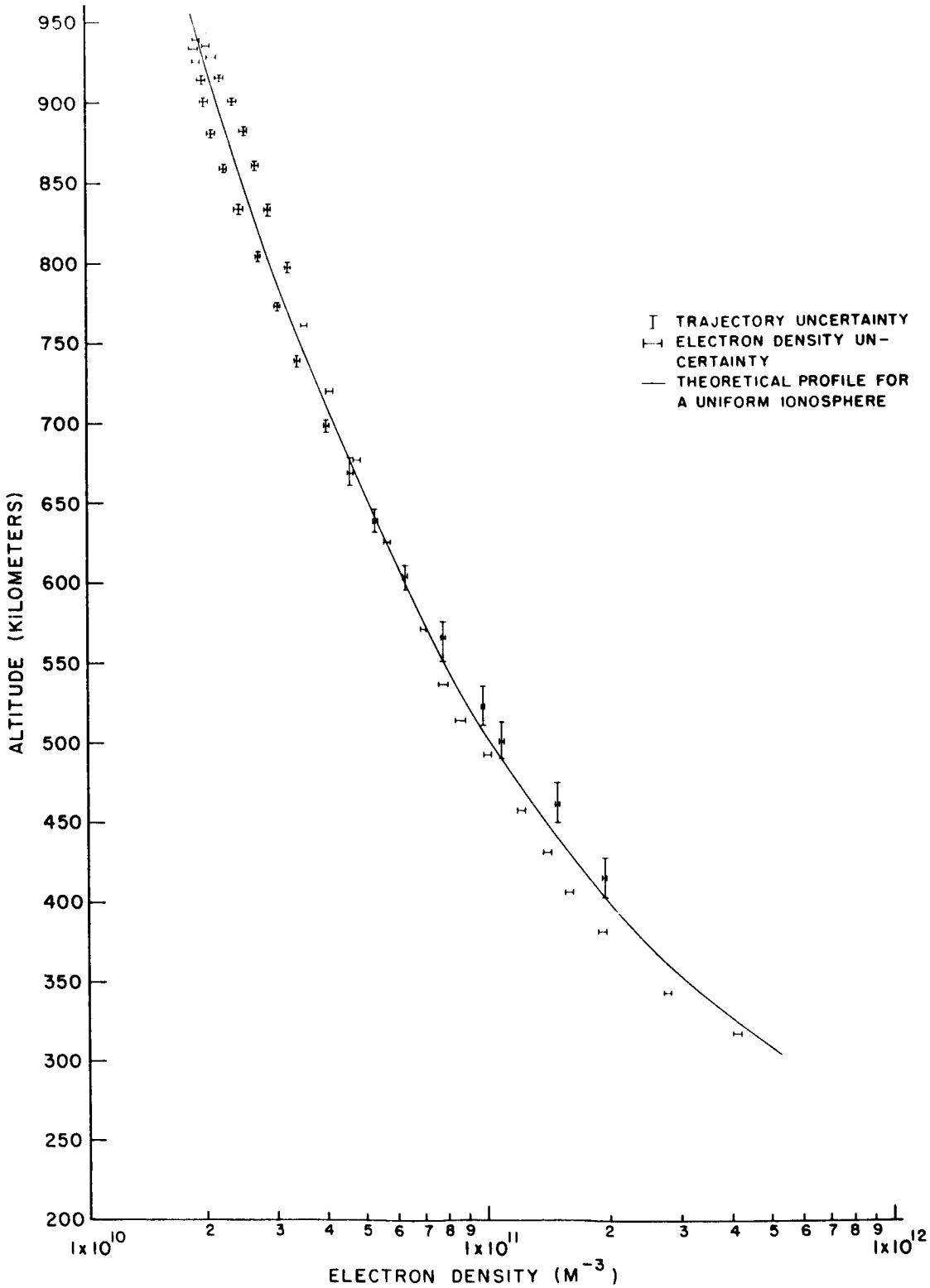

ELECTRON DENSITY PROFILE

FIGURE 5.31

was less than 1%.

The accuracy was, however, far better than the error bars indicate. The redundant phase measurement between 511 km and 535 km by the 6 Mc and 12 Mc phase channels showed a deviation in the two profiles from an average value of less than ± 1.2%. Many of the calculations in this 25 km interval coincided exactly thus giving no deviations at all. Error of this magnitude were expected more so than those of magnitudes given by the error bars placed on the profile.

What this method does is effectively measure an average electron density along a line between the Mother and Daughter payloads. When the payloads first separate, the line is short and extends out to about 5 km at the end of the experiment. While it is true that everything happening to the electron density along the line between the payloads is not known, the line does sweep out a path through the ionosphere. These measurements are, however, of higher resolution than any other known to date.

An important result from these high resolution measurements is the scale of irregularities in the ionosphere. From a close examination of the fine structure of the profile and with consideration due to the error bars, these small scale irregularities were estimated to be less than 2% per km over the densities. The large scale gradients centered around the peak of the flight and end of the flight were evaluated by assuming a completely uniform ionosphere. This assumed reference density is indicated by the smooth exponential drawn through the profile. Size of irregularities from this type of analysis are best seen in the isopynics of Figure 5.32.

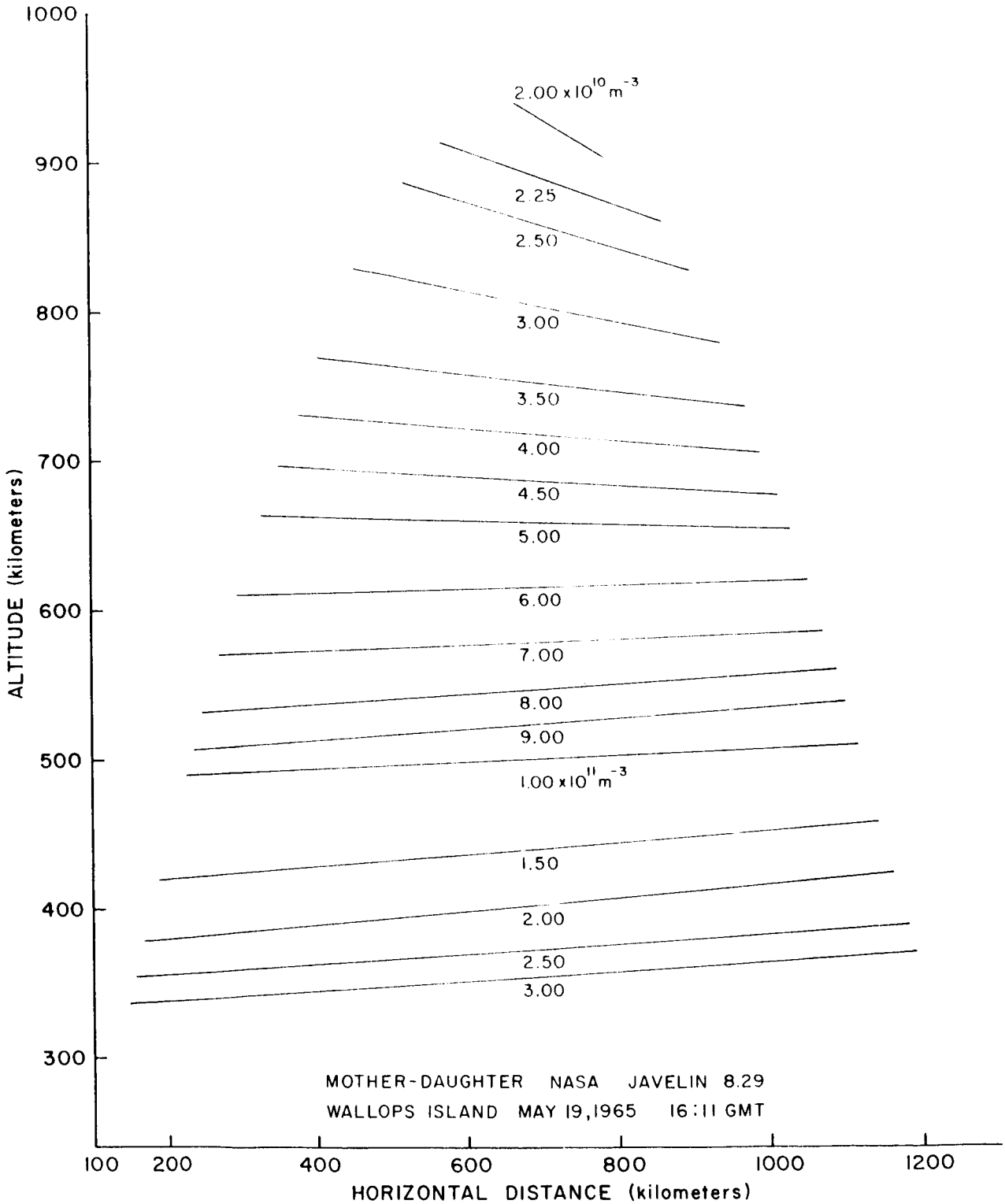

ISOPYCNICS

FIGURE 5.32

CHAPTER VI

Comparison of Results with Simultaneous Experiments

The results of the Mother-Daughter experiment were compared with electron density profiles obtained from simultaneous experiments. A planar ion probe mounted on the Mother payload made continuous measurements of the electron densities and ion densities along payload trajectory. The Alouette satellite, traveling in a north-south direction in the vicinity of Wallops Island also provided data for comparison; and a bottomside sounder, the Wallops Island ionosonde gave valuable information on the lower F region - the F_2 peak density at time of launch, the plasma frequency, and scale height.

6.1 Planar Ion Probe

A multi-gridded planar ion probe designed and constructed by Dr. L. C. Hale of Pennsylvania State University (1964), was concerned with the determination of the positive ion density, temperature, and composition, electron temperature, and the vehicle potential of the Mother. Electron densities were inferred from ion density measurements; the ionosphere was assumed to be electrically neutral. The results of the probe experiment are described in more detail by Hoffman (1966). Only portions of these results are reiterated for comparison with the Mother-Daughter propagation results.

Figure 6.1 shows the profile obtained from the ion probe, the Mother-Daughter profile, results from the Alouette satellite, and the Wallops sounding radar. The ion probe electron density profile was normalized with respect to the Mother-Daughter profile because

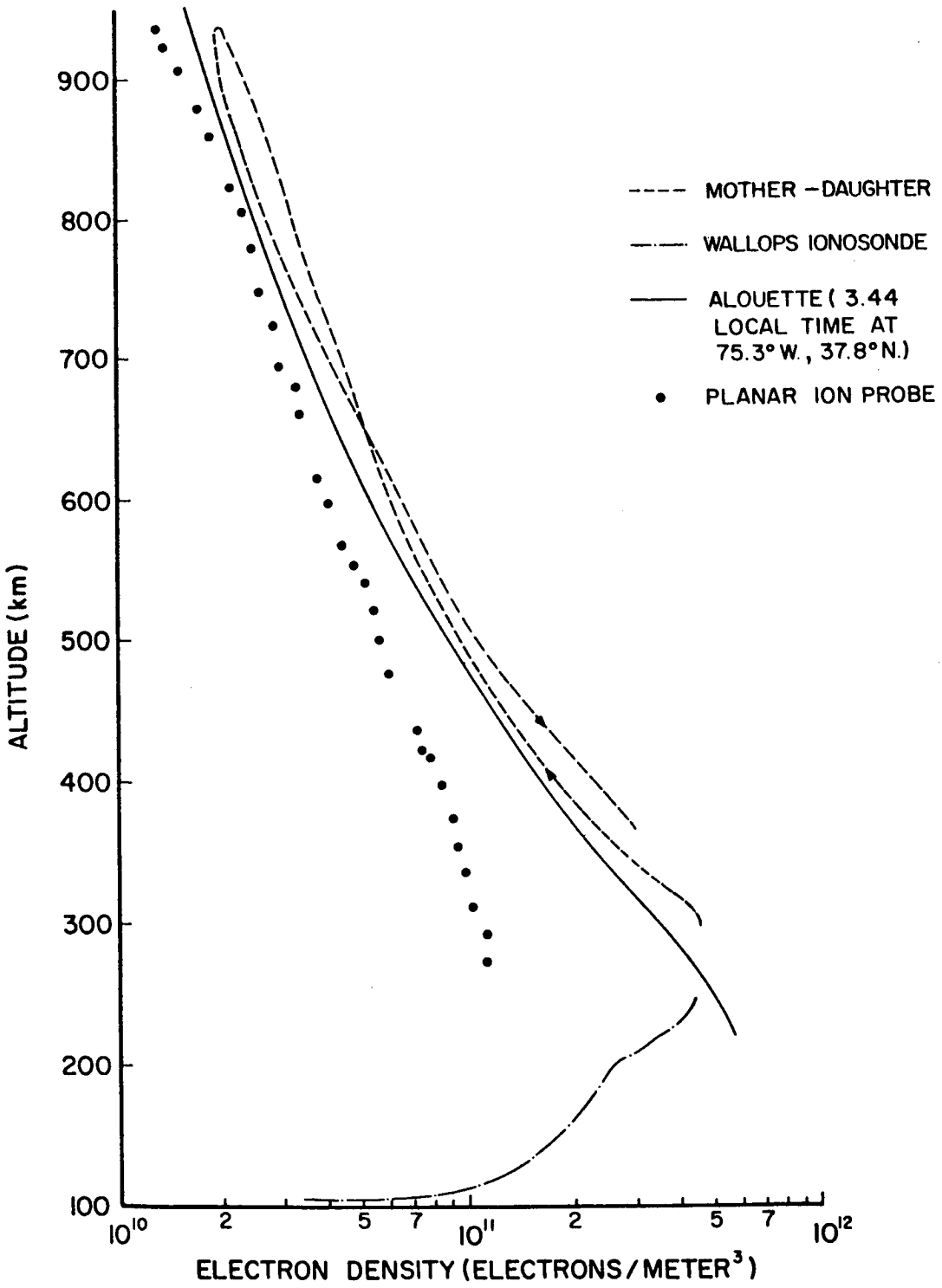

ELECTRON DENSITY PROFILES

FIGURE 6.1

of a number of overriding complicating effects encountered in analysis of the data.

Compared to ionosonde data and the Mother-Daughter results these densities were quite low. The experimental error was estimated as ±20% for the probe; however, this could not account for the large discrepancies at the lower altitudes where probe results were incorrect by a factor of four. There were reported by Hoffman (1966) to be three significant factors causing the errors in profile of Figure 6.1.

A wake from the Daughter section below an upleg altitude of 450 km caused a trail of depleted ions. This was suspected to be the cause of low measurements of the ion densities by the probe mounted on the trailing Mother. The wake, which extended to a distance of 100 meters, predominated for nearly 18 seconds after payload separation; but it did not, however, affect phase measurements on the 12 Mc channel of the Mother-Daughter experiment because the electron density controls the refractive index. Density calculations from 12 Mc phase data began at the time the wake effect was becoming negligible.

The stipulated 50% inaccuracy of probe measurements from 450 to 700 km was thought to be caused by an inaccurate geometrical determination of the grid transmission coefficient.

Above 700 km the error stemmed from the fact that vehicle velocity was no longer much greater than the probable ion velocity. The angle of influx of particles was also becoming larger. This effect combined, supposedly, with the attracting electric field of the grids

and the enlarging ion sheath so that ion currents were large and consequently yielded high densities.

6.2 Wallops Island Ionosonde

The bottomside of the F region was investigated every thirty minutes at Wallops Island on the day of launch. The profile exhibited in Figure 6.1 shows the results of the ionosonde eleven minutes before launch (20 hours zebra time). The accuracy of the profile was estimated by NASA to be within ±5%.

From the ionosonde data it was also possible to evaluate the plasma frequency in the vicinity of the F_2 peak at Wallops. A value of 6.1 Mc was found; this measurement was also verified by the rapid attenuation of the 6.13333 Mc propagation frequency as the Daughter payload re-entered the F_2 peak at 1000 seconds or 260 km on the downleg portion of the flight. There was no assessment of the horizontal gradient by this experiment.

6.3 Alouette Satellite

Results from the topside sounding satellite Alouette are also shown in Figure 6.1. The satellite was passing north to south at 19 hours 44 minutes zebra time and came within 2^{o} latitude of Wallops Island. Measurements are close to those of the Mother-Daughter experiment at the higher altitudes. It does show a disagreement near the F_2 peak with both the results of the Mother-Daughter experiment and the ground ionosonde. The unusually low F_2 peak from Alouette data is characteristic of this type experiment.

The magnitude of errors in the Alouette profile was not specified. These results are, however, subject to the many inherent

errors mentioned in Chapter I. The altitude at which densities were measured was liable to errors caused by the irregularities along the path of propagation of the sounding waves and the ducting of these waves along field lines. This ducting of waves was speculated by Jackson, Donley, Blumle, Bauer, and Fritzenreiter (1963) in a previous experiment to increase the path length and thus lower the altitude of the F_2 peak.

CHAPTER VII

Conclusions

7.1 Summary of Results

In Section 1.3 the specific objectives of this investigation were stated. All of the objectives were achieved; each is outlined here under the problem headings.

7.1.1 Methods of Analyzing F Region Electron Densities

A method of analyzing the electron density profiles in the F region was described in Chapter III. The technique relied on the phase dispersion measurements between two slowly separating rocket capsules. The phase measurements made with respect to the 73.6 Mc high frequency reference also required a separation velocity, a relative spin between the payloads, nominal payload trajectory, and a continuous measurement of the angle of propagation of the CW signals with respect to the total magnetic field vector.

7.1.2 Absolute Accuracy of the Technique

The absolute accuracy of the above method was analyzed in Section 5.4.2. The maximum error in the 12 Mc density calculations was shown in Figure 5.27 excluding trajectory errors. The 6 Mc electron density calculations were liable to the errors shown in Figure 5.26 less trajectory uncertainty. The density profile calculated from flight data showed an error less than the above predicted maximum errors. A maximum deviation of 1.2% from the average density between the 6 Mc and 12 Mc profiles in a 25 km interval showed that the accuracy was better than the predicted errors. Some

densities in this interval for 6 Mc and 12 Mc coincided and thus showed no deviation at all.

7.1.3 The Experiment and Results

The technique of propagating between two rocket capsules was accomplished using a Mother-Daughter payload Javelin 8.29 launched from Wallops Island on May 19, 1965. The data reduction technique described in Chapter IV centered about the phase reduction curve formulated for Figure 4.1. Corrections to recorded phases included the large relative spin phases and minor second order corrections dependent on receiver delays and the Faraday rotation. The electron density profiles of Figures 5.30 and 5.31 were the end result of the analysis.

7.1.4 Analysis of Profiles

The electron density profile was examined closely and a detailed study of the fine structure of the profile was made. Small scale irregularities amounted to less than 2% over densities. Large scale horizontal gradients were evident near the apogee of the trajectory and on re-entry at 500 km. Figure 5.32 showed these gradient regions.

7.1.5 Comparison with Simultaneous Experiments

The results of the Mother-Daughter experiment were compared with the onboard planar ion probe, the Wallops Island ground ionosonde, and the topside sounding Alouette satellite. Complications in the probe data made its results dubious. The ionosonde showed that the lower F region profile was in close agreement with the 12 Mc upleg

Mother-Daughter profile. The Alouette data agreed within 5% of the Mother-Daughter results above 750 km. This could be entirely accounted for by horizontal gradients of the order of those actually measured above 900 km.

7.2 Suggestions for Further Study

The large scale horizontal gradients evident in the density profile of Figure 5.30 and 5.31 have an interesting basis for further investigations. The connection between the changing propagation angle (caused by a changing magnetic field) and the electron density is also very interesting in the analysis of the horizontal gradients.

Appendix A

Complete Formula for Index of Refraction

$$\mu^2 = 1 - \frac{X}{1 - jZ - \frac{Y_T^2}{2(1-X-jZ)} \pm \left[Y_L^2 + \frac{Y_T^4}{4(1-X-jZ)^2} \right]^{\frac{1}{2}}}$$

where $Z = \nu e/\omega$

$$Y_T = \omega_H \sin \theta/\omega$$

$$Y_L = \omega_H \cos \theta/\omega$$

$$X = \omega_N^2/\omega^2$$

Appendix B

Proof $Z = \nu e/\omega \doteq 0$ for F Region Analysis

1. $\nu_e = 4.4 \times 10^{-9}(T/300)\, n_n + 6.1 \times 10^{-3}(T/300)^{-3/2}\, n_i$

   where ν_e = collision frequency

   n_i = ion density $\doteq n_e$ electron density for F region

   (1×10^4 to 1×10^6 cm^{-3})

   n_n = neutral particle density (3×10^9 cm^{-3})

   T = temperature ($1500^{\circ}K$ to $3500^{\circ}K$)

   ω = propagation frequencies - (2π) 6.13333 Mc,

   2π 12.26666 Mc, or 2π 73.60 Mc

2. $\nu_e(max) = 615$ cps

   $\nu_e(min) = 72$ cps

3. $Z_{max} = 1.59 \times 10^{-5}$

   $Z_{min} = 1.55 \times 10^{-7}$

4. Contribution of Z(maximum or minimum) in the expression for the refractive index μ is found in the term $1 - X - jZ$. Since Z_{max} and X_{max} and X_{min} with Z_{min} occur simultaneously the contribution of Z to $1 - X - jZ$ is less than 0.01%.

References

1. Bauer, S. J. and L. J. Blumle, "Mean Diurnal Variation of the Topside Ionosphere at Mid-Latitudes", Journal of Geophysical Research, Vol. 69, No. 17, September 1, 1964.

2. Bauer, S. J., L. J. Blumle, J. L. Donley, J. E. Jackson, and R. J. Fritzenreiter, "Simultaneous Rocket and Satellite Measurements of the Topside Ionosphere", Goddard Space Flight Center, Greenbelt, Maryland, X-615-63-175, August 8, 1963.

3. Bauer, S. J. and J. E. Jackson, "Rocket Measurement of the Electron Density Distribution in the Topside Ionosphere", Space Sciences Division, G.S.F.F., NASA Greenbelt, Maryland, January 5, 1962.

4. Berning, Warren W., "Charge Densities in the Ionosphere from Radio Propagation Data", Aberdeen Proving Grounds, Journal of Meteorology, Vol. 8, No. 3, June 1951.

5. Blackband, B. Burgess, I. Jones, G. Lawson, "Deduction of Ionospheric Electron Content from the Faraday Fading of Signals from Artificial Earth Satellites", Nature, April 25, 1959, Vol. 183.

6. Blumle, L. J., R. J. Fitzenreiter, J. E. Jackson, "The National Aeronautics and Space Administration Topside Sounder Program", Goddard Space Flight Center, Technical Note D-1913, based on talk presented at the American Astronautical Society, American Association for the Advancement of Science meeting at Philadelphia, Pennsylvania, December 27, 1962.

7. Bowhill, S. A., "The Formation of the Daytime Peak of the Ionosphere F_2 Layer", Ionosphere Research Laboratory, University Park, Pennsylvania, Scientific Report No. 154, January 1, 1962.

8. Bowhill, S. A., "The Faraday Rotation Rate of a Satellite Radio Signal", Journal of Atmospheric and Terrestrial Physics, Vol. 13, pp. 175-176, 1958.

9. Bowhill, S. A. and E. A. Mechtly, "An Ionosphere Electron Density Experiment Particularly Suited for Small Rockets", Ionosphere Research Laboratory, Pennsylvania State University, University Park, Pennsylvania. Reprint from Proceedings of the 2nd International Space Science Symposium 1961.

10. Bowhill, S. A. and E. R. Schmerling, "Distribution of Electrons in the Ionosphere", Ionosphere Research Laboratory, Pennsylvania State University, University Park, Pennsylvania, reprint from

Advances in Electronics and Electron Physics, 1961.

11. Boyd, R. L. and M. J. Seaton, Rocket Exploration of the Upper Atmosphere, University College, London, Interscience Publisher, Inc., New York, London, 1954.

12. Brace, L. H. and N. W. Spencer, "Ionosphere Electron Temperature Measurements and Their Implications", Goddard Space Flight Center, Greenbelt, Maryland, Journal of Geophysical Research, Vol. 68, No. 19, October 1, 1963.

13. Browne, I. C., J. V. Evans, J. K. Hargreaves, and W. A. S. Murray, "Radio Echoes from the Moon", Proceedings of the Physical Society, 69, p. 901, 1956.

14. Briggs, B. H. and M. Spencer, "Horizontal Movements in the Ionosphere", reprint Progress in Physics, 17, 245, (1954).

15. Budden, K. G., Radio Waves in the Ionosphere, Cambridge University Press, Cambridge (1961).

16. Cantrell, Wayne, "The Mother-Daughter Ionospheric Experiment Payload Description and Performance", Scientific Report 229(E) Ionosphere Research Laboratory, October 1, 1964.

17. Chapman, J. H., "A Survey of Topside Sounding of the Ionosphere", Defence Research Telecommunications Establishment, Defence Research Board, Ottawa, Canada. Paper presented at the XIII General Assembly, URSI, Tokyo, 1963.

18. Crichlow, W. Q., "Noise Investigation at V.L.F. by the N.B.S.", Proceedings of I.R.E., June 1957.

19. Defence Research Board, "Alouette Satellite 1962 Beta Alpha One", Defence Research Telecommunications Establishment, Ottawa, Canada, October 1962.

20. Doupnik, J. R. and E. R. Schmerling, "The Reduction of Ionograms from the Bottomside and Topside", Ionosphere Research Laboratory, Pennsylvania State University, University Park, Pennsylvania, Journal of Atmospheric and Terrestrial Physics, Vol. 27, 1965.

21. Fietzenreiter, R. J. and L. J. Blumle, "Analysis of Topside Sounder Records", Journal of Geophysical Research, 69, 3, Feb. 1, 1964.

22. Froehlich, J. P., "A High Frequency Phase Comparator for Rocket Instrumentation", Ionosphere Research Laboratory, University Park, Pennsylvania, Scientific Report No. 210(E), June 10, 1964.

23. Goldstein, H., Classical Mechanics, Addison-Wesley, Reading, Mass., (1950).

24. Gothard, N., "Hydromagnetic and Radio Wave Propagation in the Magnetosphere Along a Field-Aligned Plasma Stratum", Cornell University, Ithaca, New York, September 1965.

25. Gingaus, Gorozhankin, Gdalevich, Afanin, Rybchinsky, Shutte, "The Technique and Some Results of Experiments Conducted on Satellite Cosmas 2 by Means of Langmuir Probes and Ion Traps of Honeycomb Type", paper presented at the Vth International Space Science Symposium in Florence in May, 1964.

26. Hale, L. C., "A Probe Assembly for the Direct Measurement of Ionospheric Parameters", Ionosphere Research Laboratory, Pennsylvania State University, Scientific Report No. 223(E), 1964.

27. Hendricks, S. J. and Cain, J. C., "Magnetic Field Data for Trapped Particle Evaluation", Journal of Geophysical Research, Vol. 71, No. 1, January 1, 1966.

28. Hines, C. O., "Motions in the Ionosphere", Proceedings of I.R.E., 47, 177, (1959).

29. Hoffman, D. J., "The Theory and Experimental Results of an Ionospheric Probe Experiment", Scientific Report No. 260, Ionosphere Research Laboratory, University Park, Pennsylvania, January 10, 1966.

30. Jackson, J. D., Classical Electrodynamics, John Wiley and Sons, Inc., New York, (1963).

31. Jackson, John E., "Measurements in the E-Layer with the Navy Viking Rocket", U.S.N.L., Washington 25, D.C., March, 1954.

32. Jackson, J. E., "NASA Investigation of the Topside Ionosphere", X-615-63-105, May 1963, Goddard Space Flight Center, Greenbelt, Maryland. Paper presented at NATO Advanced Study Institute, Norway, April 17-26, 1963.

33. Jackson, J. E. and Kane, "Measurements of Ionospheric Electron Densities Using a R.F. Pulse Technique", Journal of Geophysical Research, 64.8, 1074, August 1959.

34. Jackson, J. E., and J. C. Seddon, "Ionosphere Electron Density Measurements with the Navy Aerobee-Hi Rocket", U.S.N.R.L., October 12, 1957.

35. King, J. W., D. Eccles, A. J. Legg and P. A. Smith with P. A. Galindo, B. A. Kaiser, D. M. Preece, and K. C. Rice, "An Explanation of Various Ionospheric Phenomena Including the Anomalous Behavior of the F-region", Radio Research Station, Ditton Park, Slough, Bucks, England, Document Number RRS/I.M. 191, December 1964.

36. King, J. W., D. Eccles, P. A. Smith, P. Dannahy, A. Legg, E. D. Olatunji, K. Rice, G. Webb and M. Williams, "Further Studies of the Topside Ionosphere Based on the Topside Sounder Satellite Data", D.S.I.R. Radio Research Station, Ditton Park, Document Number RRS/I.M. 112, December, 1963.

37. King, J. W., P. A. Smith, D. Eccles, and H. Heln, "The Structure of the Upper Ionosphere as Observed by the Topside Sounder Satellite, Alouette", D.S.I.R., Radio Research Station, Ditton Park, Document Number RRS/I.M. 94, July, 1963.

38. Knecht, R. W., and S. Russel, "Pulsed Radio Soundings of the Topside of the Ionosphere in the Presence of Spread F", Journal of Geophysical Research, Volume 67, No. 3, March 1962.

39. Knecht, R. W., and T. E. Van Zandt, "First Pulsed Radio Soundings of the Topside of the Ionosphere", Journal of Geophysical Research, Vol. 66, No. 9, September 1961.

40. Legg, A. J. and J. W. King, "Diurnal Variations of the Electron Concentration in the Ionosphere at Low Latitudes", Document No. RRS/I.M. 188, December, 1964, Radio Research Station, Ditton Park, Slough, Bucks, England.

41. Lien, J. R., R. J. Marcou, J. C. Ulwick, J. Aaron, and D. R. McMarrow, Rocket Exploration of the Upper Atmosphere, 1954, Interscience Publisher, Inc., New York.

42. Linford, L. B., "Progress Report No. 16, 1952", Contract No. W19-122 AC 15, University of Utah.

43. Lockwood, G. E. K. and Nelms, G. L., "Topside Sounder Observations of the Equatorial Anomaly". Part I: 75° W Longitude, Defence Research Telecommunications Establishment, DRTE 9511-40-5, received August 19, 1963.

44. Mechtly, E. A., "A Computer Program for Obtaining Refractive Indices and Polarizations from the Appleton-Hartree Equations and Magneto-ionic Tables for Cape Canaveral", Ionosphere Research Laboratory, University Park, Pennsylvania, Scientific Report No. 116, February 15, 1959.

45. Mitra, S. N., "A Radio Method of Measuring Winds in the Ionosphere", Proceedings of I.E.E. 96, (3), 441 (1949).

46. Moore, C., and W. Law, "Final Progress Report 1953", Contract No. AF19(122)-36, Upper Atmosphere Research Laboratory, Boston University.

47. Munro, G. H., "Traveling Ionospheric Disturbances in the F-Region", Australian Journal Physics, 11, 91 (1958).

48. Nisbet, John S., "Electron Densities in the Upper Ionosphere from Rocket Measurements", Ionosphere Research Laboratory, University Park, Pennsylvania, Scientific Report No. 126, December 10, 1959.

49. Nisbet, J. S. and S. Bowhill, "Electron Densities in the F Region of the Ionosphere from Rocket Measurements", Journal of Geophysical Research, 65, 3601, 1960.

50. Nisbet, J. S., T. P. Quinn, and B. H. Carson, "Feasibility Study of a Separating Capsule Rocket Experiment for the Accurate Determination of Absolute Electron Densities to a Height of Several Thousand Kilometers", Ionosphere Research Laboratory, Scientific Report No. 152, November 1, 1961.

51. Panofsky, W. K. H. and M. Phillips, Classical Electricity and Magnetism, Addison Wesley, Reading, Mass., (1955).

52. Pfister, W., "Magneto-Ionic Splitting Determined with the Method of Phase Integration", Preprint presented to URSI-IRE meeting April 1951, Washington, D. C.

53. Pfister, W. and J. C. Ulwick, "Analysis of Pulse-Delay from Rockets for Determination of Electron Density", Journal of Atmospheric and Terrestrial Physics, 1502, 1959.

54. Pfister, W., J. C. Ulwick, and R. P. Vancour, "Some Results of Direct Probing in the Ionosphere", Air Force Cambridge Research Laboratories, Journal Geophysical Research, Vol. 66, No. 4, April, 1961.

55. Ratcliffe, J. A., "A Survey of Existing Knowledge of Irregularities and Horizontal Movements in the Ionosphere", Phys. Soc. Rept. Ionosphere Conference 88 (1955).

56. Ratcliffe, J. A., Physics of the Upper Atmosphere, Academic Press, New York and London, (1960).

57. Ross, W. J., "The Determination of Ionospheric Electron Content from Satellite Doppler Measurements and Experimental Results", Journal of Geophysical Research, 65(a), 1960.

58. Ross, W. J., E. N. Bramley, and H. E. Ashwell, "A Phase Comparison Method of Measuring the Direction of Arrival of Ionospheric Radio-Waves", Proceedings Inst. Elec. Engineer, Part III, Vol. 98, pp. 294-302, 1951.

59. Seddon, J. Carl, "Electron Densities in the Ionosphere", U.S.N.R.L., Washington 25, D.C., Journal of Geophysical Research, Vol. 59, No. 4, December 1954.

60. Seddon, J. Carl, "Summary of Rocket and Satellite Observations Related to the Ionosphere", September 1960, National Aeronautics and Space Administration, G.S.F.C., Washington 25, D.C.

61. Seddon, J. Carl, "Propagation Measurements in the Ionosphere with the Aid of Rockets", U.S.N.R.L., Journal of Geophysical Research, Vol. 58, No. 3, September 1953.

62. Seddon, J. Carl, A. D. Pickar, and J. E. Jackson, "Continuous Electron Density Measurements Up to 200 Km", U.S.N.R.L., Washington 25, D.C., Journal of Geophysical Research December, 1954, Vol. 59, No. 4.

63. Serber, G. P., "Results from a Rocket Borne Langmuir Probe", NASA Tech. Note D-570, Goddard Space Flight Center, Greenbelt, Maryland, July 1, 1961.

64. Solomon, S. J., "Variations in the Total Electron Content of the Ionosphere at Mid-Latitude During Quiet Sun Conditions", Ionosphere Research Laboratory, Pennsylvania State University, University Park, Pennsylvania, Scientific Report No. 256, November, 1965.

65. Stratton, J. A., Electromagnetic Theory, McGraw-Hill, New York (1941).

66. Thomas, J. O., B. R. Briggs, L. Colin, M. J. Rycroft, and M. Covert, "Ionosphere Topside Sounder Studies, I - The Reduction of Alouette I Ionograms to Electron Density Profiles", Ames Research Center, California, NASA, Washington, D. C., Technical Note NASA TN D-2882, July 1965.

67. Thomas, J. O. and A. Y. Sader, "Electron Density at the Alouette Orbit", Journal of Geophysical Research, Volume 69, No. 21, November 1, 1964.

68. Ulwick, J. C., W. Pfister, R. P. Vancour, R. T. Bettinger, O. C. Haycock, and K. D. Baker, "Firing an Astrobee 200 Rocket with a Multiple Ionospheric Experiment", Proceedings of IRE, Vol. 50, No. 11, November, 1962.

69. Whipple, E. C., "Exploration of the Upper Atmosphere with the Help of the Third Soviet Sputnik", Goddard Space Flight Center, NASA Technical Note D-665.